The University Of Sheffield.

Discrete and continuum modelling of micro-lattices in dynamics

Duc Cac Diem Nguyen

Department of Civil and Structural Engineering

University of Sheffield

A thesis submitted in partial fulfilment of the requirements for the degree of

Doctor of Philosophy

2015

To my parents who have worked hard and sacrificed to provide me a precious gift of education. They have been a constant inspiration for me to work and live with my best ability and overcome difficulties with strength.

To my big family and friends who have supported me on this journey, thank you all for giving me a piece of your life.

To my cousin, Minh, who will always be in my heart. Your life indented in everyone's mind the best memories that are everlasting reminder to live life to the fullest.

Last but not least, to Mark, your love and never-ending support have been with me throughout these exciting years which were also full of stressful and exhausted moments. Your belief in me has encouraged me to head on strong. On the sideline, I hope that your proof-reading skills has improved to a new height after this. Nevertheless, there are new destinations waiting, I am looking forward to embark on our future journey together.

Declaration

I hereby declare that except where specific reference is made to the work of others, the contents of this dissertation are original and have not been submitted in whole or in part for consideration for any other degree or qualification in this, or any other University. This dissertation is the result of my own work and includes nothing which is the outcome of work done in collaboration, except where specifically indicated in the text.

Duc Cac Diem Nguyen
2015

Acknowledgements

I would like to express my special appreciation and thanks to my supervisor Professor Harm Askes, you have been a tremendous mentor for me. I would like to thank you for encouraging my research and for allowing me the freedom to explore the areas that interests me. I also want to thank the University of Sheffield and Engineering Faculty for providing me the opportunity to carry out a PhD and facilitate my PhD with the best academic environment.

I would also like to thank members in the Computational group CMD, especially people who were and are still in room D120a for being there with me during this PhD journey. I will miss this unique office space and bantering time during lunch or in Red Deer very much in the future.

A special thanks to my beloved friends, who provided my student life a sense of home and belonging. Thank you for eating with me, cooking for me, travelling with me, accommodating me, listening to my complaints and being there for me. I feel very lucky to find you all and share the friendships which could cross space and time.

Finally, I would like to thank all the staffs at the University of Sheffield for helping me along this academic journey.

Abstract

Materials with a sparse, periodic lattice microstructure exhibit excellent mechanical performance compared to their weight. Particularly, their engineered microstructure allows optimised mechanical behaviour under dynamic loading conditions. For instance, the material's microstructure can be manipulated such that wave filters emerge so that only certain frequencies can propagate through the material.

Various techniques can be used to model such materials with lattice microstructures. For instance, a discrete model can be deployed whereby every strut of the lattice structure is modelled as a beam element. However, a more efficient approach is to replace such a detailed microscopic material model with an enriched continuum model for certain dynamic problems. Compared to the classical continuum, the new model allows the microstructural effects to be captured efficiently and effectively by equipping the continuum equations of elasticity with an appropriate set of higher-order spatial derivatives; hence, a gradient elasticity formulation is obtained.

In order to link the additional constitutive coefficients of gradient elasticity to the geometric and mechanical properties of the lattice, in this thesis we use continualisation techniques whereby a representative volume element of a discrete square lattice model is translated into a homogeneous continuum formulation. Taylor series expansions and Padé approximations are usually required to ensure stability of the gradient elasticity model. The resulting continuum formulation is equipped with a range of strain gradient and inertia gradient terms. The dispersive properties of the model are then tested to check for the occurrence of wave filters. Applications of the Ru-Aifantis theorem are considered in detail. Finally, implementability with finite elements of the new continuum is examined. The research first reviews the one-dimensional case and subsequently applies the procedure to two-dimensional lattices of square, trapezium and hexagonal geometry arrangements.

Table of contents

List of figures

List of tables

Nomenclature

Roman Symbols

c_e	Wave velocity and is equal $\sqrt{\frac{E}{\rho}}$
E	Young Modulus
h	Numerical element length
i	unit imaginary number $\sqrt{-1}$
K	Stiffness matrix
l	Micro length
M	Mass matrix
t	Time
u	Horizontal displacement
v	Vertical displacement
x	Horizontal coordinate
y	Vertical coordinate

Greek Symbols

β	Ratio of beam depth over beam length
γ	Anti-clockwise angle made by the direction of wave propagation to the horizontal
ω	Angular frequency
π	$\simeq 3.14\ldots$

ρ Material density

θ Rotational displacement

Superscripts

$,j$ derivative with respect to j

Other Symbols

$\oint_\gamma$ integration around a curve γ

Chapter 1

Introduction

The aim of this research is to look for continuous models of microlattices to efficiently simulate the dispersion relations in micro-lattices, which have periodic structures. One of the methods to construct homogeneous models is to add higher order gradient terms in the equations of motion. This is called the gradient theory. The thesis describes the procedure to derive such gradient theories from physical discrete models with a variety of geometries. Three types of two dimensional microlattices which we consider in the scope of this thesis are square, trapezium and hexagonal lattices.

1.1 Wave propagation in microlattices

What are micro-lattices and what are their application?

Cellular solids are found in many natural and man-made structures from familiar cancellous or trabecular bone, wood, cork and honeycomb of bees to a variety of structures such as sandwich panels, cushioning foams, compact heat exchangers, heat resistant ceramic tiles of space shuttles and artificial biological implants. It is well known that cellular materials can extend the range of properties, static and dynamic responses, achievable by their solid counterparts (Gibson and Ashby, 1999). Also, the nature of the material, the relative density, and the underlying internal geometrical structure play a big role in improving the properties of these microstructural materials. In the last decade, cellular materials have emerged as promising multifunctional material systems (Evans et al., 1999). The wave propagation behaviour of such periodic materials show abilities to filter frequencies, a phenomenon known as pass and stop bands (Brillouin, 1953; Kittel, 1962), and to direct waves spatially known as wave beaming (Langley et al., 1997). In this research, we consider only the frequency filtering property of microstructured materials as this wave propagation behaviour currently has many applications at the micro and nano-scales such as vibration control devices, photonic devices and

energy absorption. The micro-lattices considered are comprised of many very small beams with length ranging from nanometers to milimeters and the beam sizes can be engineered by recent improved manufacturing methods such as 3D printers. Figure 1.1 presents typical micro-lattices with a very low density that can have practical application in the aerospace industry.

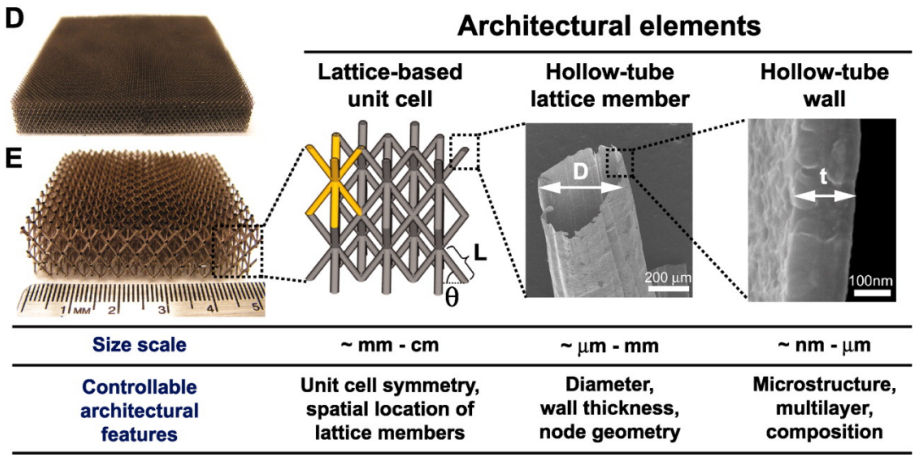

Fig. 1.1 The three dimensional micro-lattices that are created by HRL Laboratories, LLC

How to model wave propagation in microlattices and what is continualisation?

To model such materials with underlying microstructures, the most intuitive but the most cost-ineffective approach is to use a discrete model which is built by connecting individual members of a system, e.g. the discrete model of a micro-lattice material will have a system of tiny beams connected together. Therefore, there are suggestions in the literature (see the representative authors in Table 2.1) for using a continuous model instead, through the continualisation of a specific discrete representative volume element. Continualisation is a process turning a discrete model into a continuum while capturing the essentials for a specific problem and reducing computational cost. The idea of generalised (enhanced) continuum theories appeared as early as the 1800s, but it is also well-known through the efforts of the Cosserat brothers (Cosserat and Cosserat, 1909). There are currently two main ways to enrich a continuum: adding more degrees of freedom (micropolar theory) or adding higher order of strain gradients and this is one of the main topics in this thesis. For gradient elasticity, the continualisation procedure from real physical beam models still requires in-depth investigations and understanding. *This thesis focuses on the establishment of a procedure to formulate gradient continua for the wave dispersion for different arrangements of two dimensional physical beam models while comparing with popular models: the discrete models and the classical continuum. The challenge of the thesis is to develop models that capture the behaviour of micro-lattices in elasto-dynamics with the following properties:*

- *Stability*: the model is unconditionally stable in wave dispersion.
- *Robustness*: means that the continuum model has parameters that can be derived from the physical models. Moreover, the dispersion behaviour of the new continuum should outperform that of the popular classical continuum.
- *Efficiency*: easy implementation in commercial numerical methods such as finite element models.

1.2 Scope of work

The thesis constructs enhanced continua using gradient elasticity theory for linear dynamic analysis. More importantly, the application helps derive coefficients of the new C^0 continuity continuum [1] from the physical properties of the discrete models which, in this thesis, are chosen for micro-beam materials. The case for square, trapezium and diamond two dimensional trusses are implemented. The new continua are compared with the discrete and classical models on their wave dispersion behaviours. Finally, further steps are taken to facilitate easy and efficient implementation of the newly-derived gradient continuum into the finite element method for real problems by making the continuum only require C^0 continuity when discretised.

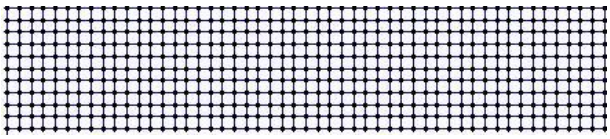

Fig. 1.2 The square lattice

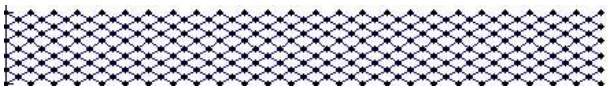

Fig. 1.3 The trapezium lattice

1.3 Outline

The thesis is structured as follows:

Chapter 2 mainly contains a literature review of different models for wave propagation in microlattices. However, before that, simple wave propagation definitions, especially the

[1] A function f is said to be (differentiability) class C^k if the derivatives f', f'',..., f^k exist and are continuous. Hence, a function of class C^0 means that it is continuous.

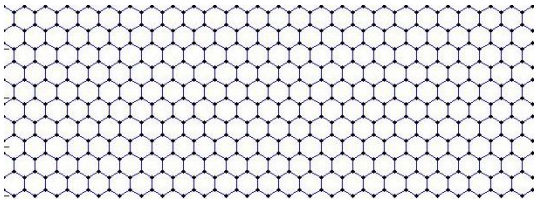

Fig. 1.4 The hexagonal lattice

Bloch-Floquet theorem, are introduced. At the end of the chapter, goals and objectives of the thesis are established together with the methodology that the thesis is based on. This serves to illustrate, in the simplest possible way, the concepts developed

Chapter 3 reviews the one dimensional case and compares this with existing models. The chapter includes a detailed derivation of chosen models following the methodology set out in Chapter 2. Additionally, the application of Ru-Aifantis theory (see footnote1, page 14), which helps the equations of motion of the continuum only require C^0 continuity (see footnote 1, page 3), is first presented in this chapter. This serves to illustrate, in the simplest possible way, the concepts developed in later chapters.

Chapters 4, 5 and 6 contain the novel contribution of this thesis. The procedure of Chapter 3 is extended from one dimension to two dimensions in order of geometric complication: the square, trapezium and hexagonal lattices. Chapter 4 also compares the derived models with existing models in the literature. Chapters 5 and 6 detail the Ru-Aifantis theorem application processes for the trapezium and hexagonal geometries. In each case, the order of the models derived is summarised in Figure 1.5.

Chapter 7 compiles all the results presented in the previous chapters and presents some discussion points. Conclusions and directions for further research on the topic are given in Chapter **??**.

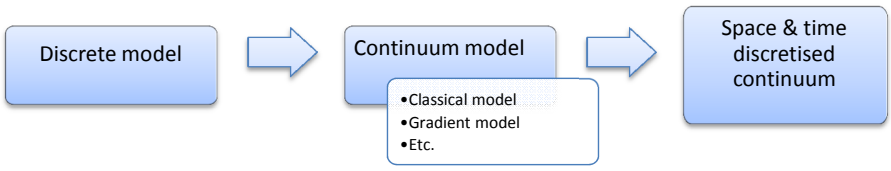

Fig. 1.5 The derivation order of models for 1D and 2D cases

Chapter 2

Wave propagation in microlattices

This chapter first gives a quick introduction of the basis of wave propagation, especially concepts of dispersion relations, in Section 2.1 and quickly reviews the basics of the Bloch-Floquet theorem in Section 2.2. The Bloch theorem is not the main focus of the thesis because it can only describe wave behaviours for one propagation angle each time; hence, the number of efficient finite element applications that can use the Bloch theorem is limited. However, the Bloch theorem provides quick analytical dispersion solutions for many cases; therefore, it is worthwhile to mention it in detail for the one-dimensional case as a limited special model to simulate dispersion of waves in periodic microstructures. In Section 2.2, there are applications of the definitions mentioned in Section 2.1. This is followed by a literature review of different models used in the simulation of wave propagation including the discrete models in Section 2.3 and different continuum models in Section 2.4. The next section formulates the goals and objectives of the thesis and establishes a procedure for four main steps to derive an efficient gradient continuum in Section 2.7. Lastly, a short introduction to three two-dimensional geometries and their relations to the 1D case is given in Section 2.8.

2.1 Wave propagation

This section provides a basic introduction to wave propagation in a medium. The content of this section can be found in any textbook, lecture notes or educational website about wave propagation. A wave speed can be understood in many ways and has been defined in different contexts; however, there are two most commmon concepts: phase speed and group speed. If we think of the wave as a sum of many frequency components, the phase speed provides the

speed at which the phase of any one component of the wave propagating in a medium:

$$v_p = \frac{\omega}{k} = \frac{\lambda}{T}, \tag{2.1}$$

where v_p is the phase speed [m/s], ω the angular frequency [rad/s], k the wavenumber [rad/m], λ is the wavelength [m] and T is the time period of the wave [s].

Meanwhile, a wave would contains different frequency components; the group speed is defined as the speed of a wave packet of a range of frequencies propagating through a medium:

$$v_g = \frac{\partial \omega(k)}{\partial k}, \tag{2.2}$$

where v_g is the group speed [m/s]. In almost all cases, a wave is mainly a movement of energy through a medium; thus, the group speed can be considered as the speed at which the wave energy travels through this medium.

The angular frequency ω cannot be chosen independently from the wavenumber k, but they are related through the dispersion relationship. For one-dimensional waves, this dispersion relation can be written as:

$$\omega = \Omega(k). \tag{2.3}$$

Hence, the phase speed can be rewritten as:

$$v_p = \frac{\Omega(k)}{k}. \tag{2.4}$$

In the special case where $\Omega(k) = ck$ where c is a constant and based on Equation (2.4), we have $v_p = c$ which means the phase speed is independent of the wave number k and also the group speed is equal to the phase speed. Such a case is said to be non-dispersive because all frequencies travel at the same phase speed c and the wave shape travels undistorted at this speed (Graff, 1975). Moreover, it also implies that all disturbances, including localised ones, propagate without change of shape. Examples of non-dispersive waves are electro-magnetic waves travelling in vacuum. However, in practice, there are many kinds of wave motion where the phase speed v_p varies with the wave number k non-linearly and the group speed is now a range of different values. Experimentalists proved that most waves in a range of materials are dispersive where components of the wave travels at different velocities (Erofeyev, 2003; Jakata and Every, 2008). In this case, the envelope of the wave packet becomes distorted as it travels. Popular examples of dispersive waves are surface waves on deep water, internal gravity waves, sound and electromagnetic waves, etc. Henceforth, to study wave propagation, it is important to find the dispersion relations $\Omega(k)$.

In this study, the wave propagation, especially the dispersion relations, of micro-beam ma-

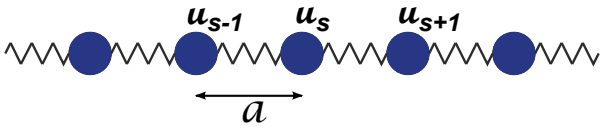

Fig. 2.1 A periodic structure with masses and springs

terials is observed using different modelling strategies. As explained above, the dispersion relation include two groups: non-dispersive and dispersive waves. However, it is well-known that wave propagation in inhomogeneous media contains dispersive waves - waves of different wavenumbers travelling at different speeds – due to the intrinsic microstructural effects (Mindlin, 1964). Moreover, the inhomegeneity of micro-beam materials is periodic; hence, they are predicted to have stop-bands which are certain regions of frequencies where there are no corresponding wavenumbers, which means only certain frequencies are allowed to travel through the materials. It is the main aim of the thesis to derive continuum models which display desirable dispersive behaviours.

2.2 Bloch-Floquet waves in periodic structures

It is useful to recall that the Bloch-Floquet theorem has limited applications for finite element methods but it provides good analytical solutions for any one frequency at a time. This section [1] introduces the basics of the Bloch-theorem which was the back-bone for key papers (Phani et al., 2006) and (Gonella and Ruzzene, 2008), and thus helps apply some of the important properties of wave propagation in periodic structures.

Consider a lattice structure, consisting of particles of mass M, separated by a distance a, and springs of stiffness C, as shown in Figure 2.1. Let u_s be the displacement of the particle at $x = s$ and t stands for time. Then the equations of motion take the form:

$$M\frac{d^2u_s}{dt^2} = C\left(u_{s+1} + u_{s-1} - 2u_s\right). \tag{2.5}$$

Assume that the displacements of the masses are time harmonic motion, that is $u_s = U_s(x)\exp(-i\omega t)$ where U_s is the magnitude, ω the angular frequency of the harmonic motion of the mass at $x = s$. The above equation can be rewritten as:

$$-M\omega^2 U_s = C\left(U_{s+1} + U_{s-1} - 2U_s\right). \tag{2.6}$$

[1] More details on this section can be found in the book Asymtotic Models of Solids with Cracks and Small Inclusions by A.B. Movchan, Department of Mathematics, University of Liverpool in LMS-EPSRC Short Instructional Courses on Advanced Methods in Linear and Nonlinear Elasticity, 28 July-1 August, which referenced back to Kittel (1996).

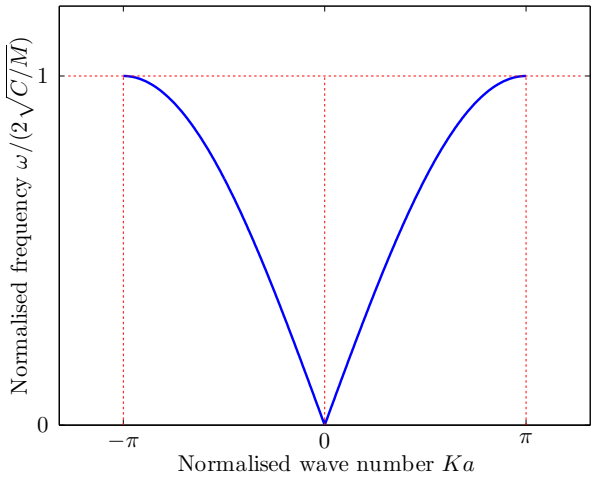

Fig. 2.2 Irreducible Brillouin zone for the lattice spring-mass problem

Solutions in the form of Bloch-Floquet waves for the above equation satisfy the following relation:

$$u_{s+n} = u_s \mathbf{e}^{inaK}, \tag{2.7}$$

where K is the Bloch parameter (or wavenumber).

Hence, the equation of motion becomes

$$-\omega^2 M U_s = 2C U_s \left(\cos\left(Ka\right) - 1\right). \tag{2.8}$$

Assuming that U_s is non-trivial, we deduce

$$\omega^2 U_s = \frac{C}{M} U_s \left(1 - \cos\left(Ka\right)\right), \tag{2.9}$$

and the non-negative roots have the form

$$\omega = \sqrt{\frac{4C}{M}} \left|\sin\left(\frac{Ka}{2}\right)\right|. \tag{2.10}$$

This is a periodic function with a period of $2\pi/a$. The interval $(-\pi/a, \pi/a)$ is known as the irreducible Brillouin zone , and it represents the range of physically significant values of the Block parameter K. Figure 2.2 shows the irreducible Brillouin zone where the horizontal axis is the normalised wave number Ka and the vertical axis is the normalised frequency $\dfrac{\omega}{2\sqrt{C/M}}$.

From the conditions of Bloch-Floquet waves, we have

$$\frac{U_{s+1}}{U_s} = \mathrm{e}^{iKa}. \tag{2.11}$$

Let $K_{max} = \pi/a$. In the continuum limit, as $a \to 0$, we have $K_{max} \to \infty$.

At the boundaries $K = \pm\pi/a$ of the Brillouin zone, the solution U_s represents a standing wave

$$U_s = U\mathrm{e}^{\pm isK_{\max}a} = U\mathrm{e}^{\pm is\pi} = U(-1)^s. \tag{2.12}$$

A standing wave is set up through successive reflections back and forward.

2.2.1 Group velocity

Using the definition in Section 2.1, the group velocity in this case is given as:

$$v_g = \frac{\partial\omega}{\partial K}. \tag{2.13}$$

Let's observe how the group velocity changes in the irreducible Brillouin zone. Figure 2.2 shows a symmetry axis at $Ka = 0$; hence, we can take into consideration only half of the irreducible Brillouin zone. First, considering the range $K \in (0, \pi/a)$, the group velocity has a value defined by the following equation:

$$v_g = \sqrt{\frac{C}{M}}a\cos(Ka/2). \tag{2.14}$$

At $K = \pi/a$, we have a group velocity $v_g = 0$ which represents a standing wave.

In the long wave limit $Ka \ll 1$, $\sin\left(\frac{Ka}{2}\right) \simeq \frac{Ka}{2}$, the solution becomes:

$$\omega(k) = 2\sqrt{\frac{C}{M}}|\sin\left(\frac{Ka}{2}\right)| = \sqrt{\frac{C}{M}}a|K|. \tag{2.15}$$

As $0 < Ka \ll 1$ then

$$\frac{\partial\omega}{\partial k} = v_g = a\sqrt{\frac{C}{M}}. \tag{2.16}$$

Thus, the group velocity v_g is independent of frequency in this limit.

The lattice structure can be modified to have different masses connected periodically to one another and this will lead to a band gap phenomenon, where a certain range of frequencies does not have corresponding wavenumbers.

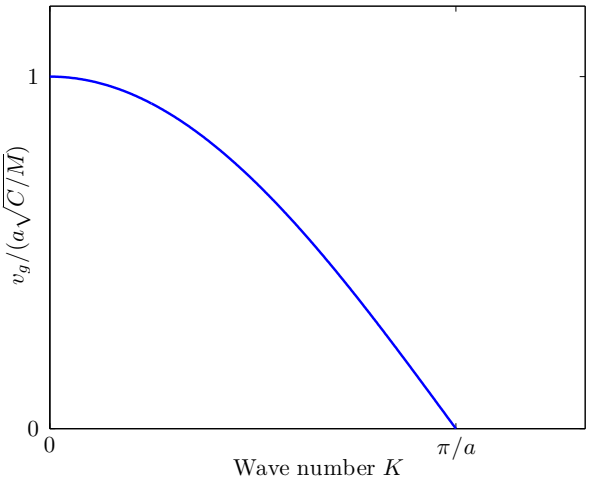

Fig. 2.3 Group velocity

After grasping some important concepts of wave propagation in microlattices, we will review different models used in wave propagation simulation for microstructured materials in the next section.

2.3 Discrete models for wave propagation in microlattice

It can be said that discrete models are the most intuitive solutions to build a simulation for micro-structured materials and we will use them as the benchmarks to compare and evaluate other models.

The spring-mass model was first derived by Born and von Karman (1912) but it was noted that the model is not an appropriate one (Berezovski et al., 2012) in some cases. However, the simple spring-mass model has been the main platform for developing different models. For instance, the simplest model of lattice vibrations is a 1D mono-atomic infinite chain of identical particles.

The spring-mass system has been developed from simple to more complicated forms with more added degrees of freedom. Firstly, at the one-dimensional level, the spring-mass system is constructed with axial springs connecting masses; the system has a typical equation $M\ddot{u} = K(\ldots + u_n)$ and this is the most common spring-mass model found in the literature. After that, the two dimensional spring-mass model was equipped with axial, shear and rotational springs (Suiker et al., 2001).

Going away from the spring-mass system, the beam models are built as a more practical discrete model to live applications such as the space grid-lattices, micro-beam materials. Phani et al. (2006) established a framework of modelling the Bloch wave theorem for different

lattice arrangements. Different beam theories are considered such as Euler, Timoshenko and Rayleigh beam theories. Additionally, different mass schemes such as consistent and lumped masses are compared. These discrete beam models are examined in the chapters discussing about the square, trapezium and hexagonal lattices.

Simple and straightforward, the discrete models can provide accurate stress and strains of individual microlattice beams. However, some specific problems, e.g. wave propagation or fracture toughness, do not require such details to be computed. Also, for dynamic problems, when the behaviour is investigated over a long period of time or when the time step is small, inclusion of unnecessary data is not beneficial. Besides, some examples of materials with microstructures are granular such ase geotechnical soil and rock layers, ballast material used in ordinary raiway tracks (Selig and Waters, 1994; Suiker et al., 1999), crystal lattice structures, carbon graphite, microlattices which are new materials found to be mechanically energy efficient and the microlattices can be artificially engineered, etc. Discrete models for the applications of the microstructures materials would mean setting up equations of motion for every single grain or beam. That would require powerful computers to solve the equations and their computational cost will be prohibitively large if a real life application of microlattices is to be considered.

2.4 Continuum models for wave propagation in micro-lattice

With the limitations mentioned in the last paragraph of the last section, it has been suggested in the literature to use continuum models instead of discrete models. The idea of generalised (enhanced) continuum theories have appeared as early as the 1800s, but it is also well-known by the efforts of the brothers Cosserat (Cosserat and Cosserat, 1909). A review on generalised continuum mechanics can be found in (Altan and Aifantis, 1997). As said in Section 1.1, continualisation is a process for turning a discrete model into a continuum while reducing computational cost but still capturing the essentials for a specific problem. A wide variety of continualisation techniques have been proposed to formulate continuum parameters of discrete materials (Pasternak and Mühlhaus, 2005; Pasternak et al., 2006). Five large categories of homogenisation methods arranged by Pasternak and Mühlhaus (2005) are listed as follows:

1. Averaging over volume element adopted in the theory of effective characteristics: Some papers which used this methods are Hill (1963), Mori and Tanaka (1973), Christensen (1979), Hashin (1988), Kachanov (1992), Nemat-Nasser and Hori (1993), Germanivich.

2. The homogenisation method is applied to materials with randomly varying elastic properties: based on averaging over realisations (ensemble averaging) (Khoroshun, 1978)

3. A group of methods based on modelling of periodically regular microstructure: such as periodical system of defects/inclusions, layers, regular granular packing, seen in Duffy and Mindlin (1957), Deresiewicz (1958), Meguid and Kalamkarov (1994).

4. Homogenisation by integral transformations: demonstrated by (Kunin, 1982, 1983). This is a special method of homogenisation applied to periodical structures only and it is based on the trigonometrical interpolation.

5. Homogenisation by differential expansions: examples are Mühlhaus and Oka (1996), Maugin (1999), Suiker et al. (2000, 2001), Lombardo and Askes (2012). The method is based on expanding the field variables into a Taylor series once a strategy to relate the discrete variables to continuum variables has been established. This method allows for higher-order theory derivations if a way to identify correspondent derivatives of the field variables in the Taylor expansions as higher-order terms can be found. This is also the method that this thesis applies and it is described in Chapters 3, 4, 5 and 6.

With different micro-structure arrangements and choices of continualisation methods, we can arrive at a wide variety of continuum in the literature. The classical continuum is the simplest and easiest continuum to be formulated but it does not contain any material length-scale. Therefore, classical continuum models often ignore the inhomogeneous effects at the micro-level and do not take into account the size effect due to the micro-structural length; thus, they produce incomplete or even misleading information about wave propagation behaviours of microstructured materials.

There are currently two main ways to enrich a continuum through the continualisation process: adding more degrees of freedom (micropolar theory) or adding a higher order of strain gradients. There are also continuum models which comprise of both additional degrees of freedom and strain gradients. There are a few ways to classify different formats of continuum theories that manifest the microstructural effects, see Askes and Aifantis (2011). In this section, we choose the most intuitive method to quickly understand the differences between gradient continuum with others. Based on the nature of the added variables of the continuum theories, they can be classified into three main categories:

- Standard continuum models: contain only translational degrees of freedom and ignore all rotational degrees of freedom. These early models can be seen in the works of Duffy and Mindlin (1957) and Deresiewicz (1958) for regular granular packing, which assumed that these continua were built for homogeneous deformation fields. Later, continuum theories with higher order gradients of strain were developed for non-homogeneous deformations to take into account the microstructural lengthscale: the use of second order gradients was proposed by (Chang and Gao, 1997, 1995), (Askes and Metrikine,

2002) and (Lombardo and Askes, 2012), fourth order gradients by (Suiker et al., 2000). All the standard models containing higher order gradients are named *gradient enhanced standard models* which are the main focus of this thesis and will be discussed further below.

- Non-standard continuum models: are constructed with additional degrees of freedom such as microstructural rotation or spin. The most typical non-standard continuum model is micro-polar theory which was first suggested by Cosserat and Cosserat (1909). The reader can read about micro-polar continuum developed for granular media by Mühlhaus and Vardoulakis (1987) and for beams by Askar and Cakmak (1968), Bazant and Christensen (1972), etc. as displayed in Table 2.1. We will not go into detail for this model later unless it appears in the context during the formulation of gradient enhanced standard models.

- Higher-order non-standard continuum models: as the name suggested, are hybrids of non-standard continuum models with high-order gradient terms. Representatives of this class are Cosserat continuum with second strain gradient terms by Mühlhaus and Oka (1996) and Suiker et al. (2000). Mindlin's model (Mindlin, 1964) could also be categorised into this group.

Except for the gradient enhanced standard models, we will not go into further details of other models as they are not the focus of the thesis.

2.5 Gradient elasticity theories

The key feature of gradient elasticity theories (models) is the introduction of higher order gradients of the field variables accompanied by internal length scales (Metrikine, 2006; Metrikine and Askes, 2002). Higher-order gradients have been incorporated into continuum formulation to capture certain properties of the continuum. Different motivations for gradient-enhanced theories can be found in (Aifantis, 1992; De Borst et al., 1997; Engelbrecht et al., 2005; Milton and Willis, 2007; Vardoulakis and Aifantis, 1994). Besides ranking the gradient continuum according to their highest order gradients, they can also be divided into two main types of higher-order gradient models: gradient elasticity and gradient plasticity (Aifantis, 1984, 1987) and then into smaller categories for linear and non-linear groups. It can be seen that gradient continuum (Chang and Gao, 1995; Mühlhaus and Oka, 1996) are based on or can be traced back to Mindlin's equation, which includes a large variety of terms. The higher-order gradients might also contain micro-inertia (Askes and Metrikine, 2002; Askes et al., 2007) for

dynamic linear elasticity. Micro-inertia terms have been considered to be numerically stable and suitable to solve boundary value problems (Fish and Chen, 2001; Rubin et al., 1995; Wang and Sun, 2002).

Models developed by (Chang and Gao, 1997, 1995), (Askes and Metrikine, 2002), (Lombardo and Askes, 2012) and (Suiker et al., 2000) resulted from the fifth homogenisation (continualisation) method (mentioned above) where different levels of truncation of the Taylor series expansion are retained. Moreover, some models when first developed include the rotational degrees of freedom which are then approximated into translational degrees of freedom. For example, Lombardo and Askes (2012) first developed equations of motion which represented micropolar theory, then rewrote the rotational variable to replace it with translational degrees of freedom. It is a well-known fact that high order strain gradients can cause dispersion instability which means no positive square of the frequency is corresponding to a certain wavenumber (Andrianov and Awrejcewicz, 2008; Andrianov et al., 2003; Chen and Fish, 2001; Collins, 1981; Pichugin et al., 2008; Rubin et al., 1995). The Padé approximants were one of the easy methods used to make modifications to lead to stable gradient-enriched model, as seen with the equation of the transverse vibrations of microstructured membranes (Andrianov and Awrejcewicz, 2008; Lombardo and Askes, 2010). Unfortunately, Lombardo and Askes (2012) noted that this approach does not always improve the model (Ostoja-Starzewski, 2002) in terms of stability. The Padé approximation shall be detailed in the next chapters for each specific case. Another shortfall of the high order strain gradients that hinders the popularity of such theories in practical application is the limited number of robust numerical implementations of gradient elasticity in the literature. An overview of different methods for implementations can be found at (Askes and Aifantis, 2011). C^0 continuity is the most desirable discretisation scheme for the popular finite element method. To enable the use of C^0 continuity (see footnote 1, page 3), the gradient continuum was modified by Aifantis (Aifantis, 1992) using a operator split to turn the fourth-order spatial continuum into two second-order spatial equations [1]. This procedure is chosen to be implemented in this thesis in Chapters 5 and 6. Further details on gradient elasticity, its application, classfication and comparison can be found in (Andrianov et al., 2009; Askes and Aifantis, 2011; Ostoja-Starzewski, 2002; Papargyri-Beskou et al., 2009).

[1] Ru-Aifantis theorem (Aifantis, 1992) utilises operator splits to rewrite second order strain gradients into an equation containing first order strain gradients. By doing so, the functions does not need C^1 continuity but instead only C^0 continuity for numerical implementations.

2.6 Continuum derived from physical models

At the one dimensional level, papers have been presented by Kunin (1982), Fish et al. (2002) and Metrikine and Askes (2002). Enhanced two-dimensional continua equipped by additional degrees of freedom have been frequently developed from continualisation of real physical systems, for example, (C.B. Banks and Sokolowski, 1968) formed an analogy between the rectangular lattices to couple stress theory. For gradient elasticity, the continualisation procedure from beam models still requires in-depth investigations and understanding. While mathematical models of the one and two dimensional case of the gradient theory using Ru-Aifantis theory (Ru and Aifantis, 1993) are well formulated and tested in (Askes et al., 2007) and Bennett and Askes (2008), a derivation of a gradient continuum from a two dimensional discrete model has been studied recently (Lombardo and Askes, 2010, 2012). This research focuses on the establishment of a procedure to formulate a gradient continuum for wave dispersion problem of a 2D physical beam model of diffrent microlattices. The approach in this research is a more general case of Lombardo and Askes (2012) and with more variety of geometries.

Table 2.1 summarises representative continuous models from different discrete models under different theories:

The entries of Table 2.1 were chosen based on the continuous models originating from a real physical model. The first seven papers use micropolar theory to approach localised failure problems in beam models and the eighth is about wave propagation problems in spring models. There are not many authors comparing the continuum they derived with discrete models (Suiker et al., 2001): Kunin (1983) uses the comparison for a cubic lattice consisting of masses that are connected by weightless rods and Suiker et al. (2001) does the comparison for a hexagonal spring-mass system solving wave propagation problems.

2.7 Aim of thesis and methodology

From Section 2.3, 2.4 and 2.6, there are a few important aspects that motivate this thesis. There are a number of continuum theories that take into account the underlying lengthscale of the microstructural materials as being more theoretically efficient replacements than the discrete model. Gradient elasticities modified by the Padé approximation and the Ru-Aifantis theorem are potential candidates in many continuum theories to produce stable dispersion relations, and only require C^0 continuity discretisation schemes for numerical implementations. A function f is said to be (differentiability) class C^k if the derivatives f', f'',..., f^k exist and are continuous. C^0 continuity can be easily applied to most of the finite element method structural analysis commercial software because of its simple shape functions. Therefore, a continuum which

No.	*Researchers*	*Continuum theory*	*Discrete element*	*Homogenisation method*	*Taylor's order*	*Problem*
1	C.B. Banks and Sokolowski (1968)	Couple stress	2D beam- rect cells	Strain energy	1st	Stress & disp of circular section
2	Askar and Cakmak (1968)	Micropolar	2D beam – rect cells with diagonals	Strain energy	1st	N/A
3	Bazant and Christensen (1972)	Micropolar	2D beam- rect cells	Strain energy	2nd	Initial stress and buckling
4	Chen et al. (1998)	Micropolar	2D beam -square, triangular & hexagonal	Strain energy	1st	Brittle fracture
5	Wang and Stronge (1999)	Micropolar	2D beam -honeycomb	Structural analysis	1st	Boundary-value
6	Warren and Byskov (2002)	Micropolar	2D beam - triangle & honeycomb	Structural analysis	2nd	N/A
7	Suiker et al. (2001)	Micropolar	2D springs – 7-cell hex & 9-cell square	Energy eqns then Lagrange eqns	1st	Dispersion relation
8	Kumar and McDowell (2004)	Micropolar	2D beam – rect, equilateral, mixed-tri , diamond	Strain energy	1st, 2nd	Stress concentration
9	Lombardo and Askes (2012)	Gradient	2D beam - square	Structural analysis	4th	Dispersion relation

Table 2.1 Different generalised models constructed from physiscal models using different continuum theories arranging according to timeline

requires only C^0 for discretisation can be considered to highly implementable.

When a continuum is discretised in space, the discretised continuum will display numerical dispersion behaviour even if the original continuum does not behave dispersively because the divided elements numerically does not propagate waves that has wavelength shorter than the element size. Hence, the dispersion behaviour should be incorporated into the continuum before the discretisation, which is the property that the classical continuum lacks.

More importantly, it is desirable to derive the gradient continuum from a physical system to enable performance comparison between the discrete model and the continuum. A physical system is defined and used as the base to formulate the coefficients of the continuum. Also, a robust method to build gradient continua from a wide variety of physical models is an advantage.

There are many routes to arrive at different mathematical continua for a same physical beam model. In the context of dynamic simulation, from the beginning, we identify a number of properties that the gradient continuum should exhibit:

- *Stability:* A stable continuum always has a corresponding frequency to any wave number in dispersion analysis.
- *Robustness:* The parameters are derived from physical models; thus, the continuum model will exhibit dispersion behaviours similar to the discrete model. In our case, we focus on the wave propagation behaviour instead of the magnitude of stresses or strains. Similar frequency bandwidths to the discrete model are an indicator of the robustness of a continuum before being discretised in space [1] that we try to achieve.
- *Implementability:* it is preferred that the final equations of motion are simple and easy to be implemented into Finite Element models. Specifically, we aim to use the C^0 continuity of the interpolation functions.

The thesis focuses on micro-lattices which are artificial highly porous micro-structured materials comprising many micro-beams with scales ranging from nano-meters to milimeters. An electron beam three-dimensional printer facilitates an adaptable fabrication of such materials with a variety of geometries at different scales. Therefore, their micro-structures can be engineered to optimise their mechanical behaviour such as wave filtering under dynamic loading conditions. However, this requires efficient and effective techniques to simulate wave propagation through such materials.

In this research, continuous models are derived using gradient theory enhanced with high-order terms, similar to the ninth entry of Table 2.1. The chosen discrete models have beam

[1] In the finite element method, to be able to model a certain problem with a defined geometry and boundary conditions, the object is often divided into appropriate smaller elements. Hence, the finite element method will 'break' a continuum model into smaller elements in space using mathematical manipulations, this process is called space discretisation.

elements arranged in different topologies ranging from one to two dimensions. Provided that a Taylor series expansion up to fourth order derivatives is considered, the homogenisation of these discrete models leads to a number of equations of motion equal to the number of degrees of freedom. If possible, the rotational degrees of freedom are approximated using translational degrees of freedom to achieve a standard model which consists of only translational degrees of freedom. This new set of equations is modified until it can achieve the expected dynamic properties which are listed above.

The stated Padé approximation method used in Askes and Metrikine (2002); Askes et al. (2007); Lombardo and Askes (2012) resembles a linear analysis and the same method is utilised in this thesis. We will keep calling this method the Padé approximation which is used to make a continuum stable in dispersion analysis, which means that for every wave number there are corresponding frequencies. Similarly, the aspect of Ru-Aifantis theorem where fourth order spatial derivatives is rewritten as a terms includes only second order spatial derivatives used in Askes et al. (2007) is re-applied in this thesis . However, this thesis seeks to widen the one-dimensional case established in Askes et al. (2007) to a more general case and to higher dimensional geometries.

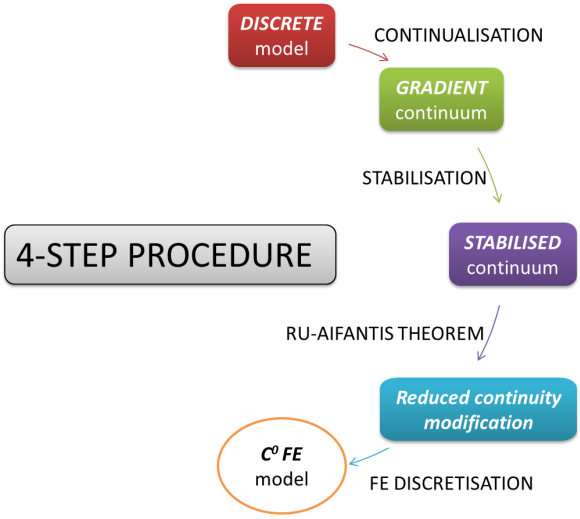

Fig. 2.4 Procedures to derive gradient continuum

We establish the 4-step procedure to derive a new gradient continuum (see Figure 2.4). Firstly, a discrete model is defined with given physical properties. Taylor series and Padé approximation are then used to continualise and stabilise the continuum. If the resulting continuum requires a higher continuity for FEM implementation, a further step applying the Ru-Aifanthis theorem (see footnote1, page 14) is carried out to arrive at the final continuum formulation. We perform dispersion analysis for each model by substituting the plane wave

equations into the continua to test the dispersion behaviour:

$$u = U \exp\left[i\left(k_x x + k_y y - \omega t\right)\right] v = V \exp\left[i\left(k_x x + k_y y - \omega t\right)\right], \tag{2.17}$$

where U ,V are the magnitude of the plane wave, k_x and k_y are the wave numbers in the x and y directions, $k = \sqrt{{k_x}^2 + {k_y}^2}$ is the wave number, ω is the angular frequency and t is time. Where possible, the models are tested with numerical examples.

We will apply the same procedure to the one dimensional case, two dimensional square, trapezium and hexagonal lattices.

2.8 Different geometries studied in the thesis and the computation methods used

Depending on the geometries, the procedure established in Figure 2.4 is modified to give the continuum model according to the goals and objectives in Section 2.7.

Generally, the well documented one-dimensional model is suitable for demonstration of the 4-step procedure but without the micro-rotation; the one dimensional case cannot manifest the relation of different continuum as well as two dimensional lattices. The one dimensional case can be considered as a benchmark and a test case as we develop other higher-dimensional cases; hence, in the next chapter we will describe the one dimensional case in detail. Then, the complication of cases gradually increases: the square lattice in Chapter 4, see Figure 1.2, the trapezium lattice in Chapter 5, see Figure 1.3 and the hexagonal lattice in Chapter 6, see Figure 1.4.

For the one-dimensional spring-mass model, the Hooke's law is applied where the stress and strain relationship in the spring is directly proportional. This spring-mass model is continualised using the Taylor series which has the form of Equation (3.5). The new continuum is modified to be stable in dispersion analysis while containing the fourth-order spatial derivatives. If the new continuum requires more than C^0 continuity, the Ru-Aifantis theory is applied. After this 4-step procedure, the continuum is discretised for finite element implementation. As a standard engineering practice, the thesis will use the well-documented and popularly calculated mass and stiffness matrices of finite elements instead of re-calculating them again. For the one-dimensional case, the consistent mass of a two-noded element can be calculated based on page 339 of Hughes (2000). A lumped mass matrix is calculated by having its diagonal elements equal to the row-sum of the corresponding rows. The consistent and lumped mass of the two-noded element can be looked up for the complete forms in Rao (2011). These matrices are displayed in Section 3.3.

For the two-dimensional cases, the discrete models are models as two-dimensional beams. The two popular beam theories, the Euler-Bernoulli and Timoshenko beam theory, are compared in this thesis. The Euler-Bernoulli beam theory is very popular in the industry. Meanwhile, the Timoshenko beam theory, different from the Euler-Bernoulli beam theory, takes into account the shear deformation and rotational inertia effects of a short beams. The calculated mass and stiffness matrices of the Euler-Bernoulli is very well-known and can be found in Bauchau and Craig (2009). Meanwhile, the Timoshenko matrices is given in Appendix A. The lumping techniques for mass matrices of the two-dimensional cases are the same row-sum operation with the one-dimensional case. Similar to the one dimension case, other steps will be applied to obtain a stable continuum requiring only C^0 continuity.

Because wave propagation is a dynamic problem, the magnitude of the time step Δt in numerical simulation plays an important role especially when explicit time scheme is used, see Equation (3.27). The time step Δt in this case is limited by a critical time step which is dictated by the speed wave and the element length. This thesis will consider how this critical time step changes with the new continuum.

Chapter 3

Wave propagation in a one-dimensional structure

It is necessary to first revise the literature and investigate the one dimensional case of the gradient theory as it will be the guideline to understand and fine-tune the new continuum in higher dimensions. This chapter uses a simple one-dimensional case to demonstrate the role of gradient elasticity in continuum models.

For dispersion and wave propagation of granular media, Mühlhaus and Oka (1996) first derived one-dimensional continuous models by using the energy functionals of the discrete model, then, extended this to three-dimensional models; and, the continuum models containing strain gradient terms were compared with the discrete models. Mühlhaus and Oka (1996) noted that the new continuum had "a combination of a Cosserat theory and a strain gradient theory". This was one of a few examples where the continuum was maintained with the material parameters of a particular discrete model for wave propagation analysis.

Early detailed reports on one dimensional case of continuum models using gradient elasticity for discrete spring-mass model can be found in (Metrikine and Askes, 2002) and (Askes and Metrikine, 2002). The two papers laid a foundation for the one dimensional model in this thesis. Metrikine and Askes (2002) discussed in detail the different continualisation methods. The standard method which this thesis uses replaces the discrete degree of freedom by a continuous field variable which retains the micro-structural properties of the discrete model. Metrikine and Askes (2002) analysed the dispersion of second-order and fourth-order models and emphasised that "a continuum model should be able to describe full frequency range". In this study, the stability and easy finite element implementation of the gradient continuum model are prioritised, see Section 2.7; therefore, only unconditionally stable second-order models (according to Metrikine and Askes (2002)) are considered further.

The following sections are arranged in the order: Section 3.1 defines a particular discrete

system, Section 3.2 gives details of the generalised continuum and contains two main continuum theories: Section 3.2.1 investigate the formation and wave propagation behaviours of the classical continuum while Section 3.2.2 investigates those aspects of the gradient continuum. Section 3.3 discusses the discretisation of both continua in space and time, and Section 3.4 concludes this chapter on one-dimensional models.

3.1 The one-dimensional discrete model

As introduced at the beginning of the chapter, this section depicts the chosen one dimensional discrete model for the study. Figure 3.1 shows a specific spring mass system where its micro-structural properties are used to derive a related continuum. The particles have mass M, connected by springs of stiffness K and the distance between two connecting balls is l. The particle dimension is insignificant at distance l and the particle deformation is infinitesimal in this study. The particles can only move in the horizontal direction. If u_n describes the displacement of a particle n and the mass density is defined by $\rho = \dfrac{M}{Al}$ and $E = \dfrac{Kl}{A}$, a discrete model can be derived as:

$$\rho \ddot{u}_n = \frac{E}{l^2}\left(u_{n+1} - 2u_n + u_{n-1}\right). \tag{3.1}$$

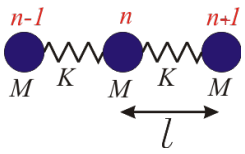

Fig. 3.1 Three successive particles in the one-dimensional discrete model

3.1.1 Dispersion analysis

The discrete displacement u_n has the harmonic plane wave equation $u_n = U\exp\left[i\left(kx_n - \omega t\right)\right]$ where U is the wave magnitude, k is the wave number and ω is the frequency. Substituting this into Equation (3.1), the dispersion relationship - the frequency ω with respect to the wave number k- can be deduced from the following periodic relationship:

$$\omega^2 = 4\frac{E}{\rho l^2}\sin^2\left(\frac{kl}{2}\right). \tag{3.2}$$

Hence, for all wavenumbers k, there is a frequency magnitude (maximum value) $\omega_{max} = \dfrac{2}{l}\sqrt{\dfrac{E}{\rho}}$ at wavenumber values $k = \frac{\pi}{2} + 2n\pi$ where $n \in \mathbb{N}$ (see Figure 3.2). Physically, the

discrete model only allows frequencies that are equal or lower than the ω_{max} to travel through the structure. Besides, the initial definition of the discrete spring-mass system implies that only waves with wavelengths larger than $2l$ or twice the inter-particle distance would be able to propagate. Therefore, it can be said that this particular discrete model has an ability to filter wave frequencies.

3.2 Generalised continuum of the one-dimensional model

This section investigates the generalised continuum based on the discrete model defined in Section 3.1. A detailed and more general approach for this spring mass system with higher order gradients can be found in (Metrikine and Askes, 2002) and (Askes and Metrikine, 2002). A general round viewpoint of modeling waves in microstructured solids in one dimensional setting can be found in (Berezovski et al., 2011). Using the standard continualisation method, the study replaces the discrete displacement with the continuum displacement $u(x,t)$ which is a function of the spatial coordinate x and time t and has to satisfy:

$$u(x,t) \approx u_n(t) \tag{3.3}$$

$$u(x+l,t) \approx u_{n+1}(t). \tag{3.4}$$

For simplicity, we replace $u(x,t) = u$, $\frac{\partial u}{\partial x}(x,t) = u_{,x}$, $\frac{\partial^2 u}{\partial x^2}(x,t) = u_{,xx}$, $\frac{\partial^3 u}{\partial x^3}(x,t) = u_{,xxx}$, $\frac{\partial^4 u}{\partial x^4}(x,t) = u_{,xxxx}$ and $\frac{\partial^2 u(x,t)}{\partial t^2} = \ddot{u}$ then substitute $u(x \pm l,t)$ for components in Equation (3.1) and a Taylor series is used to continualise the discrete model in Equation (3.1):

$$u_{n\pm1} \approx u(x \pm l,t) = u \pm u_{,x} l + \frac{u_{,xx}}{2} l^2 \pm \frac{u_{,xxx}}{6} l^3 + \frac{u_{,xxxx}}{12} l^4 \pm \ldots \tag{3.5}$$

Then, Equation (3.1) is as follows:

$$\rho \ddot{u} = \frac{E}{l^2} \begin{pmatrix} u - u_{,x} l + \frac{u_{,xx}}{2} l^2 - \frac{u_{,xxx}}{6} l^3 + \frac{u_{,xxxx}}{12} l^4 - \ldots \\ +2u+ \\ u + u_{,x} l + \frac{u_{,xx}}{2} l^2 + \frac{u_{,xxx}}{6} l^3 + \frac{u_{,xxxx}}{12} l^4 + \ldots \end{pmatrix}. \tag{3.6}$$

The previous equation is shortened to be the new equation of motion of the continuum from the Equation (3.1):

$$\rho \ddot{u} = E \left(u_{,xx} + \frac{1}{12} l^2 u_{,xxxx} \right) + \mathrm{O}(l^4), \tag{3.7}$$

where $O(l^4)$ has the exact numerical form as $\frac{E}{360} l^4 u_{,xxxxxx}$ which can be ignored due to its small magnitude compared to other terms in Equation (3.7). This equation belongs to the second-order model classification in (Metrikine and Askes, 2002) and is called the elasticity equation with a *stiffness gradient* term $El^2 u_{,xxxx}$.

Dispersion analysis: Performing the same procedure as Section 3.1.1, the following relationship is gained:

$$\omega^2 = k^2 l^2 \frac{E}{\rho}\left(1 - \frac{l^2}{12}k^2\right). \tag{3.8}$$

It is easy to notice that when $k > \frac{\sqrt{12}}{l}$, Equation (3.8) has imaginary frequencies. Thus, the continuum described by Equation (3.7) is only conditionally stable in dispersion analysis. Therefore, the next two sub-sections deal with two unconditionally stable continua which are the classical continuum and the gradient continuum originated from Equation (3.7).

3.2.1 Classical continuum of the one dimensional model

The classical continuum is the simplified version of Equation (3.7), and its dispersion equation can be written as:

$$\rho \ddot{u} = E u_{,xx} \tag{3.9}$$

$$\omega_K^2 = \frac{E}{\rho} k^2. \tag{3.10}$$

The dispersion behaviour of the classical continuum is shown in Figure 3.2. Equation (3.10) implies that the classical frequency ω_K has a linear relationship with respect to the wavenumber k and does not take into account the microstructural length l; hence, the classical continuum only displays a light dispersive behaviour and no frequency filtering ability.

It can be seen that after space discretisation in Section 3.3, the classical model appears to have frequency filtering ability which is created numerically and not desired.

3.2.2 Gradient continuum of the one dimensional model

There are many different mathematical ways to derive gradient continua from the discrete models. This section is divided into two parts: the first part presents the derivation procedure and analyses the optimisation aspect of the chosen method; meanwhile, the second part applies the so-called Ru-Aifantis theorem which is demonstrated in (Aifantis, 1992) to achieve a more efficient continuum.

Derivation procedure

The gradient continuum is based on Equation (3.7) which is thus modified using a Padé approximation to make the equation dynamically stable in the dispersion analysis. The following derivation aims at optimising the dispersion analysis results closer to the discrete model. Let S be a constant that determines how well the continuum fits to the discrete model:

$$\begin{aligned} \rho\ddot{u} &= E\left(u_{,xx} + \frac{1}{12}l^2 u_{,xxxx}\right) \\ + \quad -S\rho l^2 \ddot{u}_{,xx} &= -SEl^2 u_{,xxxx} \\ \hline \rho\ddot{u} - S\rho l^2 \ddot{u}_{,xx} &= Eu_{,xx} + El^2\left(\frac{1}{12} - S\right) u_{,xxxx}. \end{aligned} \tag{3.11}$$

The term $S\rho l^2 \ddot{u}_{,xx}$ is called an *inertia gradient* or micro-inertia term; meanwhile, the term $El^2\left(\frac{1}{12} - S\right) u_{,xxxx}$ is a *stiffness gradient* term (Askes et al., 2011). Performing dispersion analysis on the above newly formed equation, we have:

$$\omega^2 = k^2\left(\frac{12 - l^2(1-12S)k^2}{12(1+Sl^2k^2)}\right). \tag{3.12}$$

The condition for Equation (3.12) to be positive with all real values of the wave number k is that $S \geq \frac{1}{12}$. We note that when there are fourth order derivatives in the equation system, to ensure the stability (real value of ω for all real value of k), they should have the opposite signs with the second order derivatives or their coefficients are significant small so that they are negligible. As S increases, the difference in value of the frequency ω between the discrete and continuum model increases. Hence, the optimum value of S is $\frac{1}{12}$ and the optimal gradient continuum has the equation of motion and its dispersion relationship as follows:

$$\rho\ddot{u} - \frac{1}{12}\rho l^2 \ddot{u}_{,xx} = Eu_{,xx} \tag{3.13}$$

$$\omega^2 = k^2\frac{E}{\rho}\left(\frac{12}{12 + l^2k^2}\right). \tag{3.14}$$

Regarding Askes et al. (2007), we have written the one dimensional version of the equation of motion with *the additional inertia term accompanied by the material length scale parameter l that is a representation of the underlying microstructure of the material*. To compare the discrete model with the classical continuum and the gradient continuum, we draw the graph of Equation (3.10) and Equation (3.14) in Figure 3.2. Note that the discrete model is discrete in space and continuous in time; meanwhile, the classical and gradient models are continuous in both time and space.

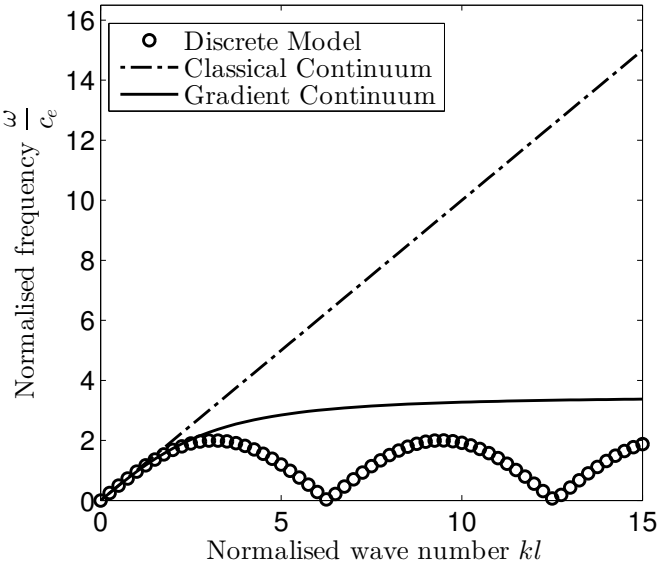

Fig. 3.2 Comparing the classical continuum and gradient continuum with the discrete model, with all structural properties E, l , ρ equal to 1, $S = 1/12$

Considering Equation (3.14), when $k \to \infty$, the frequency reaches a maximum value $\frac{12}{l^2}$. It can be thus said that this particular gradient continuum (when $S = \frac{1}{12}$) has a frequency filtering ability. Hence, $S = \frac{1}{12}$ gives the optimal continuum and requires the simpliest implementation because there is no stiffness gradient in the equation of motion and the mass gradient term can be discretised with only C^0 continuity.

On the other hand, when $S > \frac{1}{12}$, the continuum does not have the same filtering ability but the dispersion behaves with a lower gradient than the classical continuum. This case is discussed further in the next section to demonstrate how the Ru-Aifantis thoerem is applied.

Application of Ru-Aifantis theorem

If $S > \frac{1}{12}$, Equation (3.11) will retain the term $u_{,xxxx}$, which requires C^1 continuity for FEM implementation:

$$\rho\ddot{u} - S\rho l^2 \ddot{u}_{,xx} = Eu_{,xx} + \left(\frac{1}{12} - S\right) El^2 u_{,xxxx}. \tag{3.15}$$

If we define an auxiliary variable $\alpha = \mu u - \nu l^2 u_{,xx}$ where μ and ν are constants to be determined, and substitute it into Equation (3.15), we obtain:

$$\rho\ddot{u} - S\rho l^2 \frac{\mu\ddot{u} - \ddot{\alpha}}{\nu l^2} = Eu_{,xx} + \left(\frac{1}{12} - S\right) El^2 \frac{\mu u_{,xx} - \alpha_{,xx}}{\nu l^2} \tag{3.16}$$

$$\Leftrightarrow \rho\frac{S}{\nu}\ddot{\alpha} + \rho\left(1 - \frac{S\mu}{\nu}\right)\ddot{u} = E\left(\frac{1}{12} - S\right)\frac{1}{\nu}\alpha_{,xx} + E\left(1 + \left(\frac{1}{12} - S\right)\frac{\mu}{\nu}\right)u_{,xx}. \tag{3.17}$$

Equation (3.17) is paired with the rewritten form of the definition of the auxiliary variable α:

$$C\left(-\ddot{\alpha}+\mu\ddot{u}-\nu l^2\ddot{u}_{,xx}\right)=0, \tag{3.18}$$

where C is a multiplier that can be determined such that Equations (3.17) and (3.18) can be rewritten as to the following symmetric matrices after discretisation:

$$\begin{bmatrix} M_{1,1} & M_{1,2} \\ M_{2,1} & M_{2,2} \end{bmatrix} \begin{bmatrix} \ddot{\alpha} \\ \ddot{u} \end{bmatrix} = \begin{bmatrix} K_{1,1} & K_{1,2} \\ K_{2,1} & K_{2,2} \end{bmatrix} \begin{bmatrix} \alpha \\ u \end{bmatrix}, \tag{3.19}$$

where $M_{1,2}=M_{2,1}$ and $K_{1,2}=K_{2,1}=0$ in this particular case. In particular, we can determine the coefficients and multiplier so that the matrices are symmetric:

$$K_{1,2}=K_{2,1}=0 \Rightarrow \left(1+\left(\frac{1}{12}-S\right)\frac{\mu}{\nu}\right)=0 \Rightarrow \nu=\frac{(1-12S)}{12}\mu \tag{3.20}$$

$$M_{1,2}=M_{2,1} \Rightarrow \rho\left(1-\frac{S\mu}{\nu}\right)=-C \Rightarrow C=-\rho\left(\frac{12S\mu}{(1-12S)\,\mu}-1\right) \tag{3.21}$$

$$=\rho\left(\frac{1-24S}{1-12S}\right). \tag{3.22}$$

Finally, the Ru-Aifantis theorem-modified-system of equations of motion are:

$$\rho\frac{S}{\nu}\ddot{\alpha}+\rho\left(\frac{1-24S}{1-12S}\right)\ddot{u}=E\left(\frac{1}{12}-S\right)\frac{1}{\nu}\alpha_{,xx} \tag{3.23}$$

$$\rho\left(\frac{1-24S}{1-12S}\right)\ddot{\alpha}+\left(\frac{1-24S}{1-12S}\right)\left(\frac{12\nu}{1-12S}\right)\ddot{u}-\nu l^2\ddot{u}_{,xx}=0. \tag{3.24}$$

The above derivation helps demonstrate the implementation of the Ru-Aifantis theory. If we substitute the value of S into Equation (3.12), the relationship of the frequency and wave number can be plotted. We will not perform further dispersion analysis for Equation (3.23) and (3.24) (for time and space discretisation), but the process will involve solving a sixth order equation for the frequency ω.

3.3 Space and time discretisation of the continua

The dispersion analysis for the time-space discretisation continuum shall be carried out in a similar approach to Askes and Metrikine (2002)). However, we use the lumped mass scheme here. For a one dimensional two noded element with h is the length of the discretised element,

its consistent mass matrix is conventionally stated as Rao (2011):

$$M_{consistent} = \frac{1}{6}\rho h \begin{bmatrix} 1 & 2 \\ 2 & 1 \end{bmatrix}. \tag{3.25}$$

To attain the lumped mass matrix, we perform the row-sum operation on the consistent mass matrix in Equation (3.25):

$$\frac{1}{2}\rho h \begin{bmatrix} 1 & 0 \\ 0 & 1 \end{bmatrix}. \tag{3.26}$$

If the time integration follows the explicit central difference scheme, the relationship between acceleration and displacement is:

$$\begin{aligned} a_n^t &= M^{-1}\left(f - K u_t^n\right) \\ a_n^t \Delta t^2 &= u_n^{t-\Delta t} - 2u_n^t + u_n^{t+\Delta t}, \end{aligned} \tag{3.27}$$

where a_n^t is the acceleration of point n at time t, u_n^t is the displacement of point n at time t, M is the mass of point n, f is the external force, K is the stiffness of spring connecting to point n, Δt is the time step increment.

Spatial discretisation uses the plane wave equation to determine the displacement of node n at time t:

$$u_n^t = U \exp\left[i\left(knh - \omega t\right)\right], \tag{3.28}$$

where h is the length of an element and n is the position of the node.

3.3.1 Classical continuum

Using the lumped mass in Equation (3.26), the space discretised matrix form of Equation (3.9) for an element of length h is:

$$\frac{1}{2}\rho h \begin{bmatrix} 1 & 0 \\ 0 & 1 \end{bmatrix} \begin{bmatrix} a_n^t \\ a_{n+1}^t \end{bmatrix} = \frac{E}{h} \begin{bmatrix} 1 & -1 \\ -1 & 1 \end{bmatrix} \begin{bmatrix} u_n^t \\ u_{n+1}^t \end{bmatrix} \tag{3.29}$$

And the global matrix has the form as in Equation (3.30).

$$\frac{\rho h}{2}\begin{bmatrix} 1 & 0 & 0 & \cdots & 0 & 0 \\ & 2 & 0 & \cdots & 0 & 0 \\ & & 2 & \cdots & 0 & 0 \\ & & & \ddots & \vdots & \vdots \\ & \text{sym} & & & 2 & 0 \\ & & & & & 1 \end{bmatrix}\begin{bmatrix} a_1^t \\ a_2^t \\ a_3^t \\ \vdots \\ a_{n-1}^t \\ a_n^t \end{bmatrix} = \frac{E}{h}\begin{bmatrix} 1 & -1 & 0 & \cdots & 0 & 0 \\ & 2 & -1 & \cdots & 0 & 0 \\ & & 2 & \cdots & 0 & 0 \\ & & & \ddots & \vdots & \vdots \\ & \text{sym} & & & 2 & -1 \\ & & & & & 1 \end{bmatrix}\begin{bmatrix} u_1^t \\ u_2^t \\ u_3^t \\ \vdots \\ u_{n-1}^t \\ u_n^t \end{bmatrix}. \tag{3.30}$$

Consider the j^{th} equation of Equation (3.30), we have:

$$\rho h\left(a_j^t\right) = \frac{E}{h}\left(u_{j-1}^t - 2u_j^t + u_{j+1}^t\right). \tag{3.31}$$

Substituting the time integration scheme Equation (3.27) and space discretisation Equation 3.26 into the above equation:

$$\cos\left(\omega\Delta t\right) = \Delta t^2 \frac{E}{\rho h^2}\left(\cos\left(kh\right) - 1\right) + 1. \tag{3.32}$$

The graph for Equation (3.32) is shown in Figure 3.3[1] together with the discrete model and discretised continuum models.

3.3.2 Gradient continuum

Similarly, we have the matrix equation for an element:

$$\frac{\rho h}{2}\begin{bmatrix} 1 & 0 \\ 0 & 1 \end{bmatrix}\begin{bmatrix} a_n^t \\ a_{n+1}^t \end{bmatrix} + \frac{\rho l^2}{12h}\begin{bmatrix} 1 & -1 \\ -1 & 1 \end{bmatrix}\begin{bmatrix} a_n^t \\ a_{n+1}^t \end{bmatrix} = \frac{E}{h}\begin{bmatrix} 1 & -1 \\ -1 & 1 \end{bmatrix}\begin{bmatrix} u_n^t \\ u_{n+1}^t \end{bmatrix}, \tag{3.33}$$

[1] If we choose $\Delta t = \Delta t_{crit} = \frac{l}{c_e}$ where $c_e = \sqrt{\frac{E}{\rho}}$ is the wave velocity, $h = l$, the curve for ω will be a straight line.

and the global matrix has the form as in Equation (3.34):

$$\frac{\rho h}{2}\begin{bmatrix} 1 & 0 & 0 & \cdots & 0 & 0 \\ & 2 & 0 & \cdots & 0 & 0 \\ & & 2 & \cdots & 0 & 0 \\ & & & \ddots & \vdots & \vdots \\ & \text{sym} & & & 2 & 0 \\ & & & & & 1 \end{bmatrix}\begin{bmatrix} a_1^t \\ a_2^t \\ a_3^t \\ \vdots \\ a_{n-1}^t \\ a_n^t \end{bmatrix} + \frac{\rho l^2}{12h}\begin{bmatrix} 1 & -1 & 0 & \cdots & 0 & 0 \\ & 2 & -1 & \cdots & 0 & 0 \\ & & 2 & \cdots & 0 & 0 \\ & & & \ddots & \vdots & \vdots \\ & \text{sym} & & & 2 & -1 \\ & & & & & 1 \end{bmatrix}\begin{bmatrix} a_1^t \\ a_2^t \\ a_3^t \\ \vdots \\ a_{n-1}^t \\ a_n^t \end{bmatrix} = \frac{E}{h}\begin{bmatrix} 1 & -1 & 0 & \cdots & 0 & 0 \\ & 2 & -1 & \cdots & 0 & 0 \\ & & 2 & \cdots & 0 & 0 \\ & & & \ddots & \vdots & \vdots \\ & \text{sym} & & & 2 & -1 \\ & & & & & 1 \end{bmatrix}\begin{bmatrix} u_1^t \\ u_2^t \\ u_3^t \\ \vdots \\ u_{n-1}^t \\ u_n^t \end{bmatrix}. \tag{3.34}$$

Consider the j^{th} equation of the matrix in Equation (3.34)

$$\rho h a_j^t + \frac{1}{12}\rho\frac{l^2}{h}\left(-a_{j-1}^t + 2a_j^t - a_{j+1}^t\right) + \frac{E}{h}\left(-u_{j-1}^t + 2u_j^t - u_{j+1}^t\right) = 0. \tag{3.35}$$

Multiplying both sides of the equation with $12\frac{h}{l^2\rho}$ and replacing $\frac{E}{\rho}$ by ${c_e}^2$, we have after time and space discretisation:

$$\cos(\omega\Delta t) = \frac{24\frac{h^2}{l^2\Delta t^2} + \frac{4-4\cos(kh)}{\Delta t^2} + 12\frac{{c_e}^2}{l^2}(2\cos(kh)-2)}{24\frac{h^2}{l^2\Delta t^2} + \frac{-4\cos(kh)+4}{\Delta t^2}}. \tag{3.36}$$

If we choose the time step Δt equal to $\frac{l}{c_e}$, the value of the frequency can be determined by the following equation

$$\cos(\omega\Delta t) = \frac{24\frac{h^2}{l^2} - 20 + 20\cos(kh)}{24\frac{h^2}{l^2} - 4\cos(kh) + 4}. \tag{3.37}$$

The graph illustrating the relationships of ω against k for all three models (discrete, classical and discretised gradient continuum model) is plotted in Figure 3.3 where $h = l$.

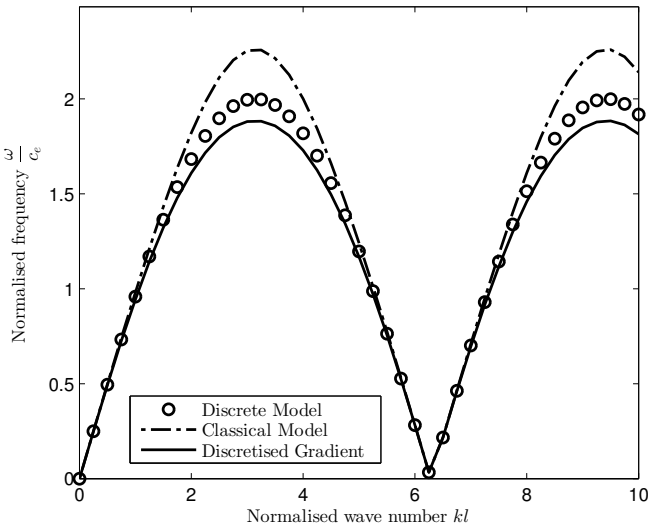

Fig. 3.3 Dispersion analysis of discretised continua in comparison with the discrete model of the one dimensional case

3.4 Discussion and conclusions on the one-dimensional case

Considering both the classical and the gradient continuum derived in Section 3.2, they are special cases of the equation of motion of Type I derived by Mindlin to introduce a general theory of elasticity with microstructure (Mindlin, 1964):

$$\rho\left(\ddot{u}_i - {b_1}^2\ddot{u}_{i,jj} - {b_2}^2\ddot{u}_{j,ij}\right) = (\lambda+\mu)\,u_{j,ij} + \mu u_{i,jj} - 2(a_1+a_2+a_5)u_{j,ijkk} - 2(a_3+a_4)u_{i,jjkk}. \tag{3.38}$$

In the above equation, the parameters a_i, $i = 1,2,3,4,5$ are related to strain gradients and the parameters b_i, $i = 1,2,3,4,5$ are related to inertia gradients; and, these parameters are dependent on material properties. Hence, the described continualisation procedure of the discrete model helps determine these material parameters for the continua.

Comparing the dispersive behaviours of the continua, the gradient curve proves to be more efficient to capture the peak frequency propagated in the one dimensional structure than the classical curve, see Figure 3.2.

For the discretised continua, because the relationships $\omega - k$ are cosine functions, see Equation (3.32) and (3.37), the curves repeat periodically along the increment of the wave number k, Figure 3.3. It is significant for the microstructural length l to be equal to numerical length h to obtain the most similar behaviour of the frequency ω (the curves meet the horizontal axis at the same position). At a time step close to the critical time step, the gradient continuum proves to be more accurate (the difference with the discrete model is smaller).

We set up a following simple numerical example depicted in Figure 3.4 to compare the new

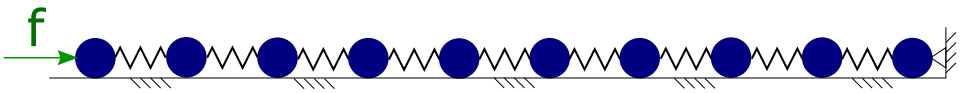

Fig. 3.4 A one dimensional numerical problem for finite element model implementation.

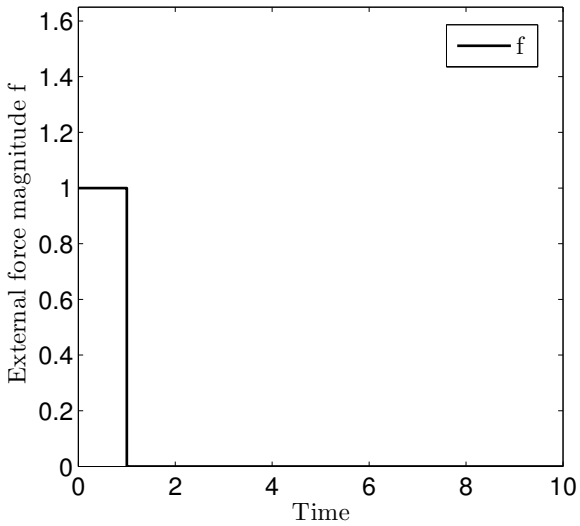

Fig. 3.5 Force of Heaviside function is depicted against time. The unit on the graph is for demonstration purpose only.

gradient continuum with the discrete model. The whole system is in one-dimensional space and the masses and springs can only display in the horizontal directions. A Heaviside force which is shown in Figure 3.5 with respect to time is applied to the left hand side end of the mass-spring chain and the right hand side end of the system is fixed. In this thesis, the popular explicit time integration method is used to model the dynamical behaviour of the system in Figure 3.4. There is a big disadvantage of the explicit scheme: it is conditionally stable when the simulation time step is less or equal the critical time step (Askes et al., 2011). If the time step is larger than the critical time step, which for the explicit scheme integration used in our numerical method is determined by the Courant condition (Bathe (2006)): $\Delta t_{crit} \leq \frac{2}{\omega_{\max}}$, the displacements of finite element model grows very large and unrealistic.

Finite element implementation of the gradient continuum displays a similar average maximum amplitude of the wave propagation with the discrete model. This is the displacement of the first node of a long string. The fluctuation of displacement of the gradient model in Figure 3.6 is because this time step is not the critical time step for this model.

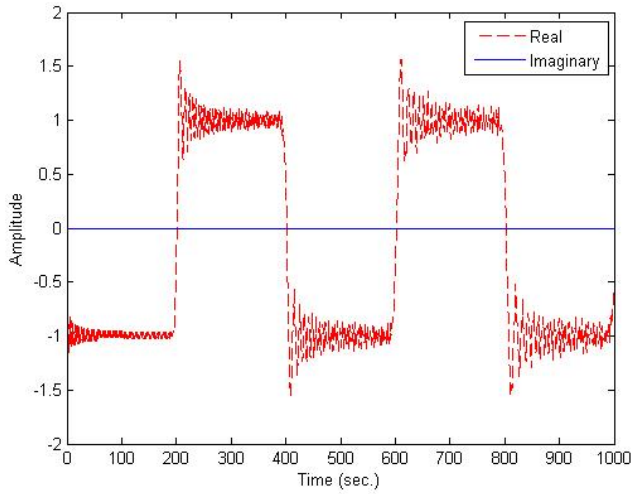

Fig. 3.6 Numerical behaviour of the 1D gradient model under Heaviside function.

Chapter 4

Wave propagation in the square lattice

The square lattice is considered to be the simplest two dimensional geometry in this study due to its symmetry in both principal axes. Before studying other more complicated geometries, this chapter investigates the square lattice in the following order: the discrete model in Section 4.1, classical and gradient models in Section 4.2, space and time discretised models in Section 4.3 and numerical examples in Section 4.4.

4.1 Discrete model of the square lattice

In this section, the square lattice is first introduced in the discrete form and dispersion analysis corresponding to the defined model is presented.

4.1.1 Definition of the square lattice

The two dimensional square lattice is depicted in Figure 4.1 where beams of equal lengths are connected to each other at a 90° angle. The representative volume element (RVE) is presented as the part of the micro-lattice surrounded by the dashed red square in Figure 4.1. However, the beam cannot be shortened by half to fit into the RVE because the shorter the beam is, the smaller wavelength the beam would allow to travel through itself. Hence, the full beam length l is used to model the equilibrium forces and moment about the red point and then divide these forces by the area of the representative element as in Figure 4.1. In Figure 4.1, the node, marked in red, is used as the central point for continualisation by Taylor series.

- For the square geometry, see Figure 4.1, the representative volume element (RVE) only requires a single joint to ensure the symmetry for simple mathematical formulations. This RVE of the microlattice is modelled as a rigid-joint network of four uniform beams having cross section A, length l, material density ρ and Young's modulus E.

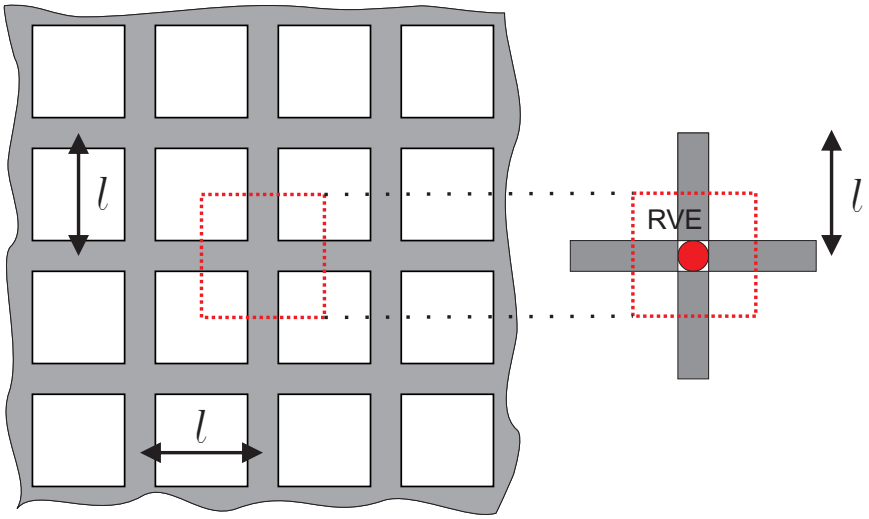

Fig. 4.1 The 2D square microlattice with the definition of a representative volume element in a red dashed square with the length scale l and the details of the RVE square lattice

- Different beam theories can be used to model each individual beam, such as Euler-Bernoulli, Timoshenko, Rayleigh beam theories, etc. In this study, the microlattices have slender beams where β is the depth over length ratio, $\beta \leq \frac{1}{10}$ and the Euler-Bernoulli beam theory is used to model the behaviour of the discrete microbeams. It is acknowledged that Euler-Bernoulli beam theory exhibits anomalous behaviour in dynamics; however, these undesirable effects can be shown not to affect the subsequent derivations shown below. In the main body of the thesis, only results from Euler-Bernoulli beam theory are presented (Equation (4.2)), the results by Timoshenko beam theory are displayed in Appendix B.1.

- Similarly, different mass matrices can be used to model each individual beam, such as lumped mass (Equation (4.1)) or consistent mass matrices. In the main body of the thesis, only results from a lumped mass scheme are presented; the results from consistent mass matrices are displayed in Appendix B.1.

- For simplicity, the mass matrix of the beam element is lumped as in Equation (4.1). The beam stiffness matrix used is the common two-dimensional stiffness matrix of Euler-Bernoulli beam theory in Equation (4.2): Next, the global matrix is built for the RVE system.

$$\mathbf{M}^{(e)} = \frac{\rho A l}{2} diag\left(1, 1, \frac{\delta}{12l^2}, 1, 1, \frac{\delta}{12l^2}\right), \tag{4.1}$$

where δ is a constant which usually takes the value of 1.

$$\mathbf{K}^{(e)} = \begin{bmatrix} A & 0 & 0 & -A & 0 & 0 \\ & \frac{12I_z}{L^2} & \frac{6I_z}{L} & 0 & -\frac{12I_z}{L^2} & \frac{6I_z}{L} \\ & & 4I_z & 0 & \frac{6I_z}{L} & 2I_z \\ & & & A & 0 & 0 \\ & \text{sym} & & & \frac{12I_z}{L^2} & -\frac{6I_z}{L} \\ & & & & & 4I_z \end{bmatrix}, \tag{4.2}$$

where $I_z = \frac{d^4}{12}$ and d is the beam depth.

4.1.2 Dispersion analysis of the discrete model

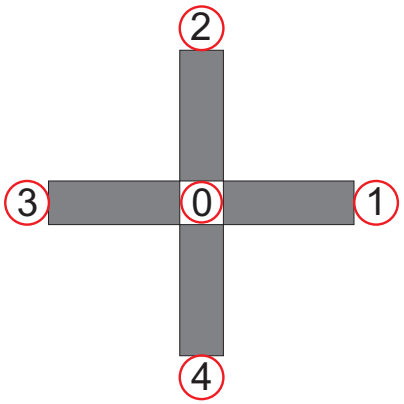

Fig. 4.2 Finite element analysis on the discrete model. Node numbering of the discrete system containing the RVE unit.

As explained in Section 4.1.1, the system of four beams on the right side of Figure 4.1 are chosen to carry out the dispersion analysis. The five nodes are numbered anti-clockwise as in Figure 4.2 and have coordinates $(0,0)$, $(1,0)$, $(0,1)$, $(-1,0)$ and $(0,-1)$. In this section, u_n and v_n describes the horizontal and vertical displacements of node number n; θ_n stands for the rotation, a_n, b_n and c_n for horizontal, vertical and rotational accelerations. With the mass matrices M and stiffness matrices K defined in Equations (4.1) and (4.2) for each beam of length l, the term $M\overline{a} + K\overline{u}$ can be written where $\overline{a}$ and $\overline{u}$ are the column vectors for displacement and acceleration for each beam. Because node number 0 is fully surrounded by four beams, we can assume external forces and moment equilibrium about node 0 and write the following three equations of motion:

$$\frac{E\beta^2}{l}\left(\beta^2\left(2u_0-u_2-u_4-\frac{1}{2}l\theta_2+\frac{1}{2}l\theta_4\right)+(2u_0-u_1-u_3)\right)+2\rho\beta^2 la_0=0 \tag{4.3}$$

$$\frac{E\beta^2}{l}\left(\beta^2\left(2v_0-v_1-v_3-\frac{1}{2}l\theta_3+\frac{1}{2}l\theta_1\right)+(2v_0-v_2-v_4)\right)+2\rho\beta^2 lb_0=0 \tag{4.4}$$

$$\frac{E\beta^4}{l^2}\left(l^2\left(\frac{4\theta_0}{3}+\frac{\theta_1}{6}+\frac{\theta_2}{6}+\frac{\theta_3}{6}+\frac{\theta_4}{6}\right)+\frac{l}{2}(u_2-u_4+v_3-v_1)\right)+\frac{1}{6}\rho\beta^2 l^3 c_0=0. \tag{4.5}$$

The first two Equations (4.3) and (4.4) represent the forces acting on point 0 in the x and y directions, while Equation (4.5) stands for the moment about point 0. The number of equations of motion required to carried out the dispersion analysis is equal to the number of degrees of freedom of all the nodes inside the representative volume element. However, the system might not be stable and some manipulations are required to modify the system.

Comparing the first two Equations (4.3) and (4.4), the variables u and v are interchangeable; that means when a force acting on point 0 at an angle of 45°, the horizontal and vertical displacement u and v will have the same value, or it can be said that the system is symmetrical through the line at 45° to the horizontal. Within the two-dimensional cases, this property is attributed only to the square lattice and should be maintained after the discrete model is continualised. Hence, this property is used later to evaluate the continuum model. On the other hand, if the force acts on point 0 at an angle of 0° to the horizontal line, it is easier for the structure to propagate the force in the horizontal direction than the perpendicular direction to the force; hence, a larger portion of the wave travels in the horizontal direction (compression wave) and components having lower energy (which normally have higher frequencies) struggle to propagate through the vertical direction. This results in the compression wave having a much higher frequency magnitude than the shear wave at this angle (0° to the horizontal line).

After obtaining the three equations of motion, dispersion analysis can be carried out by replacing the displacements by the harmonic plane wave equation with respect to the coordinates (x,y) of the nodes:

$$\begin{aligned} u_n &= U\exp\left[i\left(k\cos\gamma x_n + k\sin\gamma y_n - \omega t\right)\right] \\ v_n &= V\exp\left[i\left(k\cos\gamma x_n + k\sin\gamma y_n - \omega t\right)\right] \\ \theta_n &= W\exp\left[i\left(k\cos\gamma x_n + k\sin\gamma y_n - \omega t\right)\right]. \end{aligned} \tag{4.6}$$

After these substitutions, the three equation of motions (Equations (4.3), (4.4) and (4.5)) transform into:

$$\frac{E}{l}\left(\begin{array}{l}\beta^2\left(\begin{array}{l}2Ue^{i(-\omega t)}-Ue^{i(k\sin\gamma-\omega t)}-Ue^{i(-k\sin\gamma-\omega t)}\\-\frac{1}{2}lWe^{i(k\sin\gamma-\omega t)}+\frac{1}{2}lWe^{i(-k\sin\gamma-\omega t)}\end{array}\right)\\+\left(2Ue^{i(-\omega t)}-Ue^{i(k\cos\gamma-\omega t)}-Ue^{i(-k\cos\gamma-\omega t)}\right)\end{array}\right)-i2\rho l\omega Ue^{i(-\omega t)}=0 \quad (4.7)$$

$$\frac{E}{l}\left(\begin{array}{l}\beta^2\left(\begin{array}{l}2Ve^{i(-\omega t)}-Ve^{i(k\cos\gamma-\omega t)}-Ve^{i(-k\cos\gamma-\omega t)}\\-\frac{1}{2}lWe^{i(-k\cos\gamma-\omega t)}+\frac{1}{2}lWe^{i(k\cos\gamma-\omega t)}\end{array}\right)\\+\left(2Ve^{i(-\omega t)}-Ve^{i(k\sin\gamma-\omega t)}-Ve^{i(-k\sin\gamma-\omega t)}\right)\end{array}\right)-i2\rho l\omega Ve^{i(-\omega t)}=0 \quad (4.8)$$

$$\frac{E\beta^2}{l^2}\left(\begin{array}{l}l^2\left(\begin{array}{l}\frac{4We^{i(-\omega t)}}{3}+\frac{We^{i(k\cos\gamma-\omega t)}}{6}+\frac{We^{i(k\sin\gamma-\omega t)}}{6}\\+\frac{We^{i(-k\cos\gamma-\omega t)}}{6}+\frac{We^{i(-k\sin\gamma-\omega t)}}{6}\end{array}\right)\\+\frac{l}{2}\left(\begin{array}{l}Ue^{i(k\sin\gamma-\omega t)}-Ue^{i(-k\sin\gamma-\omega t)}\\+Ve^{i(-k\cos\gamma-\omega t)}-Ve^{i(k\cos\gamma-\omega t)}\end{array}\right)\end{array}\right)-\frac{1}{6}i\rho l^3\omega We^{i(-\omega t)}=0. \quad (4.9)$$

The system is then solved as an eigen-value problem where the variables are $[U,V,W]$; if E, l, ρ, β are predefined, the determinant of the system is a function of $[\omega,k,\gamma]$. For non-trivial solutions of the system comprised of the above three equations, the determinant has to be zero. For each pair of $[k,\gamma]$, there are three corresponding values of ω and all these values are real for the discrete model of the square lattice.

Note: To simplify the system, the normalised frequency is defined as $\frac{\omega l}{c_e}$ where $c_e=\sqrt{\frac{E}{\rho}}$ and normalised wave number as kl.

The results of this section will be compared with other models in Section 4.2, in particular Figure 4.4 for the propagation angle $\gamma=\frac{\pi}{2}$.

4.2 Generalised model of the square lattice

The process in this section is similar to the method found in (Lombardo and Askes (2012)), however, with a more general input of the discrete model where the rotational variable is taken into account.

As mentioned in Section 4.1.1, different mass schemes and different beam theories can be deployed when constructing the discrete model. However, these different inputs only result in different coefficients but do not produce extra terms. The main body of the thesis concentrates

on the combination of the lumped mass and the Euler-Bernoulli beam theories. The other combination with consistent mass and Timoshenko beam theory are explored in Appendix B.1. The equations of motion after continualisation using lumped mass scheme and Euler-beam theory, see Section 4.1.1, are:

$$2\rho\ddot{u} = E\left(u_{,xx} + \beta^2 u_{,yy} + \beta^2\theta_{,y}\right) + \frac{El^2}{12}\left(u_{,xxxx} + \beta^2 u_{,yyyy} + 2\beta^2\theta_{,yyy}\right) \tag{4.10}$$

$$2\rho\ddot{v} = E\left(v_{,yy} + \beta^2 v_{,xx} - \beta^2\theta_{,x}\right) + \frac{El^2}{12}\left(v_{,yyyy} + \beta^2 v_{,xxxx} - 2\beta^2\theta_{,xxx}\right) \tag{4.11}$$

$$\frac{\delta}{6E\beta^2}\rho l^2\ddot{\theta} + 2\theta = v_{,x} - u_{,y} - \frac{l^2}{6}\left(\theta_{,xx} + \theta_{,yy} - v_{,xxx} + u_{,yyy}\right). \tag{4.12}$$

Consider the three equations (4.10), (4.11) and (4.12):

- If we keep the derivatives up to second order and omit the rotational degree of freedom, we have equations of classical elasticity theory.
- If we keep the derivatives up to second order, we have equations of micropolar elasticity or Cosserat theory (Pavlov et al., 2006; Vasiliev et al., 2002, 2010). The basis and developments of micropolar elasticity can be found in Eringen (1966); Eringen and Kafadar (1976); Mindlin and Tiersten (1962); Nowacki (1970). The microrotational degrees of freedom are often called Cosserat rotations giving tribute to the brothers Cosserat and Cosserat (1909) who were the first to propose the theory.
- If we keep the derivatives up to fourth order, we have equations which mimic micromorphic elasticity (Eringen, 1967; Eringen and Kafadar, 1976) or the Mindlin continuum (Mindlin, 1964).

Dispersion analysis for these equations uses the following plane wave relationships (similar to the set of Equation (12) of Suiker et al. (2001) to obtain an eigen-value problem:

$$\begin{aligned} u(x,y,t) &= U\exp\left[i\left(k\cos\gamma x + k\sin\gamma y - \omega t\right)\right] \\ v(x,y,t) &= V\exp\left[i\left(k\cos\gamma x + k\sin\gamma y - \omega t\right)\right] \\ \theta(x,y,t) &= W\exp\left[i\left(k\cos\gamma x + k\sin\gamma y - \omega t\right)\right]. \end{aligned} \tag{4.13}$$

The determinant of the Eigen problem containing the frequency is a cubic function, which has three distinctive real roots. However, these three roots are not positive with all wave numbers, or it can be said that this system is unconditionally stable. The route to stabilise

this continuum is thought to be more difficult with three variables; hence, in this study, the rotational variable θ is translated into other variables and thus can be eliminated from the equations of motion to enable simpler stabilisation steps.

4.2.1 Reduced degree-of-freedom continuum

To simplify the problem and to eliminate A_{ijk}, firstly, the rotational degree of freedom θ is rewritten in terms of u and v. The paper by Lombardo and Askes (2012), with a different set of equations of motion, uses all three equations of motions to extract θ. In this thesis, we only use Equation (4.12) to approximate θ. A detailed derivation is displayed in Appendix B.2:

$$\theta = \frac{\rho l^2}{24E\beta^2}\left(\ddot{u}_{,y} - \ddot{v}_{,x}\right) + \frac{1}{2}\left(v_{,x} - u_{,y}\right) - \frac{l^2}{12}\left(-v_{,xxx} + v_{,xyy} + u_{,yyy} - u_{,xxy}\right). \tag{4.14}$$

Substituting this result into the Equations (4.10) and (4.11), we have new equations of motion:

$$2\rho\ddot{u} + \frac{\rho l^2}{24}\left(\ddot{v}_{,xy} - \ddot{u}_{,yy}\right) = E\left(u_{,xx} + \frac{\beta^2}{2}u_{,yy} + \frac{\beta^2}{2}v_{,xy}\right) + \frac{E\beta^2 l^2}{12}\left(u_{,xxyy} - u_{,yyyy} + \frac{u_{,xxxx}}{\beta^2} + v_{,xxxy}\right). \tag{4.15}$$

$$2\rho\ddot{v} + \frac{\rho l^2}{24}\left(\ddot{u}_{,xy} - \ddot{v}_{,xx}\right) = E\left(v_{,yy} + \frac{\beta^2}{2}v_{,xx} + \frac{\beta^2}{2}u_{,xy}\right) + \frac{E\beta^2 l^2}{12}\left(v_{,xxyy} - v_{,xxxx} + \frac{v_{,yyyy}}{\beta^2} + u_{,xyyy}\right). \tag{4.16}$$

The two new equations of motion produce unstable dispersion relationships when substituting the terms with Equations 4.13, see Figure 4.3. Therefore, a further step is required to stabilise the system using the Padé approximation. These two new equations are classified as the gradient-enhanced continuum.

4.2.2 Classical continuum

Similar to the one-dimensional case, the equations of motion for the classical continuum contains all the second order derivative terms in Equation (4.15) and (4.16):

$$2\rho\ddot{u} = E\left(u_{,xx} + \frac{\beta^2}{2}u_{,yy} + \frac{\beta^2}{2}v_{,xy}\right) \tag{4.17}$$

$$2\rho\ddot{v} = E\left(v_{,yy} + \frac{\beta^2}{2}v_{,xx} + \frac{\beta^2}{2}u_{,xy}\right). \tag{4.18}$$

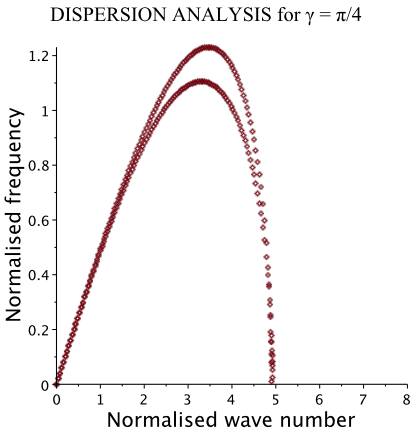

Fig. 4.3 Dispersion analysis for the unstable continuum of Equations (4.15) and (4.16). The lower curve presents the shear wave component and the higher curve presents the compression wave component. The normalised wave number is kl and the normalised frequency is $\frac{\omega l}{c_e}$.

Again, Equations 4.13 are used for dispersion analysis of these two new equations.

Figure 4.4 compares the dispersion behaviour of a classical continuum represented by Equations (4.17) and (4.18) with the dispersion behaviour of other models.

4.2.3 Stabilised gradient continuum

The Padé approximation is mainly used during the stabilisation step. If we denote Equation (4.15) as $\mathscr{R}$ and Equation (4.16) as $\mathscr{Z}$, we shall calculate (ignoring all terms $(\mathrm{O})\,(l^4)$):

$$\mathscr{R} + a\mathscr{R}_{,xx} + b\mathscr{R}_{,yy} + c\mathscr{Z}_{,xy} \tag{4.19}$$

$$\mathscr{Z} + d\mathscr{Z}_{,xx} + e\mathscr{Z}_{,yy} + c\mathscr{R}_{,xy}, \tag{4.20}$$

where a, b, c, d and e are the multipliers that are determined later so that the new expressions (4.19) and (4.20) shall be stable in the dispersion analysis. For the square lattice, the x and y directions are interchangeable, which leads to $a = d$ and $b = e$. This arrangement is intended to introduce variable coefficients of the terms that we need to eliminate. Other additions such as $f\mathscr{R}_{,xy}$ to Equation (4.19) are not included because they bring in even more unstable terms into the system. If we choose $a = e = -\frac{1}{12}$, $b = d = -\frac{1}{24}$ and $c = 0$, we have the following

equations:

$$2\rho\ddot{u}+\frac{\rho l^2}{24}\left(\ddot{v}_{,xy}-3\ddot{u}_{,yy}-4\ddot{u}_{,xx}\right)=E\left(u_{,xx}+\frac{\beta^2}{2}u_{,yy}+\frac{\beta^2}{2}v_{,xy}\right)+ \\ +\frac{El^2}{48}\left(-5\beta^2u_{,yyyy}+\left(2\beta^2-2\right)u_{,xxyy}+2\beta^2v_{,xxxy}-\beta^2v_{,xyyy}\right) \tag{4.21}$$

$$2\rho\ddot{v}+\frac{\rho l^2}{24}\left(\ddot{u}_{,xy}-3\ddot{v}_{,xx}-4\ddot{v}_{,yy}\right)=E\left(v_{,yy}+\frac{\beta^2}{2}v_{,xx}+\frac{\beta^2}{2}u_{,xy}\right)+ \\ +\frac{El^2}{48}\left(-5\beta^2v_{,xxxx}+\left(2\beta^2-2\right)v_{,xxyy}+2\beta^2u_{,xyyy}-\beta^2u_{,xxxy}\right). \tag{4.22}$$

Further considerations are taken to simplify the two Equations (4.21) and (4.22):

- For the terms of the forms $\mathscr{X}_{,iijj}$ where $i,j=x,y$: After differentiation, their coefficients have $\left(1-\beta^2\right)l^2$ (the largest numerical coefficient of all the fourth order spatial derivatives) and $\cos^2\gamma\sin^2\gamma$ which has an absolute maximum value of 0.25 when $\gamma=\pi/4$
- For the terms of the forms $\mathscr{X}_{,iiij}$ where $i,j=x,y$: After differentiation, their coefficients have β^2l^2 and $\cos^3\gamma\sin\gamma$ or $\sin^3\gamma\cos\gamma$. These two trigonometry terms have an absolute maximum value of 0.325 when $\gamma=0.5236$ and $\gamma=1.0472$.
- For the terms of the forms $\mathscr{X}_{,iiii}$ where $i=x,y$: After differentiation, their coefficients have β^2l^2 and $\cos^4\gamma$ or $\sin^4\gamma$. These two trigonometry terms have an absolute maximum value of 1 when $\gamma=0,\pi/2$.
- When performing stability analysis of the Equations (4.21) and (4.22) at the above critical values of γ , comparing with the discrete model, it was found that:
  - Terms $\mathscr{X}_{,iiij}$ have insignificant effects on the magnitude of frequencies.
  - For the frequency magnitude the compression wave is hardly affected by other terms other than $\mathscr{X}_{,iiii}$;
  - Meanwhile, the frequency magnitude of the shear wave, if including the terms $\mathscr{X}_{,iiii}$, is overestimated as the wave number increases.

From these observation, it is reasonable and acceptable to ignore the terms $\mathscr{X}_{,ijjj}$ and $\mathscr{X}_{,iiij}$ in Equation (4.21) and (4.22):

$$2\rho\ddot{u}+\frac{\rho l^2}{24}\left(\ddot{v}_{,xy}-3\ddot{u}_{,yy}-4\ddot{u}_{,xx}\right)=E\left(u_{,xx}+\frac{\beta^2}{2}u_{,yy}+\frac{\beta^2}{2}v_{,xy}\right)+ \\ \frac{El^2}{48}\left(\left(2\beta^2-2\right)u_{,xxyy}\right) \tag{4.23}$$

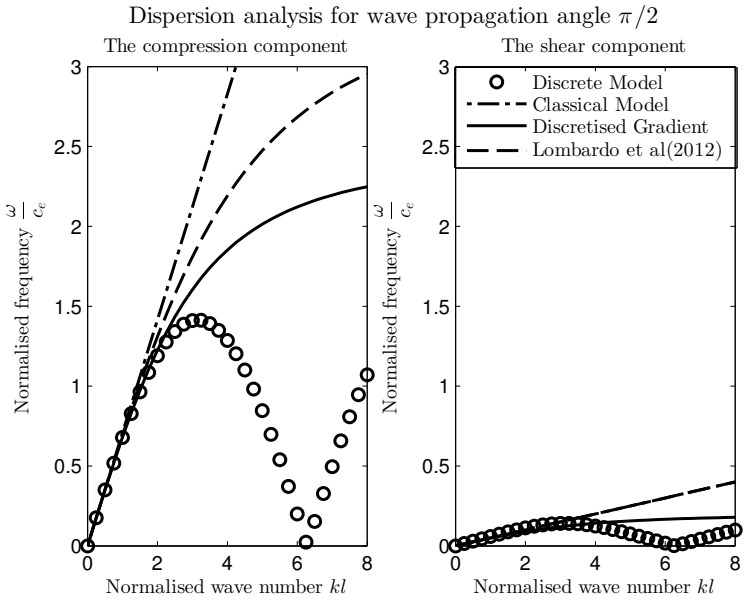

Fig. 4.4 Dispersion analysis for the stabilised continuum in comparison with discrete model, classical continuum and Lombardo's continuum

$$2\rho\ddot{v}+\frac{\rho l^2}{24}\left(\ddot{u}_{,xy}-3\ddot{v}_{,xx}-4\ddot{v}_{,yy}\right)=E\left(v_{,yy}+\frac{\beta^2}{2}v_{,xx}+\frac{\beta^2}{2}u_{,xy}\right)+ \\ +\frac{El^2}{48}\left(\left(2\beta^2-2\right)v_{,xxyy}\right), \tag{4.24}$$

which provide the dispersion graph Figure 4.4.

The new continuum has a closer match to the discrete model, displaying a better wave filter property compared to the other two continua, especially the classical continuum. It should be noted that the discrete model is discretised in space; hence, its curves periodically meet the horizontal axis. If we discretise the new continuum in space, we would also be able to have its curves periodically meet the horizontal axis.

All the terms in Equations (4.23) and (4.24) are able to be discretised with only C^0 continuity. Therefore, we can go straight to the FEM implementation step without using the Ru-Aifantis theorem as in the trapezium case. Note that there are many ways to stabilise a system. The system achieved above is only one of many possible stabilised continuum. We choose this particular route because the final continuum is simple to use.

4.3 Space and time discretisation for continua

As comparisons of the dispersion relations are made between discrete model with continuum models, it is important to note that, different from the continuum, the discrete model is discretised in space. Therefore, for better comparisons, the continuum are discretised first in space and then in time. Section 4.3.1 explains the choice of discretisation scheme. The next section reviews the discretisation procedure with dispersion analysis graphs. Finally, numerical examples are built in the final section to demonstrate the practical application of the continuum.

4.3.1 Discretisation schemes

For space discretisation and time discretisation, to get the best match with the discrete model as seen in the one-dimensional case Section 3.4, the size of numerical discretised element size shall be equal to the structural lengthscale. After discretisation, the dispersion curves have the form of the arccos (or $\cos^{-1}$) function with respect to the wave number k. This is in agreement with the 1D case.

It is well-known that the explicit scheme often overestimates while the implicit scheme underestimates the numerical solutions, and lumped mass underestimates while consistent mass overestimates the solutions. Therefore, when modelling, two common combinations are the explicit scheme together with the lumped mass and the implicit scheme together with the consistent mass. We shall use explicit scheme and the lumped mass to discretise the new continuum in this research.

4.3.2 Shape functions and element matrices and central difference scheme

As mentioned before, Equations (4.23) and (4.24) only require C^0 continuity for finite element implementation even with the fourth order spatial derivatives $\mathscr{X}_{,iijj}$. There are many ways to stabilise the system; and if there are terms $\mathscr{X}_{,iiii}$ existing, we can use Ru-Aifantis theorem to reduce the continuity requirement to C^0.

To spatially discretise the continuum, we use the trial functions:$u \approx \mathbf{Nu}$ and $v \approx \mathbf{Nv}$ where $\mathbf{N}$ contains the linear shape functions. Equations (4.23) and (4.24) are discretised in the matrix form, Ω is the element volume, ρ is the material density, E is the Young's modulus, l is the structural lengthscale:

$$\begin{bmatrix} \mathbf{M}_{uu} & \mathbf{M}_{uv} \\ \mathbf{M}_{uv} & \mathbf{M}_{vv} \end{bmatrix} \begin{bmatrix} \ddot{\mathbf{u}} \\ \ddot{\mathbf{v}} \end{bmatrix} + \begin{bmatrix} \mathbf{K}_{uu} & \mathbf{K}_{uv} \\ \mathbf{K}_{uv} & \mathbf{K}_{vv} \end{bmatrix} \begin{bmatrix} \mathbf{u} \\ \mathbf{v} \end{bmatrix} = \begin{bmatrix} f_u \\ f_v \end{bmatrix}, \tag{4.25}$$

where

$$\mathbf{M}_{uu} = \int_{\Omega} \mathbf{N}^T 2\rho \mathbf{N} dV + \int_{\Omega} \mathbf{N}_{,y}^T \frac{1}{8} \rho l^2 \mathbf{N}_{,y} dV + \int_{\Omega} \mathbf{N}_{,x}^T \frac{1}{6} \rho l^2 \mathbf{N}_{,x} dV \tag{4.26}$$

$$\mathbf{M}_{vv} = \int_{\Omega} \mathbf{N}^T 2\rho \mathbf{N} dV + \int_{\Omega} \mathbf{N}_{,x}^T \frac{1}{8} \rho l^2 \mathbf{N}_{,x} dV + \int_{\Omega} \mathbf{N}_{,y}^T \frac{1}{6} \rho l^2 \mathbf{N}_{,y} dV \tag{4.27}$$

$$\mathbf{M}_{uv} = -\int_{\Omega} \mathbf{N}_{,y}^T \frac{1}{24} \rho l^2 \mathbf{N}_{,x} dV \tag{4.28}$$

$$\mathbf{K}_{uu} = \int_{\Omega} \mathbf{N}_{,x}^T E \mathbf{N}_{,x} dV + \int_{\Omega} \mathbf{N}_{,y}^T \frac{\beta^2}{2} E \mathbf{N}_{,y} dV - \int_{\Omega} \mathbf{N}_{,xy}^T \frac{\left(\beta^2 - 1\right) E l^2}{24} \mathbf{N}_{,xy} dV \tag{4.29}$$

$$\mathbf{K}_{vv} = \int_{\Omega} \mathbf{N}_{,y}^T E \mathbf{N}_{,y} dV + \int_{\Omega} \mathbf{N}_{,x}^T \frac{\beta^2}{2} E \mathbf{N}_{,x} dV - \int_{\Omega} \mathbf{N}_{,xy}^T \frac{\left(\beta^2 - 1\right) E l^2}{24} \mathbf{N}_{,xy} dV \tag{4.30}$$

$$\mathbf{K}_{uv} = \int_{\Omega} \mathbf{N}_{,x}^T \frac{\beta^2}{2} E \mathbf{N}_{,y} dV. \tag{4.31}$$

Note that the matrix system in Equation (4.25) is symmetric through the diagonal which is a sign that the system has no energy losses. Next, the common explicit time scheme based on central differences Hughes (2000), is applied:

$$\begin{aligned} \ddot{u}_n^t \Delta t^2 &= u_n^{t-\Delta t} - 2u_n^t + u_n^{t+\Delta t} \\ \ddot{v}_n^t \Delta t^2 &= v_n^{t-\Delta t} - 2v_n^t + v_n^{t+\Delta t}, \end{aligned} \tag{4.32}$$

where $u_n^t(x_n, y_n, t) = U \exp\left[i\left(k_x x_n + k_y y_n - \omega t\right)\right]$ and $v_n^t(x_n, y_n, t) = V \exp\left[i\left(k_x x_n + k_y y_n - \omega t\right)\right]$.

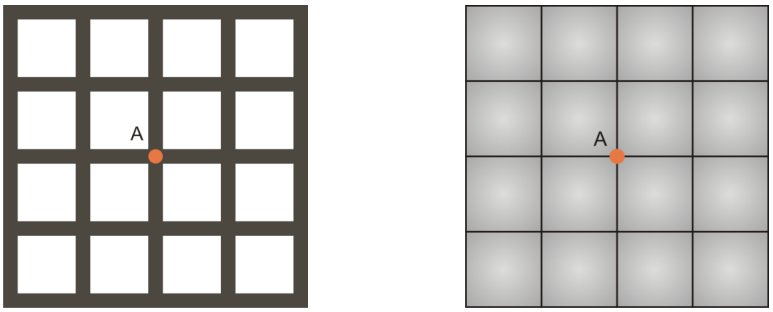

(a) The discrete model (b) The continuum model

Fig. 4.5 The location of the orange middle point A in the discrete model and the corresponding continuum model

If we consider the dispersion analysis of a point A in Figure 4.5 for the new continuum which is discretised in space and time, we can write the two equilibrium equations for the horizontal and vertical directions, we can achieve Table 4.1 to compare with the discrete model.

The discrete model has three frequencies corresponding to three degrees of freedom: compression, shear and rotation frequencies.

4.4 Numerical example

The problem is set up as in Figure 4.6. A 2D beam with an underlying square microlattice is set up as in Figure 4.6a and the similar arrangement in the discretised continuum form is depicted in Figure 4.6b. The discretised element length of the continuum model is equal to the microstructural lengthscale l. The discrete and continuum models are tested against each other. The shape of the discrete model and the continuum model are all chosen such that the continuum model would be able to simulate similar boundary conditions to those of the discrete model. Forces of the Heaviside function over time, see Figure 3.5, are applied to the left end of the structures. The right-hand side of each structure is fixed. The vertical degrees of freedom of all nodes are fixed. Therefore, the problem is predicted to behave as the one-dimensional case, see Figure 3.6.

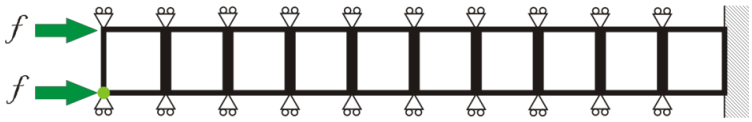

(a) The discrete model

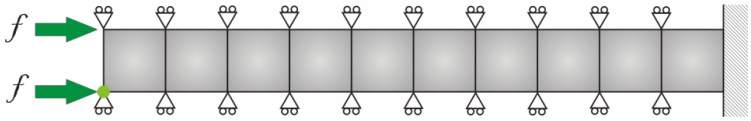

(b) The continuum model

Fig. 4.6 Depiction of numerical problems for the square lattice

With the problem defined as earlier, the models are input into a Matlab program to observe the displacement of the green points in Figure 4.6 over time. Figure 4.7 compares the performances of the discrete model in Figure 4.7a and the continuum model in Figure 4.7b. It is easy to see that during the first period (initial 30 seconds) when the wave first time travels from the left hand side to the fixed right hand end of the structure, the amplitudes and the time of both models are similar.

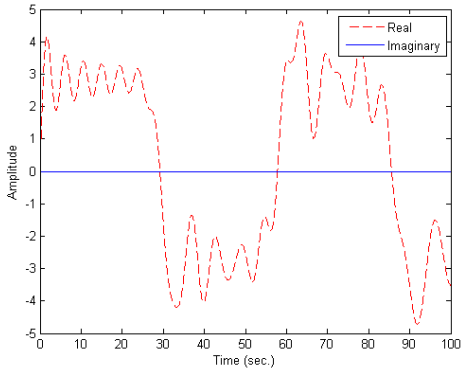

(a) The discrete model

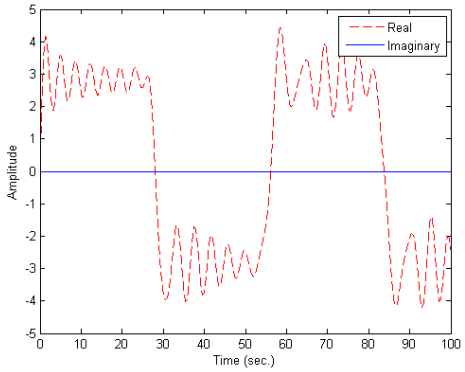

(b) The gradient continuum model

Fig. 4.7 Numerical results for the square lattice - The displacement of the light green point in Figure 4.6b and Figure 4.6a, respectively, over time; the time step is 0.02

Stage	**Classical model**	**Gradient model**
Continuum model	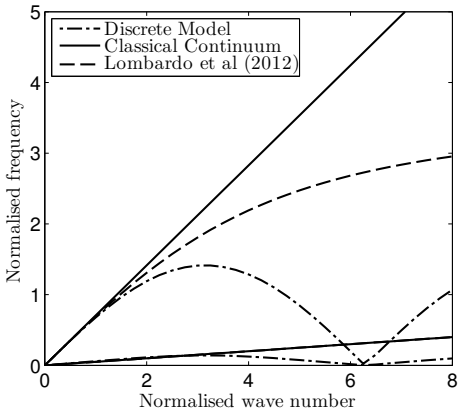	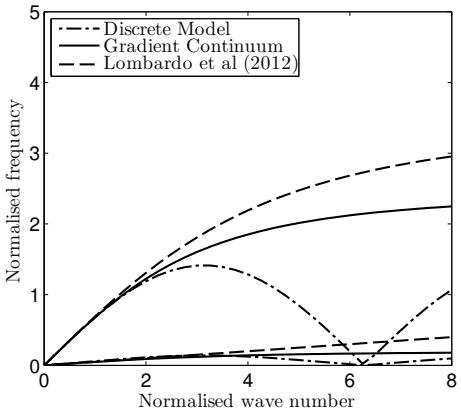
Discretised model in *space*	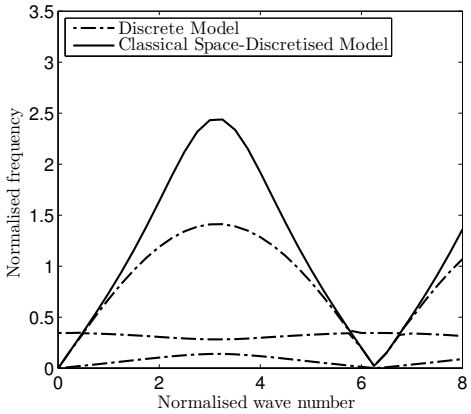	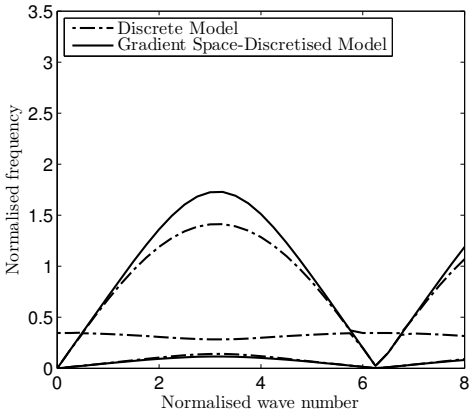
Discretised model in *space and time*	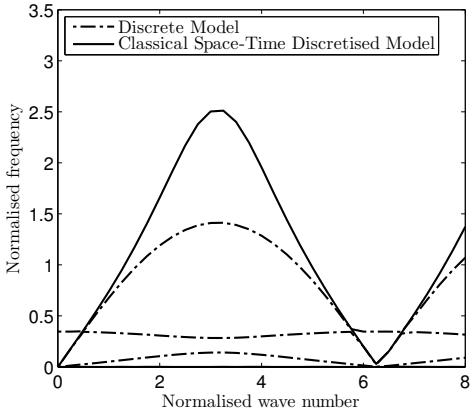	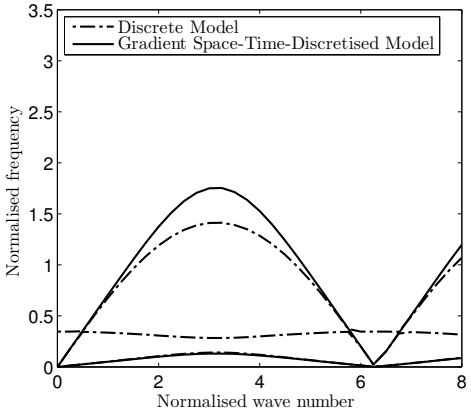

Table 4.1 Square lattice - Comparison of the dispersion behaviour of the classical and gradient model under different stages for $\gamma = \pi/2$. The normalised wave number is kl and the normalised frequency is $\dfrac{\omega}{c_e}$. Every model has two curves which are depicted by the same type line, for e.g. the in the Stage Continuum model, the classical model column, the discrete model has two dash-dot curves, the lower curve represents the shear component and the higher curve represents the compression component. The same is applied for other models.

Stage	Classical model	Gradient model
Continuum model	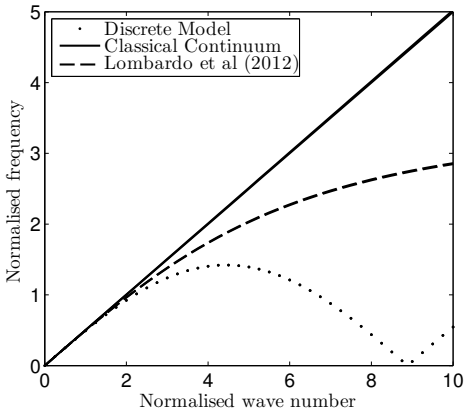	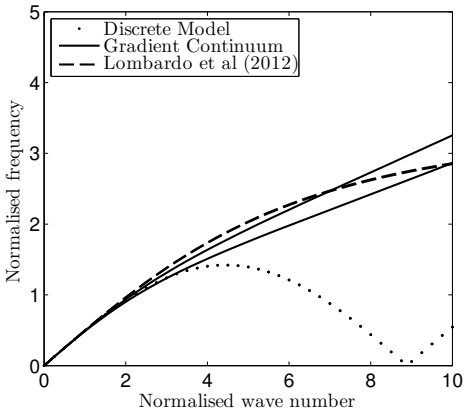
Discretised model in *space*	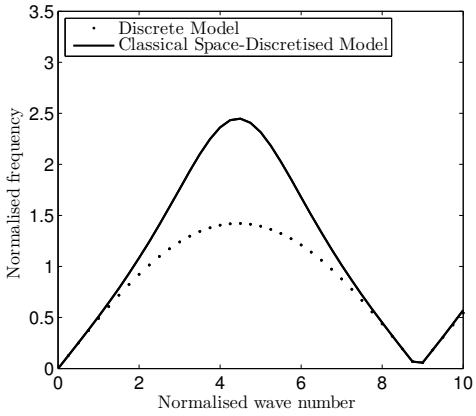	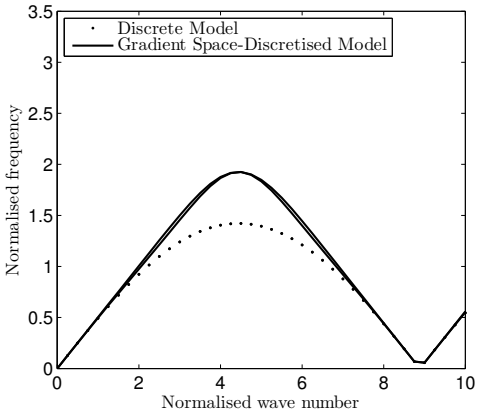
Discretised model in *space and time*	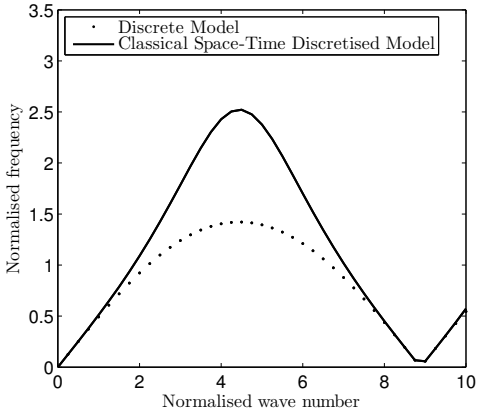	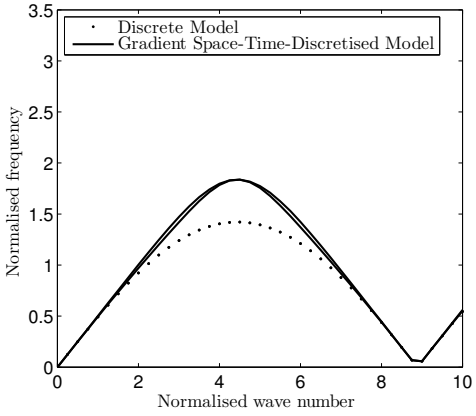

Table 4.2 Square lattice - Comparison of the dispersion behaviour of the classical and gradient model under different stages for $\gamma = \pi/4$. The normalised wave number is kl and the normalised frequency is $\dfrac{\omega}{c_e}$.

Chapter 5

Wave propagation in the trapezium lattice

The trapezium lattice has a more complicated geometry than the square lattice. It can be said that the trapezium lattice is a more general case than the square lattice or that the square one is a special case of the trapezium one. This chapter explores different models to simulate wave propagation in trapezium lattices. The arrangement of this chapter is very similar to the previous Chapter 4 with the following order: the discrete model in Section 5.1, classical and gradient models in Section 5.2, space and time discretised models in Section 5.3 and numerical examples in Section 5.4. However, because of the trapezium geometry which leads to mathematical complications that cannot be ignored, Section 5.2 also treat the Ru-Aifantis theorem in detail.

5.1 Discrete model of the trapezium lattice

In this section, the trapezium lattice is first introduced in the discrete form and dispersion analysis corresponding to the defined model is presented.

5.1.1 Definition of the trapezium lattice

We choose the smaller opening angle between two beams as $\varphi = 60^\circ$ as in Figure 5.2.

- For the trapezium geometry, see Figure 5.1, the representative volume element (RVE) only requires a single joint to ensure the symmetry for simple mathematical formulations, see Figure 5.2. This RVE of the microlattice is modelled as a rigid-joint network of four uniform beams having cross section A, length l, material density ρ and Young's modulus E.

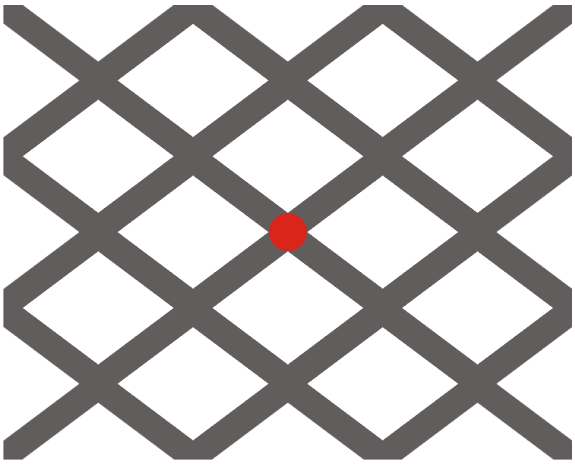

Fig. 5.1 The 2D discrete model of a trapezium lattice

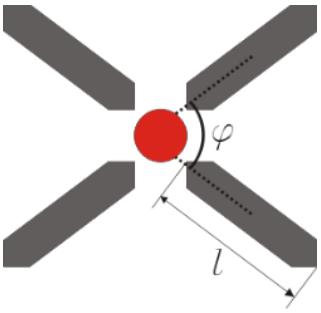

Fig. 5.2 Detailed diagram of a RVE of the trapezium lattice

- Different beam theories can be used in this step. In this paper, the microlattices have slender beams where β is the depth over length ratio, $\beta \leq \frac{1}{10}$ and the Euler-Bernoulli beam theory is used to model the behaviour of the discrete microbeams. It is acknowledged that Euler-Bernoulli beam theory can exhibit anomalous behaviour in dynamics; however, these undesirable effects can be shown not to effect the subsequent derivations shown below.

- For simplicity, the mass matrix of the beam element is lumped as follows

$$\mathbf{M}^{(e)} = \frac{\rho A l}{2} diag\left(1, 1, \frac{\delta}{12l^2}, 1, 1, \frac{\delta}{12l^2}\right)$$

  where *delta* is a constant which usually takes the value of 1. The beam stiffness matrix used is the common two-dimensional stiffness matrix of Euler-Bernoulli beam theory, see Equation (4.2).

  Next, the global matrix is built for the RVE system and the equilibrium is considered at the midde node in the RVE (the red node in Figure 5.2).

5.1.2 Dispersion analysis

As explained in Section 4.1.1, the system of four beams on the right side of Figure 5.2 is chosen to carry out the dispersion analysis. The five nodes are numbered anti-clockwise as in Figure 5.3 and have coordinates as $(0,0)$, $\left(\frac{\sqrt{3}}{2}, \frac{L}{2}\right)$, $\left(-\frac{\sqrt{3}}{2}, \frac{L}{2}\right)$, $\left(-\frac{\sqrt{3}}{2}, -\frac{L}{2}\right)$ and

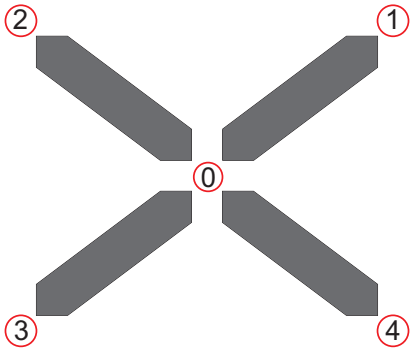

Fig. 5.3 Finite element analysis on the discrete model. Node numbering of the discrete system containing the RVE unit.

$\left(\frac{\sqrt{3}}{2}, -\frac{L}{2}\right)$. In this section, u_n and v_n describe the horizontal and vertical displacements of node number n; θ_n stands for the rotation, a_n, b_n and c_n for horizontal, vertical and rotational accelerations. With the mass matrices M and stiffness matrices K defined in Equations (4.1) and (4.2) for each beam of length l, the term $M\overline{a} + K\overline{u}$ can be written where $\overline{a}$ and $\overline{u}$ are the column vectors for displacement and acceleration for each beam. Because the node number 0 is fully surrounded by four beams, we can assume equilibrium of node 0 and write the following three equations of motion:

$$\left(\begin{array}{l} \frac{1}{16}\left(-\theta_1-\theta_2+\theta_3+\theta_4\right)\beta^4 \\ +\frac{1}{16L}\left(\begin{array}{l}\left(4u_0-u_1-u_2-u_3-u_4-\sqrt{3}v_2+\sqrt{3}v_1-\sqrt{3}v_4+\sqrt{3}v_3\right)\beta^4 \\ +\left(3\left(4u_0-u_1-u_3-u_2-u_4\right)+\sqrt{3}\left(-v_3+u_4-v_1+v_2\right)\right)\beta^2\end{array}\right)\end{array}\right) E+\frac{\rho L\beta^2}{2}a_0=0 \tag{5.1}$$

$$\left(\begin{array}{l} \frac{\sqrt{3}}{16}\left(-\theta_2+\theta_1+\theta_4-\theta_3\right)\beta^4 \\ +\frac{1}{16L}\left(\begin{array}{l}\left(3\left(4v_0-v_1-v_2-v_3-v_4\right)+\sqrt{3}\left(u_1-u_2+u_3-u_4\right)\right)\beta^4 \\ +\left(4v_0-v_4-v_3-v_2-v_1+\sqrt{3}\left(u_4+u_2-3u_1-u_3\right)\right)\beta^2\end{array}\right)\end{array}\right) E+\frac{\rho L\beta^2}{2}b_0=0 \tag{5.2}$$

$$\left(\begin{array}{l}\frac{L}{24}\left(8\theta_0+\theta_2+\theta_1+\theta_4+\theta_3\right)\beta^4 \\ +\frac{1}{16}\left(u_2+u_1-u_3-u_4-\sqrt{3}v_1+\sqrt{3}v_3+\sqrt{3}v_2-\sqrt{3}v_4\right)\beta^4\end{array}\right)E+\frac{\rho L^3\beta^2\delta}{24}c_0=0 \quad (5.3)$$

These equations can be divided on both sides by a constant for simplification and easy future manipulation. The first two Equations (5.1) and (5.2) represent the forces acting on point 0 in the x and y directions, while Equation (5.3) stands for the moment about point 0. However, the system might not be stable for dispersion analysis and some manipulations are required to modify the system.

Comparing the first two Equations (5.1) and (5.2), different from the square lattice case, the variables u and v are non-interchangeable because the trapezium does not have a symmetric axis at 45° to the horizontal line. Hence, there is no angle of propagation that the horizontal and vertical displacements u and v will have the same value. On the other hand, if the force acts on point 0 at an angle of 60° to the horizontal line (perpendicular to the beam connecting point 2 and 4 in Figure 5.3), it is easy for the structure to propagate the force energy in the 30° direction than the direction perpendicular to the force; hence, the frequency amplitude of the shear component at this angle is much smaller to the one of the compression wave. We will check whether this property is still maintained in the continuum form.

After obtaining the three equations of motion, dispersion analysis can be carried out by replacing the displacements with the harmonic plane wave equations:

$$\begin{aligned} u_n &= U\exp\left[i\left(k\cos\gamma x_n+k\sin\gamma y_n-\omega t\right)\right] \\ v_n &= V\exp\left[i\left(k\cos\gamma x_n+k\sin\gamma y_n-\omega t\right)\right] \\ \theta_n &= W\exp\left[i\left(k\cos\gamma x_n+k\sin\gamma y_n-\omega t\right)\right] \end{aligned} \quad (5.4)$$

where u_n, v_n and θ_n are the horizontal, vertical and rotational degrees of freedom of a node numbered n, x_n and y_n are the horizontal and vertical coordinates of that node at time t.

Substituting the coordinates (x,y) of the nodes in the RVE of the trapezium to the plane wave equations, we have:

$$u_0 = U\exp\left[i\left(-\omega t\right)\right] \quad (5.5)$$

$$u_{1-4} = u_0\exp\left[i\left(\pm\frac{\sqrt{3}}{2}k\cos\gamma\pm\frac{1}{2}k\sin\gamma-\omega t\right)\right] \quad (5.6)$$

$$v_0 = V\exp\left[i\left(-\omega t\right)\right] \tag{5.7}$$

$$v_{1-4} = v_0\exp\left[i\left(\pm\frac{\sqrt{3}}{2}k\cos\gamma\pm\frac{1}{2}k\sin\gamma-\omega t\right)\right] \tag{5.8}$$

$$\theta_0 = W\exp\left[i\left(-\omega t\right)\right] \tag{5.9}$$

$$\theta_{1-4} = W\exp\left[i\left(\pm\frac{\sqrt{3}}{2}k\cos\gamma\pm\frac{1}{2}k\sin\gamma-\omega t\right)\right] \tag{5.10}$$

After these substitutions, the three equation of motions (Equations (5.1), (5.2) and (5.3)) transform into:

$$\left(\begin{array}{l}\left(\begin{array}{l}-We^{i\left(\frac{\sqrt{3}}{2}k\cos\gamma+\frac{1}{2}k\sin\gamma-\omega t\right)}-We^{i\left(-\frac{\sqrt{3}}{2}k\cos\gamma+\frac{1}{2}k\sin\gamma-\omega t\right)}\\ +We^{i\left(-\frac{\sqrt{3}}{2}\cos\gamma-\frac{1}{2}k\sin\gamma-\omega t\right)}+We^{i\left(\frac{\sqrt{3}}{2}k\cos\gamma-\frac{1}{2}k\sin\gamma-\omega t\right)}\end{array}\right)\beta^2\\ +\frac{1}{L}\left(\begin{array}{l}\left(\begin{array}{l}4Ue^{i(-\omega t)}-Ue^{i\left(\frac{\sqrt{3}}{2}k\cos\gamma+\frac{1}{2}k\sin\gamma-\omega t\right)}-Ue^{i\left(-\frac{\sqrt{3}}{2}k\cos\gamma+\frac{1}{2}k\sin\gamma-\omega t\right)}\\ -Ue^{i\left(-\frac{\sqrt{3}}{2}\cos\gamma-\frac{1}{2}k\sin\gamma-\omega t\right)}-Ue^{i\left(\frac{\sqrt{3}}{2}k\cos\gamma-\frac{1}{2}k\sin\gamma-\omega t\right)}\\ -\sqrt{3}Ve^{i\left(-\frac{\sqrt{3}}{2}k\cos\gamma+\frac{1}{2}k\sin\gamma-\omega t\right)}+\sqrt{3}Ve^{i\left(\frac{\sqrt{3}}{2}k\cos\gamma+\frac{1}{2}k\sin\gamma-\omega t\right)}\\ -\sqrt{3}Ve^{i\left(\frac{\sqrt{3}}{2}k\cos\gamma-\frac{1}{2}k\sin\gamma-\omega t\right)}+\sqrt{3}Ve^{i\left(-\frac{\sqrt{3}}{2}\cos\gamma-\frac{1}{2}k\sin\gamma-\omega t\right)}\end{array}\right)\beta^2\\ +\left(\begin{array}{l}12Ue^{i(-\omega t)}-3Ue^{i\left(\frac{\sqrt{3}}{2}k\cos\gamma+\frac{1}{2}k\sin\gamma-\omega t\right)}-3Ue^{i\left(-\frac{\sqrt{3}}{2}\cos\gamma-\frac{1}{2}k\sin\gamma-\omega t\right)}\\ -3Ue^{i\left(-\frac{\sqrt{3}}{2}k\cos\gamma+\frac{1}{2}k\sin\gamma-\omega t\right)}-3Ue^{i\left(\frac{\sqrt{3}}{2}k\cos\gamma-\frac{1}{2}k\sin\gamma-\omega t\right)}\\ -\sqrt{3}Ve^{i\left(-\frac{\sqrt{3}}{2}\cos\gamma-\frac{1}{2}k\sin\gamma-\omega t\right)}+\sqrt{3}Ve^{i\left(\frac{\sqrt{3}}{2}k\cos\gamma-\frac{1}{2}k\sin\gamma-\omega t\right)}\\ -\sqrt{3}Ve^{i\left(\frac{\sqrt{3}}{2}k\cos\gamma+\frac{1}{2}k\sin\gamma-\omega t\right)}+\sqrt{3}Ve^{i\left(-\frac{\sqrt{3}}{2}k\cos\gamma+\frac{1}{2}k\sin\gamma-\omega t\right)}\end{array}\right)\end{array}\right)\frac{E}{16}\\ +\frac{\rho L}{2}U\omega^2e^{i(-\omega t)}=0\end{array}\right) \tag{5.11}$$

$$\left(\begin{array}{l}
\dfrac{\sqrt{3}}{16}\left(\begin{array}{l}
-We^{i\left(-\frac{\sqrt{3}}{2}k\cos\gamma+\frac{1}{2}k\sin\gamma-\omega t\right)}+We^{i\left(\frac{\sqrt{3}}{2}k\cos\gamma+\frac{1}{2}k\sin\gamma-\omega t\right)}\\
+We^{i\left(\frac{\sqrt{3}}{2}k\cos\gamma-\frac{1}{2}k\sin\gamma-\omega t\right)}-We^{i\left(-\frac{\sqrt{3}}{2}\cos\gamma-\frac{1}{2}k\sin\gamma-\omega t\right)}
\end{array}\right)\beta^2\\
+\dfrac{1}{16L}\left(\begin{array}{l}
\left(\begin{array}{l}
12Ve^{i(-\omega t)}-3Ve^{i\left(\frac{\sqrt{3}}{2}k\cos\gamma+\frac{1}{2}k\sin\gamma-\omega t\right)}-3Ve^{i\left(-\frac{\sqrt{3}}{2}k\cos\gamma+\frac{1}{2}k\sin\gamma-\omega t\right)}\\
-3Ve^{i\left(-\frac{\sqrt{3}}{2}\cos\gamma-\frac{1}{2}k\sin\gamma-\omega t\right)}-3Ve^{i\left(\frac{\sqrt{3}}{2}k\cos\gamma-\frac{1}{2}k\sin\gamma-\omega t\right)}\\
+\sqrt{3}Ue^{i\left(\frac{\sqrt{3}}{2}k\cos\gamma+\frac{1}{2}k\sin\gamma-\omega t\right)}-\sqrt{3}Ue^{i\left(-\frac{\sqrt{3}}{2}k\cos\gamma+\frac{1}{2}k\sin\gamma-\omega t\right)}\\
+\sqrt{3}Ue^{i\left(-\frac{\sqrt{3}}{2}\cos\gamma-\frac{1}{2}k\sin\gamma-\omega t\right)}-\sqrt{3}Ue^{i\left(\frac{\sqrt{3}}{2}k\cos\gamma-\frac{1}{2}k\sin\gamma-\omega t\right)}
\end{array}\right)\beta^2\\
+\left(\begin{array}{l}
4Ve^{i(-\omega t)}-Ve^{i\left(\frac{\sqrt{3}}{2}k\cos\gamma-\frac{1}{2}k\sin\gamma-\omega t\right)}-Ve^{i\left(-\frac{\sqrt{3}}{2}\cos\gamma-\frac{1}{2}k\sin\gamma-\omega t\right)}\\
-Ve^{i\left(-\frac{\sqrt{3}}{2}k\cos\gamma+\frac{1}{2}k\sin\gamma-\omega t\right)}-Ve^{i\left(\frac{\sqrt{3}}{2}k\cos\gamma+\frac{1}{2}k\sin\gamma-\omega t\right)}\\
+\sqrt{3}Ue^{i\left(\frac{\sqrt{3}}{2}k\cos\gamma-\frac{1}{2}k\sin\gamma-\omega t\right)}+\sqrt{3}Ue^{i\left(-\frac{\sqrt{3}}{2}k\cos\gamma+\frac{1}{2}k\sin\gamma-\omega t\right)}\\
-\sqrt{3}Ue^{i\left(\frac{\sqrt{3}}{2}k\cos\gamma+\frac{1}{2}k\sin\gamma-\omega t\right)}-\sqrt{3}Ue^{i\left(-\frac{\sqrt{3}}{2}\cos\gamma-\frac{1}{2}k\sin\gamma-\omega t\right)}
\end{array}\right)
\end{array}\right)E\\
+\dfrac{\rho L}{2}V\omega^2e^{i(-\omega t)}=0
\end{array}\right. \tag{5.12}$$

$$\left(\begin{array}{l}
\dfrac{L}{24}\left(\begin{array}{l}
8We^{i(-\omega t)}+We^{i\left(-\frac{\sqrt{3}}{2}k\cos\gamma+\frac{1}{2}k\sin\gamma-\omega t\right)}+We^{i\left(\frac{\sqrt{3}}{2}k\cos\gamma+\frac{1}{2}k\sin\gamma-\omega t\right)}\\
+We^{i\left(\frac{\sqrt{3}}{2}k\cos\gamma-\frac{1}{2}k\sin\gamma-\omega t\right)}+We^{i\left(-\frac{\sqrt{3}}{2}\cos\gamma-\frac{1}{2}k\sin\gamma-\omega t\right)}
\end{array}\right)\beta^2\\
+\dfrac{1}{16}\left(\begin{array}{l}
Ue^{i\left(-\frac{\sqrt{3}}{2}k\cos\gamma+\frac{1}{2}k\sin\gamma-\omega t\right)}+Ue^{i\left(\frac{\sqrt{3}}{2}k\cos\gamma+\frac{1}{2}k\sin\gamma-\omega t\right)}\\
-Ue^{i\left(-\frac{\sqrt{3}}{2}\cos\gamma-\frac{1}{2}k\sin\gamma-\omega t\right)}-Ue^{i\left(\frac{\sqrt{3}}{2}k\cos\gamma-\frac{1}{2}k\sin\gamma-\omega t\right)}\\
-\sqrt{3}Ve^{i\left(\frac{\sqrt{3}}{2}k\cos\gamma+\frac{1}{2}k\sin\gamma-\omega t\right)}+\sqrt{3}Ve^{i\left(-\frac{\sqrt{3}}{2}\cos\gamma-\frac{1}{2}k\sin\gamma-\omega t\right)}\\
+\sqrt{3}Ve^{i\left(-\frac{\sqrt{3}}{2}k\cos\gamma+\frac{1}{2}k\sin\gamma-\omega t\right)}-\sqrt{3}Ve^{i\left(\frac{\sqrt{3}}{2}k\cos\gamma-\frac{1}{2}k\sin\gamma-\omega t\right)}
\end{array}\right)\beta^2
\end{array}\right)E\\
+\dfrac{\rho L^3\delta}{24}W\omega^2e^{i(-\omega t)}=0
\end{array}\right. \tag{5.13}$$

The system is then solved as an eigen-value problem where the variables are $[U,V,W]$; if E, l, ρ, β are predefined, the determinant of the system is a function of $[\omega,k,\gamma]$. For non-trivial solutions for the system, the determinant has to be zero. For each pair of $[k,\gamma]$, there are three corresponding values of ω and all these values are real for the discrete model of the square

lattice.

Note: To simplify the system, the normalised frequency is defined as $\frac{\omega l}{c_e}$ where $c_e = \sqrt{\frac{E}{\rho}}$ and the normalised wave number as kl.

The curves of Figure 4.4 show all values of the normalised frequency ω against the normalised wave number k for the propagation angle $\gamma = \frac{\pi}{2}$. The results of this section will be compared with later models in Section 5.2, in particular Figures 5.5 and 5.6 for the different propagation angles.

5.2 Generalised continuum

We use Taylor's series expansion, to the fourth and third order for spatial variables and rotational variables respectively, to continualise the trapezium unit lattice constructed from Euler-Bernoulli beam theory and the lumped mass scheme. The approach is explained in detail in (Lombardo and Askes (2012)). The equations of motion for a RVE in the x-direction, y-direction and rotation in the plane x-y are written as:

$$2\rho\ddot{u} + E\begin{pmatrix} -\frac{1}{8}\left(\beta^2+3\right)\left(3u_{,xx}+u_{,yy}\right)+\frac{3}{4}\left(\beta^2-1\right)v_{,xy} \\ -\frac{l^2}{384}\left(\beta^2+3\right)\left(9u_{,xxxx}+u_{,yyyy}+18u_{,xxyy}\right) \\ +\frac{1}{32}\left(\beta^2-1\right)\left(3v_{,xxxy}+v_{,xyyy}\right)-\frac{\beta^2}{48}\left(24\theta_{,y}+9\theta_{,xxy}+\theta_{,yyy}\right) \end{pmatrix} = 0 \qquad (5.14)$$

$$2\rho\ddot{v} + E\begin{pmatrix} -\frac{1}{8}\left(3\beta^2+1\right)\left(v_{,yy}+3v_{,xx}\right)+\frac{3}{4}\left(\beta^2-1\right)u_{,xy} \\ -\frac{l^2}{384}\left(1+3\beta^2\right)\left(v_{,yyyy}+18v_{,xxyy}+9v_{,xxxx}\right) \\ +\frac{1}{32}\left(\beta^2-1\right)\left(u_{,xyyy}+3u_{,xxxy}\right)+\frac{3}{16}\beta^2\left(8\theta_{,x}+l^2\theta_{,xyy}+l^2\theta_{,xxx}\right) \end{pmatrix} = 0 \qquad (5.15)$$

$$2\rho l^2\ddot{\theta} + \beta^2 E\begin{pmatrix} 3l^2\theta_{,xx}+l^2\theta_{,yy}+24\theta+6u_{,y}-18v_{,x} \\ +\frac{9}{4}l^2u_{,xxy}-\frac{9}{4}l^2v_{,xyy}+\frac{1}{4}l^2u_{,yyy}-\frac{9}{4}l^2v_{,xxx} \end{pmatrix} = 0 \qquad (5.16)$$

where u, v and θ are horizontal, vertical and rotational displacements of the middle node (red node in Figure 5.2) respectively.

Dispersion analysis for these equations uses the following plane wave relationships to

obtain an eigen-value problem:

$$\begin{aligned} u(x,y,t) &= U\exp\left[i\left(k\cos\gamma x + k\sin\gamma y - \omega t\right)\right] \\ v(x,y,t) &= V\exp\left[i\left(k\cos\gamma x + k\sin\gamma y - \omega t\right)\right] \\ \theta(x,y,t) &= W\exp\left[i\left(k\cos\gamma x + k\sin\gamma y - \omega t\right)\right] \end{aligned} \tag{5.17}$$

where we will substitute $x = 0$, $y = 0$ and $t = 0$.

5.2.1 Reduced degree-of-freedom continuum

In this step, the rotational degree of freedom will be eliminated for the following reasons:

- The route to stabilise the rotational degree of freedom is complicated. The difficulty lies in the odd number of order of derivatives which are unstable.
- Translating the rotation into spatial displacements helps reduce the size of the global matrix by a third in two dimensional cases. For three-dimensional microlattices, we would be able to reduce the computation cost by half by eliminating the rotation variables.

Similarly we rewrite θ with respect to other linear variables as (see Section C.2 for full derivation):

$$\theta = \frac{\rho l^2}{48\lambda^2 E}\delta\left(\ddot{u}_{,y} - 3\ddot{v}_{,x}\right) - \frac{1}{4}u_{,y} + \frac{3}{4}v_{,x} - \frac{1}{16}l^2 u_{,xxy} + \frac{1}{16}l^2 v_{,xyy} \tag{5.18}$$

This step allows us to eliminate θ and reduce the equations of motions (assume that $\beta^2 \ll 1$ due to $\beta \leq \frac{1}{10}$, $l \leq \frac{1}{10}$ because this is a microstructural material and $\delta = 1$; hence, we can ignore all terms $O(\beta^2)$, $O\left(\beta^2 l^2\right)$ and $O\left(l^4\right)$):

$$\begin{aligned} &2\rho\ddot{u} - \frac{\rho l^2}{96}\ddot{u}_{,yy} + \frac{\rho l^2}{32}\ddot{v}_{,xy} = E\left(\frac{9}{8}u_{,xx} + \frac{3}{8}u_{,yy} + \frac{3}{4}v_{,xy}\right) \\ &+El^2\left(\frac{9}{128}u_{,xxxx} + \frac{9}{64}u_{,xxyy} + \frac{1}{128}u_{,yyyy} + \frac{3}{32}v_{,xxxy} + \frac{1}{32}v_{,xyyy}\right) \end{aligned} \tag{5.19}$$

$$\begin{aligned} &2\rho\ddot{v} - \frac{3\rho l^2}{32}\ddot{v}_{,xx} + \frac{\rho l^2}{32}\ddot{u}_{,xy} = E\left(\frac{1}{8}v_{,yy} + \frac{3}{8}v_{,xx} + \frac{3}{4}u_{,xy}\right) + \\ &+El^2\left(\frac{1}{384}v_{,yyyy} + \frac{3}{128}v_{,xxxx} + \frac{3}{64}v_{,xxyy} + \frac{1}{32}u_{,xyyy} + \frac{3}{32}u_{,xxxy}\right) \end{aligned} \tag{5.20}$$

Dispersion analysis is carried out for the two new equations of motion by substituting the terms with plane wave Equations (5.17) to achieve an eigen-value problem. Similar to the square lattice case, the new two equations of motion produce an unstable dispersion relationship which is shown in Figure 5.4.

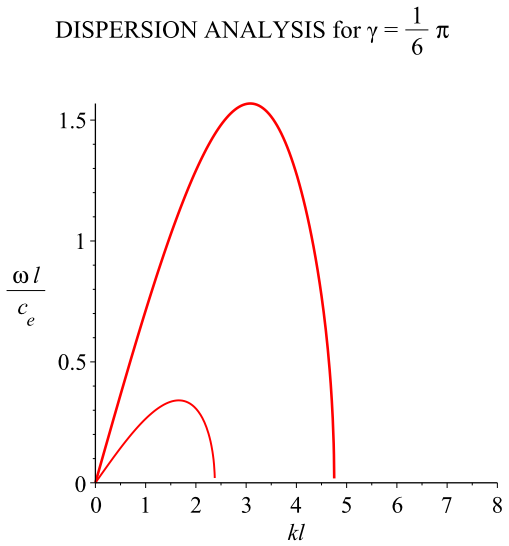

Fig. 5.4 Dispersion analysis for the unstable continuum of Equations (5.19) and (5.20). The lower curve represents the shear component and the higher curve represents the compression component.

Further modification is carried out in the next parts for stabilisation and easy implementation in finite element modelling.

5.2.2 Classical continuum

Similar to one-dimensional and the square lattice cases, the equations of motion for the classical continuum contains all the second order derivative terms in Equation (5.19) and (5.20):

$$2\rho\ddot{u} = E\left(\frac{9}{8}u_{,xx} + \frac{3}{8}u_{,yy} + \frac{3}{4}v_{,xy}\right) \tag{5.21}$$

$$2\rho\ddot{v} = E\left(\frac{1}{8}v_{,yy} + \frac{3}{8}v_{,xx} + \frac{3}{4}u_{,xy}\right) \tag{5.22}$$

Table 5.1 presenting the dispersion relation of the classical continuum is displayed in the next section.

5.2.3 Stabilised gradient continuum

For stable dispersion behaviour, the rules of thumb are:

- That the coefficients of fourth order differential terms (of the form $\mathscr{X}_{,iijj}$where $i, j = x, y, t$) shall have opposite signs with the coefficients of second order differential terms

(of the form $\mathscr{X}_{,ii}$ where $i,j = x,y,t$). This is because the plane wave equations have imaginary numbers.

- The differential terms of the form $\mathscr{X}_{,ij}$ or $\mathscr{X}_{,iiij}$ where $i,j = x,y$ shall have smaller or even negligible coefficients of the corresponding same order differential terms of the forms $\mathscr{X}_{,ii}$ or $\mathscr{X}_{,iijj}$. The reason is that k_x and k_y are associated with $\cos\gamma$ and $\sin\gamma$ where γ is the propagation angle of the wave. The sign of a $(\cos\gamma)^{2n+1}(\sin\gamma)^{2n+1}$ where $n = 0,1$ is difficult to determine, but it can be a positive or a negative term. Hence, to ensure stability, these terms must be formulated such that they are are much smaller than the permanently stable terms, or made to disappear from the set.

Using the similar method in Section 4.2.3, if we denote Equation (5.19) as $\mathscr{R}$ and Equation (5.20) as $\mathscr{Z}$, we shall calculate (ignoring all terms $(\mathrm{O})\,(l^4)$):

$$\mathscr{R} + B\mathscr{R}_{,xx} + C\mathscr{R}_{,yy} + H\mathscr{Z}_{,xy} \tag{5.23}$$

$$\mathscr{Z} + F\mathscr{Z}_{,xx} + G\mathscr{Z}_{,yy} + H\mathscr{R}_{,xy} \tag{5.24}$$

where B, C, F, G and H are the multipliers that are determined later so that the new expressions (5.23) and (5.24) shall be stable in the dispersion analysis. The expressions (5.23) and (5.24) in detailed forms are:

$$\begin{aligned}
&2\rho\ddot{u} + \left(2C\rho l^2 - \frac{\rho l^2}{96}\right)\ddot{u}_{,yy} + \left(2H\rho l^2 + \frac{\rho l^2}{32}\right)\ddot{v}_{,xy} + 2B\rho l^2\ddot{u}_{,xx} = E\,(\cdots)\\
&El^2\left[\left(\frac{9}{128} + \frac{9B}{8}\right)u_{,xxxx} + \left(\frac{9}{64} + \frac{9C}{8} + \frac{3B}{8} + \frac{3H}{4}\right)u_{,xxyy} + \left(\frac{1}{128} + \frac{3C}{8}\right)u_{,yyyy}\right]\\
&\qquad + El^2\left[\left(\frac{3}{32} + \frac{3B}{4} + \frac{3H}{8}\right)v_{,xxxy} + \left(\frac{1}{32} + \frac{3C}{4} + \frac{H}{8}\right)v_{,xyyy}\right]
\end{aligned}$$

$$\begin{aligned}
&2\rho\ddot{v} + \left(2F\rho l^2 - \frac{3\rho l^2}{32}\right)\ddot{v}_{,xx} + \left(2H\rho l^2 + \frac{\rho l^2}{32}\right)\ddot{u}_{,xy} + 2G\rho l^2\ddot{v}_{,yy} = E\,(\cdots)\\
&+El^2\left[\left(\frac{1}{384} + \frac{G}{8}\right)v_{,yyyy} + \left(\frac{3}{64} + \frac{F}{8} + \frac{3G}{8} + \frac{H}{4}\right)v_{,xxyy} + \left(\frac{3}{128} + \frac{3F}{8}\right)v_{,xxxx}\right]\\
&\qquad + El^2\left[\left(\frac{1}{32} + \frac{3G}{4} + \frac{3H}{8}\right)u_{,xyyy} + \left(\frac{3}{32} + \frac{3F}{4} + \frac{9H}{8}\right)u_{,xxxy}\right]
\end{aligned}$$

To eliminate the terms $\mathscr{X}_{xxxy}$ and $\mathscr{X}_{xyyy}$, the following set of relations is one possible route:

$$C = \frac{-4H-1}{24} \qquad B = \frac{-4H-1}{8} \tag{5.25}$$

$$F = \frac{-12H-1}{8} \qquad G = \frac{-12H-1}{24} \tag{5.26}$$

From here, the stability of wave propagation of the above set of equations depends on the arbitrary constant H. The proper range of H values changes as the angle γ of the trial solutions (plane wave equations) changes. Other values of γ are also examined to ensure that when $H \geq 0$, the set of equations (5.2.3) and (5.2.3) is always stable regardless of the γ value. If we have obtained a suitable value for H (see explanation in Appendix C.3), we have the following stable set of equations:

$$\begin{aligned}
&2\rho\ddot{u} - \left(\frac{3}{32}+\frac{H}{3}\right)\rho l^2 \ddot{u}_{,yy} - \left(H+\frac{1}{4}\right)\rho l^2 \ddot{u}_{,xx} + \left(\frac{1}{32}+2H\right)\rho l^2 \ddot{v}_{,xy} \\
=&E\left(\frac{9}{8}u_{,xx}+\frac{3}{8}u_{,yy}+\frac{3}{4}v_{,xy}\right) + \\
&\qquad El^2\left(-\left(\frac{9}{128}+\frac{H}{16}\right)u_{,xxxx} + \left(\frac{3}{64}+\frac{3}{8}H\right)u_{,xxyy} - \left(\frac{1}{128}+\frac{H}{16}\right)u_{,yyyy}\right)
\end{aligned} \tag{5.27}$$

$$\begin{aligned}
&2\rho\ddot{v} - \left(\frac{11}{32}+3H\right)\rho l^2 \ddot{v}_{,xx} - \left(H+\frac{1}{12}\right)\rho l^2 \ddot{v}_{,yy} + \left(2H+\frac{1}{32}\right)\rho l^2 \ddot{u}_{,xy} \\
=&E\left(\frac{1}{8}v_{,yy}+\frac{3}{8}v_{,xx}+\frac{3}{4}u_{,xy}\right) + \\
&\qquad + El^2\left(-\left(\frac{1}{384}+\frac{H}{16}\right)v_{,yyyy} - \left(\frac{3}{128}+\frac{9H}{16}\right)v_{,xxxx} + \left(\frac{1}{64}-\frac{H}{8}\right)v_{,xxyy}\right)
\end{aligned} \tag{5.28}$$

Figure 5.5a and Figure 5.5b compare different stabilised continua with the discrete model. When $\gamma = \pi/3$, near $k = 0$, we can see that the longitudinal wave has a nearly zero slope. This is because the direction of the wave hits the beams perpendicularly as demonstrated in the right hand diagram in Figure 5.8. Similarly to the square lattice in the latter session, beams that are perpendicular to the initial direction of wave propagation are not effective to transfer the wave energy, and hence only a narrow frequency band are allowed to go through these members. Generally, in these two figures, for the wave number region $[0, \pi]$, the continuum performs very close to the discrete model. Again, it is noted that the discrete model is already discretised in space while the continuum is not.

Next, we will apply the Ru-Aifantis theorem to the fourth order space derivatives $\mathscr{X}_{iiii}$ of the above set of Equations (5.27) and (5.28) so that we can use C^0 continuity for a finite element implement.

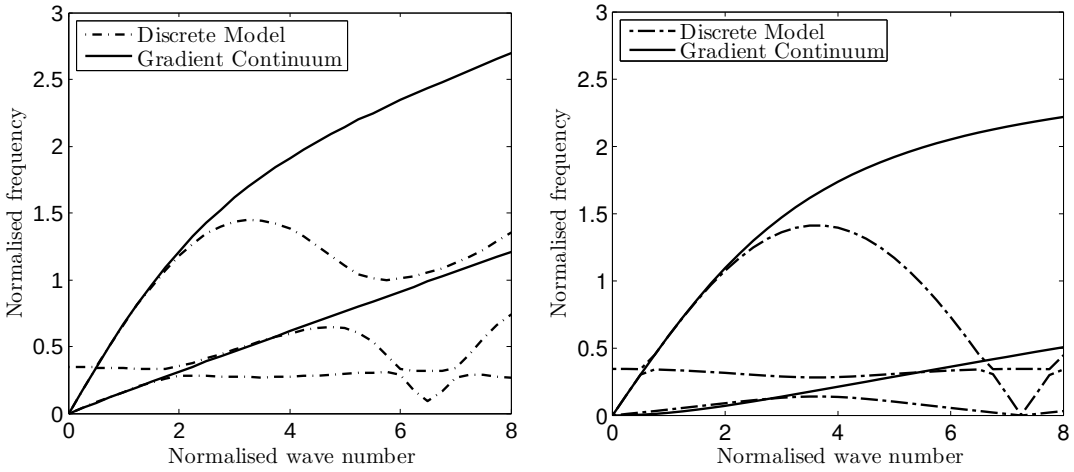

(a) $\gamma = \pi/4$ (b) $\gamma = \pi/3$

Fig. 5.5 Dispersion analysis for the stabilised gradient continuum of the trapezium for different propagation angles γ. The normalised wave number has the formula of kl, the normalised frequency $\dfrac{\omega}{c_e}$. For each model, there are two curves, the lower curve represents the shear component and the higher curve represents the compression component.

5.2.4 Ru-Aifantis theorem application

In this section, a symbolic derivation is presented first. After we obtain the symbolic equations of motion, numeric values are substituted to demonstrate the symmetric dynamic system ready for numerical spatial discretisations.

When using the Ru-Aifantis theory, each point will have four degrees of freedom, two originals and two auxiliaries; hence the stiffness or mass matrix for one square element will have the dimensions of 16x16. Both sides of Equations (5.27) and (5.28) are multiplied by 160 for easy presentation. The new system reads:

$$320\rho\ddot{u} - \left(15 + \frac{160}{3}H\right)\rho l^2 \ddot{u}_{,yy} - (160H + 40)\,\rho l^2 \ddot{u}_{,xx} + (5 + 320H)\,\rho l^2 \ddot{v}_{,xy} =$$
$$E\,(180u_{,xx} + 60u_{,yy} + 120v_{,xy})$$
$$+ El^2\left[-\left(\frac{45}{4} + 10H\right)u_{,xxxx} + \left(\frac{15}{2} + 60H\right)u_{,xxyy} - \left(\frac{5}{4} + 10H\right)u_{,yyyy}\right] \tag{5.29}$$

$$320\rho\ddot{v} - (55+480H)\,\rho l^2\ddot{v}_{,xx} - \left(160H+\frac{40}{3}\right)\rho l^2\ddot{v}_{,yy} + (320H+5)\,\rho l^2\ddot{u}_{,xy} =$$
$$E\,(20v_{,yy}+60v_{,xx}+120u_{,xy})$$
$$+El^2\left[-\left(\frac{5}{12}+10H\right)v_{,yyyy} - \left(\frac{15}{4}+90H\right)v_{,xxxx} + \left(\frac{5}{2}-20H\right)v_{,xxyy}\right] \tag{5.30}$$

For Equations (5.29) and (5.30), u and v appear together in the equations. Similar to the one dimensional case, to apply Ru-Aifantis theory for Equations (5.29) and (5.30), the two new auxiliary displacements a and b are defined as following:

$$a = su - ml^2u_{,xx} - nl^2u_{,yy} \tag{5.31}$$
$$b = \varsigma v - \mu l^2 v_{,xx} - \nu l^2 v_{,yy} \tag{5.32}$$

where s, m, n, ς, μ and ν are arbitrary coefficients whose values shall be determined later.

After eliminating the $\mathscr{X}_i iii$ terms in Equations (5.29) and (5.30), we want to finally achieve this matrix system after FE discretisations:

$$\begin{bmatrix} M_{1,1} & M_{1,2} & M_{1,3} & 0 \\ M_{2,1} & M_{2,2} & 0 & M_{2,4} \\ M_{3,1} & 0 & M_{3,3} & 0 \\ 0 & M_{4,2} & 0 & M_{4,4} \end{bmatrix} \begin{bmatrix} \ddot{u} \\ \ddot{v} \\ \ddot{a} \\ \ddot{b} \end{bmatrix} - \begin{bmatrix} K_{1,1} & K_{1,2} & K_{1,3} & 0 \\ K_{2,1} & K_{2,2} & 0 & K_{2,4} \\ K_{3,1} & 0 & K_{3,3} & 0 \\ 0 & K_{4,2} & 0 & K_{4,4} \end{bmatrix} \begin{bmatrix} u \\ v \\ a \\ b \end{bmatrix} = \begin{bmatrix} f_u \\ f_v \\ 0 \\ 0 \end{bmatrix} \tag{5.33}$$

with $M_{1,2} = M_{2,1}$, $M_{1,3} = M_{3,1}$, $M_{2,4} = M_{4,2}$, $K_{1,2} = K_{2,1}$, $K_{1,3} = K_{3,1}$ and $K_{2,4} = K_{4,2}$.

Note: Regarding the one-dimensional case, the auxiliary variables were placed before the main variables in the acceleration and displacement column vectors. Meanwhile, for the two-dimensional cases, the main variables are placed before because each equation of motion has both main variables.

To construct such matrices, it is required to consider all four equations from which the matrices are built together. It is obvious that the first and second equations built from the matrices in Equation (5.33) are based on the two equations of motion (5.29) and (5.30). On the other hand, the third and fourth equations are developed from the definition of a and b - Equations (5.31) and (5.32). In detail, the third equation reads $(M_{3,1}\ddot{u} + M_{3,3}\ddot{a}) - (K_{3,1}u + K_{3,3}a) = 0$, which can be fulfilled with $M_{3,1}\ddot{u} + M_{3,3}\ddot{a} = 0$ and $K_{3,1}u + K_{3,3}a = 0$. It is easier to satisfy these two conditions using the definition of a and b - Equations (5.31) and (5.32).

Consider developing the first equation by the matrix from Equation (5.29), the terms having fourth derivatives, $u_{,xxxx}$ and $u_{,yyyy}$ on the right hand side of equation (5.29) are replaced

by the term $K_{1,3}a$ in the first equation of the matrix. Hence, $K_{1,3}a$ needs to contain the form $qa_{,xx}+ra_{,yy}$ which is equivalent to the main variables by using the definition of a in Equation (5.31), where q and r are arbitrary coefficients whose values shall be determined later:

$$\left.\begin{aligned} qa_{,xx} &= qsu_{,xx} - qml^2u_{,xxxx} - qnl^2u_{,xxyy} \\ ra_{,yy} &= rsu_{,yy} - rml^2u_{,xxyy} - rnl^2u_{,yyyy} \end{aligned}\right\} \rightarrow \begin{aligned} qm &= SXXXX1 = \frac{45}{4} + 10H \\ rn &= SYYYY1 = \frac{5}{4} + 10H \end{aligned} \tag{5.34}$$

where $SXXXX1$ is the coefficient of the term $u_{,xxxx}$ and $SYYYY1$ is the coefficient of the term $u_{,yyyy}$ in Equation (5.29).

The condition $K_{1,3} = K_{3,1}$ to preserve the symmetry of the system means that $K_{3,1}u$ also contains $qu_{,xx}+ru_{,yy}$. Moreover, the assumption that $K_{3,1}u+K_{3,3}a=0$ from the third equation of the matrix is based on Equation (5.31) leads to $K_{3,1}u{=}qu_{,xx}+ru_{,yy}-\frac{p}{l^2}u$ and $K_{3,3}=-\frac{p}{sl^2}a$ where $\{p/q/r\}$ has the same ratio as $\{s/m/n\}$. This discussion can be presented as following:

$$\begin{cases} K_{3,1} = K_{1,3} \\ K_{1,3}a \text{ has} qa_{xx} + ra_{,yy} \\ K_{3,1}u + K_{3,3}a \sim \dfrac{su - ml^2u_{,xx} - nl^2u_{,yy} - a}{l^2} = 0 \end{cases} \Rightarrow \begin{cases} K_{1,3}a = \left(-\dfrac{p}{l^2}a + qa_{,xx} + ra_{,yy}\right) \\ K_{3,1}u = \left(-\dfrac{p}{l^2}u + qu_{,xx} + ru_{,yy}\right) \\ \forall \{p/q/r\} = \{s/m/n\} \end{cases}$$

Therefore, the following relationships are obtained:

$$\begin{cases} \dfrac{m}{s} = \dfrac{q}{p} \rightarrow m = \dfrac{sq}{p} \rightarrow qm = q^2\dfrac{s}{p} = \dfrac{45}{4} + 10H \\ \dfrac{n}{s} = \dfrac{q}{p} \rightarrow n = \dfrac{sr}{p} \rightarrow rn = r^2\dfrac{s}{p} = \dfrac{5}{4} + 10H \end{cases} \tag{5.35}$$

And the constants have their values with respect to H:

$$\frac{s}{p} = t; q = \sqrt{\frac{1}{t}\left(\frac{45}{4} + 10H\right)}; r = \sqrt{\frac{1}{t}\left(\frac{5}{4} + 10H\right)}; m = \sqrt{t\left(\frac{45}{4} + 10H\right)}; n = \sqrt{t\left(\frac{5}{4} + 10H\right)} \tag{5.36}$$

One can apply the same procedure to the auxiliary variable b:

$$\left.\begin{aligned}\varpi\mu &= \varpi^2\frac{\varsigma}{\pi} = \frac{15}{42} - 90H\\ \vartheta\nu &= \vartheta^2\frac{\varsigma}{\pi} = \frac{5}{12} + 10H\end{aligned}\right\} \Rightarrow \begin{cases}\varpi = \sqrt{\frac{1}{\tau}\left(\frac{15}{4} - 90H\right)}\;;\; \vartheta = \sqrt{\frac{1}{\tau}\left(\frac{5}{12} + 10H\right)}\;;\frac{\varsigma}{\pi} = \tau;\\ \mu = \sqrt{\tau\left(\frac{15}{4} - 90H\right)};\nu = \sqrt{\tau\left(\frac{5}{12} + 10H\right)}\end{cases} \tag{5.37}$$

With a suitable value of H, the auxiliary variables can be rewritten with respect to t, τ, s and ς from Equation (5.31) and (5.32) as:

$$a = su - \sqrt{t\left(\frac{45}{4} + 10H\right)}l^2u_{,xx} - \sqrt{t\left(\frac{5}{4} + 10H\right)}l^2u_{,yy} \tag{5.38}$$

$$b = \varsigma v - \sqrt{\tau\left(\frac{15}{4} - 90H\right)}l^2v_{,xx} - \sqrt{\tau\left(\frac{5}{12} + 10H\right)}l^2v_{,yy} \tag{5.39}$$

However, for a clear presentation, the more symbolic set of Equations (5.31) and (5.32) shall be displayed for the rest of the derivation. Further variations of Equations (5.31) and (5.32) are:

$$u = \frac{a}{s} + \frac{m}{s}l^2u_{,xx} + \frac{n}{s}l^2u_{,yy} \tag{5.40}$$

$$v = \frac{b}{\varsigma} + \frac{\mu}{\varsigma}l^2v_{,xx} + \frac{\nu}{\varsigma}l^2v_{,yy} \tag{5.41}$$

and

$$\frac{E}{t}s\frac{su - ml^2u_{,xx} - nl^2u_{,yy} - a}{l^2} = \frac{E}{t}s\left(-\frac{a}{l^2} + s\frac{u}{l^2} - mu_{,xx} - nu_{,yy}\right) = 0 \tag{5.42}$$

$$\frac{E}{\tau}\varsigma\frac{\varsigma v - \mu l^2v_{,xx} - \nu l^2v_{,yy} - b}{l^2} = \frac{E}{\tau}\varsigma\left(-\frac{b}{l^2} + \varsigma\frac{v}{l^2} - \mu v_{,xx} - \nu v_{,yy}\right) = 0 \tag{5.43}$$

After defining the auxiliary variables in preparation of the Ru-Aifantis theorem application, the left hand side of Equation (5.29) is modified by rewriting $320\rho\ddot{u}$ using Equation

(5.40) and introducing $m\rho l^2\ddot{u}_{xx}$ and $n\rho l^2\ddot{u}_{yy}$ into the equation:

$$\begin{aligned}
LHS &= 320\rho\ddot{u} - \left(15+\frac{160}{3}H\right)\rho l^2\ddot{u}_{,yy} - (160H+40)\,\rho l^2\ddot{u}_{,xx} + (5+320H)\,\rho l^2\ddot{v}_{,xy} \\
&= \underbrace{\left(\rho\ddot{a}+m\rho l^2\ddot{u}_{,xx}+n\rho l^2\ddot{u}_{,yy}\right)}_{320\rho\ddot{u}}\underbrace{-m\rho l^2\ddot{u}_{,xx}-n\rho l^2\ddot{u}_{,yy}}_{\text{new terms added}} + \left(\underbrace{n}_{\text{new}}-15-\frac{160}{3}H\right)\rho l^2\ddot{u}_{,yy} \\
&\quad + \left(\underbrace{m}_{\text{new}}-160H-40\right)\rho l^2\ddot{u}_{,xx} + (5+320H)\,\rho l^2\ddot{v}_{,xy} \\
&= \rho\ddot{a} - m\rho l^2\ddot{u}_{,xx} - n\rho l^2\ddot{u}_{,yy} + \left(2n-15-\frac{160}{3}H\right)\rho l^2\ddot{u}_{,yy} + (2m-160H-40)\,\rho l^2\ddot{u}_{,xx} \\
&\quad + (5+320H)\,\rho l^2\ddot{v}_{,xy}
\end{aligned}$$

The terms $-m\rho l^2\ddot{u}_{xx}$ and $-n\rho l^2\ddot{u}_{yy}$ are then rewritten using Equation (5.40):

$$\begin{aligned}
LHS &= \rho\ddot{a} - m\rho l^2\left(\frac{1}{s}\ddot{a}_{,xx}+\frac{1}{s}ml^2\ddot{u}_{,xxxx}+\frac{1}{s}nl^2\ddot{u}_{,xxyy}\right) - n\rho l^2\left(\frac{1}{s}\ddot{a}_{,yy}+\frac{1}{s}ml^2\ddot{u}_{,xxyy}+\frac{1}{s}nl^2\ddot{u}_{,yyyy}\right) \\
&\quad + \left(2n-15-\frac{160}{3}H\right)\rho l^2\ddot{u}_{,yy} + (2m-160H-40)\,\rho l^2\ddot{u}_{,xx} + (5+320H)\,\rho l^2\ddot{v}_{,xy}
\end{aligned} \tag{5.44}$$

It is acceptable to ignore all $O\left(l^4\right)$ terms because:

- The lengthscale l of each beam in microlattice materials is very small.
- Hence, the numerical coefficient of $-\mathrm{O}\left(l^4\ddot{u}_{ijkl}\right)$ terms are considerably much smaller than $\mathrm{O}\left(l^2\ddot{u}_{,ij}\right)$.

Finally, the left hand side of Equation (5.29) (or Equation (5.44)) is approximated as:

$$\begin{aligned}
LHS = \rho l^2 &\left[(2m-160H-40)\,\ddot{u}_{,xx} + \left(2n-15-\frac{160}{3}H\right)\ddot{u}_{,yy}\right] \\
&+ (5+320H)\,\rho l^2\ddot{v}_{,xy} + \rho\left[\ddot{a} - \frac{1}{s}ml^2\ddot{a}_{,xx} - \frac{1}{s}nl^2\ddot{a}_{,yy}\right]
\end{aligned} \tag{5.45}$$

Next, the right hand side of Equation (5.29) is modified; the fourth order derivatives $\mathscr{X}_{iiii}$

are replaced by using Equation (5.40):

$$RHS = E\left(180u_{,xx} + 60u_{,yy} + 120v_{,xy}\right) + El^2\left(\frac{15}{2} + 60H\right)u_{,xxyy} - El^2\left(\underbrace{\left(\frac{45}{4} + 10H\right)}_{qm}u_{,xxxx} + \underbrace{\left(\frac{5}{4} + 10H\right)}_{rn}u_{,yyyy}\right) \tag{5.46}$$

$$RHS = E\left(180u_{,xx} + 60u_{,yy} + 120v_{,xy}\right) + \left(\frac{15}{2} + 60H\right)El^2u_{,xxyy} + E\left(qa_{,xx} - qsu_{,xx} + qnl^2u_{,xxyy}\right) + E\left(ra_{,yy} - rsu_{,yy} + rml^2u_{,xxyy}\right) \tag{5.47}$$

Equation (5.42) is then added to the right hand side:

$$RHS = E\left[180u_{,xx} + 60u_{,yy} + 120v_{,xy} + qa_{xx} + ra_{,yy} - qsu_{,xx} - rsu_{,yy} + (qn + rm)l^2u_{,xxyy}\right] + \left(\frac{15}{2} + 60H\right)l^2u_{,xxyy} + \underbrace{\frac{E}{t}s\left(-\frac{a}{l^2} + s\frac{u}{l^2} - mu_{,xx} - nu_{,yy}\right)}_{=0} \tag{5.48}$$

$$RHS = E\left[\begin{array}{l}\frac{s^2}{t}\frac{u}{l^2} + \left(180 - qs - \frac{sm}{t}\right)u_{,xx} + \left(60 - rs - \frac{sn}{t}\right)u_{,yy} \\ + \left(qn + rm + \frac{15}{2} + 60H\right)l^2u_{,xxyy}\end{array}\right] + E120v_{,xy} + E\left(qa_{,xx} + ra_{,yy} - \frac{sa}{tl^2}\right) \tag{5.49}$$

Similarly the same procedure is applied to both sides of Equation (5.30). First one consid-

ers the left hand side of Equation (5.30):

$$LHS = 320\rho\ddot{v} - (55+480H)\,\rho l^2 \ddot{v}_{,xx} - \left(160H+\frac{40}{3}\right)\ddot{v}_{,yy} + (320H+5)\,\rho l^2 \ddot{u}_{,xy} \tag{5.50}$$

$$= \rho\left(\ddot{b} + \mu l^2 \ddot{v}_{,xx} + \nu l^2 \ddot{v}_{,yy}\right) - \mu\rho l^2 \ddot{v}_{,xx} - \nu\rho l^2 \ddot{v}_{,yy} + \left(\nu - \left(160H+\frac{40}{3}\right)\right)\rho l^2 \ddot{v}_{,,yy} \tag{5.51}$$

$$+ (\mu - (55+480H))\,\rho l^2 \ddot{v}_{,xx} + (320H+5)\,\rho l^2 \ddot{u}_{,xy}$$

$$= \rho\ddot{b} - \mu\rho l^2\left(\ddot{b}_{,xx} + \mu l^2 \ddot{v}_{,xxxx} + \nu l^2 \ddot{v}_{,xxyy}\right) - \nu\rho l^2\left(\ddot{b}_{,yy} + \mu l^2 \ddot{v}_{,xxyy} + \nu l^2 \ddot{v}_{,yyyy}\right) \tag{5.52}$$

$$+ \left(2\nu - 160H - \frac{40}{3}\right)\rho l^2 \ddot{v}_{,yy} + (2\mu - 55 - 480H)\,\rho l^2 \ddot{v}_{,xx} + (320H+5)\,\rho l^2 \ddot{u}_{,xy}$$

$$\approx (320H+5)\,\rho l^2 \ddot{u}_{,xy} + \left(2\nu - 160H - \frac{40}{3}\right)\rho l^2 \ddot{v}_{,yy} + (2\mu - 55 - 480H)\,\rho l^2 \ddot{v}_{,xx}$$

$$+ \rho\left(\ddot{b} - \mu l^2 \ddot{b}_{,xx} - \nu l^2 \ddot{b}_{,yy}\right) \tag{5.53}$$

Thus the right hand side of Equation (5.30) is modified in the following steps:

$$\begin{aligned} RHS =& E\left(20v_{,yy} + 60v_{,xx} + 120u_{,xy}\right) \\ &+ El^2\left(-\left(\frac{5}{12}+10H\right)v_{,yyyy} - \left(\frac{15}{4}+90H\right)v_{,xxxx} + \left(\frac{5}{2}-20H\right)v_{,xxyy}\right) \\ =& E\left(20v_{,yy} + 60v_{,xx} + 120u_{,xy}\right) + E\left(\frac{5}{2}-20H\right)l^2 v_{,xxyy} + E\left(\varpi b_{,xx} - \varpi\varsigma v_{,xx} + \varpi\nu l^2 v_{,xxyy}\right) \\ &+ E\left(\vartheta b_{,yy} - \vartheta\varsigma v_{,yy} + \vartheta\mu l^2 v_{,xxyy}\right) \end{aligned} \tag{5.54}$$

$$\begin{aligned} RHS =& E\left(\begin{array}{l} 20v_{,yy} + 60v_{,xx} + 120u_{,xy} + \varpi b_{,xx} + \vartheta b_{,yy} - \varpi\varsigma v_{,xx} - \vartheta\varsigma v_{,yy} \\ + \left(\varpi\nu + \vartheta\mu + \frac{5}{2} - 20H\right)l^2 v_{,xxyy} \end{array}\right) \\ &+ \frac{E}{\tau}\varsigma\left(-\frac{b}{l^2} + \varsigma\frac{v}{l^2} - \mu v_{,xx} - \nu v_{,yy}\right) \\ =& E\left[120u_{,xy} + \frac{\varsigma^2}{\tau}\frac{v}{l^2} + \left(60 - \varsigma\varpi - \frac{\varsigma\mu}{\tau}\right)v_{,xx} + \left(20 - \varsigma\vartheta - \frac{\varsigma\nu}{\tau}\right)v_{,yy}\right] \\ &+ E\left(\varpi\nu + \vartheta\mu + \frac{5}{2} - 20H\right)l^2 v_{,xxyy} + E\left(-\varsigma\left(\frac{b}{\tau l^2}\right) + \varpi b_{,xx} + \vartheta b_{,yy}\right) \end{aligned} \tag{5.55}$$

Therefore, to be able to use the Ru-Aifantis theorem, Equations (5.29) and (5.30) are

modified into:

$$\begin{aligned}
&\rho l^2\left[(2m-160H-40)\,\ddot{u}_{,xx}+\left(2n-15-\frac{160}{3}H\right)\ddot{u}_{,yy}\right]\\
&\qquad+(5+320H)\,\rho l^2\ddot{v}_{,xy}+\rho\left(\ddot{a}-\frac{m}{s}l^2\ddot{a}_{,xx}-\frac{n}{s}l^2\ddot{a}_{,yy}\right)\\
=&E\left[s^2\frac{u}{tl^2}+\left(180-qs-\frac{sm}{t}\right)u_{,xx}+\left(60-rs-\frac{sn}{t}\right)u_{,yy}+\left(qn+rm+\frac{15}{2}+60H\right)l^2u_{,xxyy}\right]\\
&+E120v_{,xy}+E\left[qa_{,xx}+ra_{,yy}-s\frac{a}{tl^2}\right]
\end{aligned}\tag{5.56}$$

$$\begin{aligned}
&(320H+5)\,\rho l^2\ddot{u}_{,xy}+\left(2\nu-160H-\frac{40}{3}\right)\rho l^2\ddot{v}_{,yy}\\
&\qquad+(2\mu-55-480H)\,\rho l^2\ddot{v}_{,xx}+\rho\left(\ddot{b}-\frac{\mu}{\varsigma}l^2\ddot{b}_{,xx}-\frac{\nu}{\varsigma}l^2\ddot{b}_{,yy}\right)\\
=&E\left[120u_{,xy}+\varsigma^2\frac{v}{\tau l^2}+\left(60-\varsigma\varpi-\frac{\varsigma\mu}{\tau}\right)v_{,xx}+\left(20-\varsigma\vartheta-\frac{\varsigma\nu}{\tau}\right)v_{,yy}\right]\\
&+E\left(\varpi\nu+\vartheta\mu+\frac{5}{2}-20H\right)l^2v_{,xxyy}+E\left[-\varsigma\left(\frac{b}{\tau l^2}\right)+\varpi b_{,xx}+\vartheta b_{,yy}\right]
\end{aligned}\tag{5.57}$$

And the other two equations to form the symmetric matrices are as follows; note that two sides of the equations below are identities of Equations (5.38) and (5.39):

$$\rho\left[\ddot{u}-\frac{1}{s}ml^2\ddot{u}_{,xx}-\frac{1}{s}nl^2\ddot{u}_{,yy}\right]-\frac{1}{s}\rho\ddot{a}=\frac{E}{t}\left[-s\frac{u}{l^2}+mu_{,xx}+nu_{,yy}\right]+\frac{E}{tl^2}a \tag{5.58}$$

$$\rho\left[\ddot{v}-\frac{1}{\varsigma}\mu l^2\ddot{v}_{,xx}-\frac{1}{\varsigma}\upsilon l^2\ddot{v}_{,yy}\right]-\frac{\rho\ddot{b}}{\varsigma}=\frac{E}{\tau}\left[-\varsigma\frac{v}{l^2}+\mu v_{,xx}+\nu v_{,yy}\right]+\frac{E}{\tau l^2}b \tag{5.59}$$

The four equations (5.56), (5.57), (5.58) and (5.59) are the equations of motion of the gradient continuum modified by Ru-Aifantis theorem.

If we choose a set of numeric values: $s=2$, $p=\frac{10240}{891}$, $q=\frac{2}{3}$, $r=\frac{2}{9}$, $m=\frac{297}{16}$, $n=\frac{99}{16}$, $\varsigma=2$, $\pi=\frac{10240}{891}$, $\varpi=\frac{2}{3}$, $\vartheta=\frac{2}{9}$, $\mu=\frac{297}{16}$, $\nu=\frac{99}{16}$ and $H=10$, we have the following equations of motion:

$$\begin{aligned}
&\rho l^2\left[-\frac{39}{8}\ddot{u}_{,xx}-\frac{79}{24}\ddot{u}_{,yy}\right]+9\rho l^2\ddot{v}_{,xy}+\rho\left(\ddot{a}-\frac{297}{5120}l^2\ddot{a}_{,xx}-\frac{99}{5120}l^2\ddot{a}_{,yy}\right)\\
=&E\left[\frac{3276800}{891}\frac{u}{l^2}-\frac{740}{3}u_{,xx}-\frac{740}{9}u_{,yy}+\frac{33}{2}l^2u_{,xxyy}\right]\\
&+E120v_{,xy}+E\left[\frac{2}{3}a_{,xx}+\frac{2}{9}a_{,yy}-\frac{10240}{891}\frac{a}{l^2}\right]
\end{aligned}\tag{5.60}$$

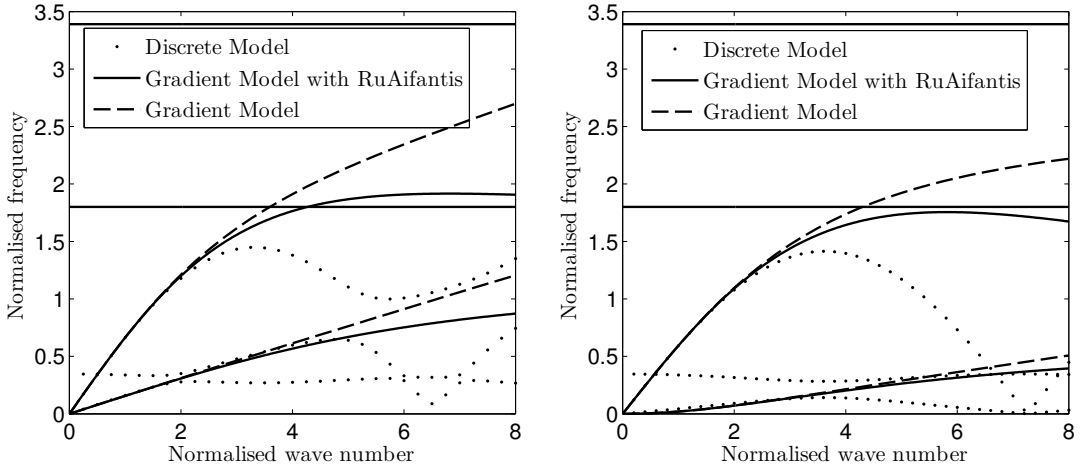

(a) $\pi/4$ (b) $\pi/3$

Fig. 5.6 Dispersion analysis for the gradient continuum with Ru-Aifantis theory compared with original gradient continuum and discrete models at propagation angles of $\pi/4$ and $\pi/3$. The normalised wave number has the formula of kl, the normalised frequency $\dfrac{\omega}{c_e}$. For each model, there are two curves, the lower curve represents the shear component and the higher curve represents the compression component.

$$\begin{aligned} &9\rho l^2\ddot{u}_{,xy} - \frac{17}{24}\rho l^2\ddot{v}_{,yy} - \frac{137}{8}\rho l^2\ddot{v}_{,xx} + \rho\left(\ddot{b} - \frac{351}{5120}l^2\ddot{b}_{,xx} - \frac{117}{5120}l^2\ddot{b}_{,yy}\right) \\ =&E\left[120u_{,xy} + \frac{3276800}{3159}\frac{v}{l^2} - \frac{740}{9}v_{,xx} - \frac{740}{27}v_{,yy}\right] \\ &+E\frac{11}{2}v_{,xxyy} + E\left[-\frac{10240}{3159}\left(\frac{b}{l^2}\right) + \frac{2}{9}b_{,xx} + \frac{2}{27}b_{,yy}\right] \end{aligned} \tag{5.61}$$

$$\rho\left[\ddot{u} - \frac{297}{5120}l^2\ddot{u}_{,xx} - \frac{99}{5120}l^2\ddot{u}_{,yy}\right] - \frac{1}{320}\rho\ddot{a} = E\left[-\frac{10240}{891}\frac{u}{l^2} + \frac{2}{3}u_{,xx} + \frac{2}{9}u_{,yy}\right] + \frac{32}{891}\frac{E}{l^2}a \tag{5.62}$$

$$\rho\left[\ddot{v} - \frac{351}{5120}l^2\ddot{v}_{,xx} - \frac{117}{5120}l^2\ddot{v}_{,yy}\right] - \frac{1}{320}\rho\ddot{b} = E\left[-\frac{10240}{3159}\frac{v}{l^2} + \frac{2}{9}v_{,xx} + \frac{2}{27}v_{,yy}\right] + \frac{32}{3159}\frac{E}{l^2}b \tag{5.63}$$

In Figure 5.6, the gradient model has four curves for the four variables u, v, a and b. The curves for the variables a and b are straight lines and their positions can be changed by changing the values of the arbitrary constants in the application of the Ru-Aifantis theorem. It

is preferred that the positions of the curves for these two auxiliary variables a and b are lower than the maximum frequency of the compression curve because then the numerical critical time step for this continuum depends only on the compression curve.

5.2.5 Summary of steps to implement the Ru-Aifantis theorem for the gradient continuum

The above section explains in details the implementation of the Ru-Aifantis theorem to reduce the continuity requirements when the continuum is applied to finite element models. This section summaries simplifying steps to implement the Ru-Aifantis theorem on a stable gradient continuum.

1. Step 1: From the equations of motion of the newly derived stable continuum (for e.g. Equations (5.27) and (5.28)), we extract the coefficients of the two equations. If we call the first equation of motion for equilibrium in x-direction (for e.g. Equation (5.27)) $Eqn1$ and the second equation of motion for equilibrium in y-direction (for e.g. Equation (5.28)) $Eqn2$, and the function to get the coefficient of a term x in an Equation X as $coeff(X,x)$, we can define the following variables from the coefficients of the two equations as follows:

   From $Eqn1$:

$$M_{TT1} = \frac{coeff(Eqn1,\ddot{u})}{\rho}; \qquad M_{YY1} = \frac{coeff(Eqn1,\ddot{u}_{,yy})}{\rho L^2} \tag{5.64}$$

$$M_{XX1} = \frac{coeff(Eqn1,\ddot{u}_{,xx})}{\rho L^2}; \qquad M_{XY1} = \frac{coeff(Eqn1,\ddot{v}_{,xy})}{\rho L^2} \tag{5.65}$$

$$S_{XX1} = \frac{coeff(Eqn1,u_{,xx})}{E}; \qquad S_{YY1} = \frac{coeff(Eqn1,u_{,yy})}{E} \tag{5.66}$$

$$S_{XY1} = \frac{coeff(Eqn1,v_{,xy})}{E}; \qquad S_{XXXX1} = \frac{coeff(Eqn1,u_{,xxxx})}{EL^2} \tag{5.67}$$

$$S_{XXYY1} = \frac{coeff(Eqn1,u_{,xxyy})}{EL^2}; \qquad S_{YYYY1} = \frac{coeff(Eqn1,u_{,yyyy})}{EL^2} \tag{5.68}$$

From $Eqn2$:

$$M_{TT2} = \frac{coeff(Eqn2, \ddot{v})}{\rho}; \qquad M_{YY2} = \frac{coeff(Eqn2, \ddot{v}_{,yy})}{\rho L^2} \tag{5.69}$$

$$M_{XX2} = \frac{coeff(Eqn2, \ddot{v}_{,xx})}{\rho L^2}; \qquad M_{XY2} = \frac{coeff(Eqn2, \ddot{u}_{,xy})}{\rho L^2} \tag{5.70}$$

$$S_{XX2} = \frac{coeff(Eqn2, v_{,xx})}{E}; \qquad S_{YY2} = \frac{coeff(Eqn2, v_{,yy})}{E} \tag{5.71}$$

$$S_{XY2} = \frac{coeff(Eqn2, u_{,xy})}{E}; \qquad S_{XXXX2} = \frac{coeff(Eqn2, v_{,xxxx})}{EL^2} \tag{5.72}$$

$$S_{XXYY2} = \frac{coeff(Eqn2, v_{,xxyy})}{EL^2}; \qquad S_{YYYY2} = \frac{coeff(Eqn2, v_{,yyyy})}{EL^2} \tag{5.73}$$

2. Step 2: Given the variables from Step 1, we can calculate the variables which help facilitate the Ru-Aifantis theorem that are mentioned in Section 5.2.4. Note that t_1, s_1, p_1, q_1, r_1, m_1, n_1 in this section are similar to t, s, p, q, r, m, n in the Section 5.2.4, and t_2, s_2, p_2, q_2, r_2, m_2, n_2 are similar to τ, ς, π, ϖ, ϑ, μ, ν. But they are not the same because the equations of motion used in this section has not been multiplied by a factor of 160 for presentation purpose.

   Firstly, we need to choose initial values for t_1 which for simplication can be a common factor of both S_{XXXX1} and S_{YYYY1}, t_2 which can be a common factor of both S_{XXXX1} and S_{YYYY1} and trial values for s_1 and s_2. After we choose a value for t_1 and s_1, the other variables can be calculated with respect to t_1 and s_1:

$$p_1 = \frac{s_1}{t_1}; \qquad q_1 = \sqrt{\frac{S_{XXXX1}}{t_1}}; \qquad r_1 = \sqrt{\frac{S_{YYYY1}}{t_1}} \tag{5.74}$$

$$m_1 = \sqrt{t_1 S_{XXXX1}}; \qquad n_1 = \sqrt{t_1 S_{YYYY1}} \tag{5.75}$$

   After we choose a value for t_2 and s_2, the other variables can be calculated with respect to t_1 and s_1:

$$p_1 = \frac{s_2}{t_2}; \qquad q_1 = \sqrt{\frac{S_{XXXX2}}{t_2}}; \qquad r_1 = \sqrt{\frac{S_{YYYY2}}{t_2}} \tag{5.76}$$

$$m_1 = \sqrt{t_2 S_{XXXX2}}; \qquad n_1 = \sqrt{t_2 S_{YYYY2}} \tag{5.77}$$

3. Step 3: We use the variables from step 1 and step 2 to rewrite the two original equa-

tions of motion of the stable continuum (for e.g. (5.27) and (5.28)) into four following equations:

$$\begin{aligned}
&\rho l^2\left[-\left(\frac{M_{TT1}}{s_1}m_{xx1}+m_{xx1}-M_{XX1}\right)\ddot{u}_{,xx}-\left(\frac{M_{TT1}}{s_1}n_{yy1}+n_{yy1}-M_{YY1}\right)\ddot{u}_{,yy}\right]+M_{XY1}\rho l^2\ddot{v}_{,xy}\\
&+\rho\left(\left(\frac{M_{TT1}}{s_1}\right)\ddot{a}-\left(\frac{M_{TT1}}{s_1}\frac{m_{xx1}}{s_1}\right)l^2\ddot{a}_{,xx}-\left(\frac{M_{TT1}}{s_1}\frac{n_{yy1}}{s_1}\right)l^2\ddot{a}_{,yy}\right)\\
=&E\left[(p_1s_1)\frac{u}{l^2}-(q_1s_1+p_1m_1-S_{XX1})u_{,xx}-(r_1s_1+p_1n_1-S_{YY1})u_{,yy}\right]\\
&+E\left[(r_1m_1+q_1n_1+S_{XXYY1})l^2u_{,xxyy}\right]\\
&+S_{XY1}Ev_{,xy}+E\left[q_1a_{,xx}+r_1a_{,yy}-p_1\frac{a}{l^2}\right]
\end{aligned}\tag{5.78}$$

$$\begin{aligned}
&M_{XY2}\rho l^2\ddot{u}_{,xy}-\left(\frac{M_{TT2}}{s_2}n_{yy2}+n_{yy2}-M_{YY2}\right)\rho l^2\ddot{v}_{,yy}-\left(\frac{M_{TT2}}{s_2}m_{xx2}+m_{xx2}-M_{XX2}\right)\rho l^2\ddot{v}_{,xx}\\
&+\rho\left(\left(\frac{M_{TT2}}{s_2}\right)\ddot{b}-\left(\frac{M_{TT2}}{s_2}\frac{m_{xx2}}{s_2}\right)l^2\ddot{b}_{,xx}-\left(\frac{M_{TT2}}{s_2}\frac{n_{yy2}}{s_2}\right)l^2\ddot{b}_{,yy}\right)\\
=&E\left[S_{XY2}u_{,xy}+(p_2s_2)\frac{v}{l^2}-(q_2s_2+p_2m_2-S_{XX2})v_{,xx}-(r_2s_2+p_2n_2-S_{YY2})v_{,yy}\right]\\
&+E(r_2m_2+q_2n_2+S_{XXYY2})v_{,xxyy}+E\left[-p_2\left(\frac{b}{l^2}\right)+q_2b_{,xx}+r_2b_{,yy}\right]
\end{aligned}\tag{5.79}$$

$$\rho\left[\ddot{u}-\frac{m_1}{s_1}l^2\ddot{u}_{,xx}-\frac{n_1}{s_1}l^2\ddot{u}_{,yy}\right]-\frac{1}{s_1}\rho\ddot{a}=E\left[-p_1\frac{u}{l^2}+\frac{p_1}{s_1}m_1u_{,xx}+\frac{p_1}{s_1}n1u_{,yy}\right]+\frac{p_1}{s_1}\frac{E}{l^2}a\tag{5.80}$$

$$\rho\left[\ddot{v}-\frac{m_2}{s_2}l^2\ddot{v}_{,xx}-\frac{n_2}{s_2}l^2\ddot{v}_{,yy}\right]-\frac{1}{s_2}\rho\ddot{b}=E\left[-p_2\frac{v}{l^2}+\frac{p_2}{s2}m_2v_{,xx}+\frac{p_2}{s_2}n_2v_{,yy}\right]+\frac{p_2}{s_2}\frac{E}{l^2}b\tag{5.81}$$

After obtaining the four equations, dispersion analysis of the four equations should be checked for different angles of propagation. The values of t_1, t_2, s_1 and s_2 can be re-chosen and the three steps are iterated until the dispersion curves of the new continuum closely match the dispersion curves of the discrete model. The above three steps can be programmed using symbolic mathematic softwares to ease the procedure.

5.3 Space and time discretisation

As comparisons of the dispersion relations are made between the discrete model with the continuum models, it is important to note that, different from the continuum, the discrete model is discretised in space. Therefore, for better comparisons, the continuum is discretised first in space and then in time. Section 5.3.1 explains the choice of discretisation scheme and briefs the discretisation procedure with tables compiling dispersion relation graphs. Finally, numerical examples are built in the final section to demonstrate the practical application of the continuum.

5.3.1 Discretisation schemes and the discretisation procedure

As seen in the one-dimensional case of Section 3.4 and the square lattice case of Section 4.3.1, for space discretisation and time discretisation, to get the best match with the discrete model, the size of the numerical discretised element must be taken equal to be the structural length-scale l of the individual beam. Two common combinations for numerical implementations are the explicit scheme together with the lumped mass and the implicit scheme together with the consistent mass. We shall use an explicit scheme and the lumped mass to discretise the new continuum in this thesis. As the Ru-Aifantis theorem is used in Section 5.2.4 to modify the equations of motion to require only C^0 continuity, the set of Equations (5.50), (5.54), (5.56) and (5.57) can easily use the similar trial functions and space discretisation procedure to Section 4.3.2:

We discretise the equations of motion in space by using $u \approx \mathbf{Nu}$, $v \approx \mathbf{Nv}$, $a \approx \mathbf{Na}$ and $b \approx \mathbf{Nb}$ where $\mathbf{N}$ comprises the linear shape functions. Equations (4.23) and (4.24) are discretised in the matrix form, Ω is the element volume, ρ is the material density, E is the Young's modulus, l is the structural lengthscale:

$$\begin{bmatrix} \mathbf{M_{uu}} & \mathbf{M_{uv}} & \mathbf{M_{ua}} & 0 \\ \mathbf{M_{uv}} & \mathbf{M_{vv}} & 0 & \mathbf{M_{vb}} \\ \mathbf{M_{ua}} & 0 & \mathbf{M_{aa}} & 0 \\ 0 & \mathbf{M_{vb}} & 0 & \mathbf{M_{bb}} \end{bmatrix} \begin{bmatrix} \ddot{u} \\ \ddot{v} \\ \ddot{a} \\ \ddot{b} \end{bmatrix} + \begin{bmatrix} \mathbf{K_{uu}} & \mathbf{K_{uv}} & \mathbf{K_{ua}} & 0 \\ \mathbf{K_{uv}} & \mathbf{K_{vv}} & 0 & \mathbf{K_{vb}} \\ \mathbf{K_{ua}} & 0 & \mathbf{K_{aa}} & 0 \\ 0 & \mathbf{K_{vb}} & 0 & \mathbf{K_{bb}} \end{bmatrix} \begin{bmatrix} u \\ v \\ a \\ b \end{bmatrix} = \begin{bmatrix} f_u \\ f_v \\ 0 \\ 0 \end{bmatrix} \tag{5.82}$$

where

$$
\begin{aligned}
\mathbf{M}_{uu} &= -\int_\Omega \mathbf{N}_{,y}^T \left(2n - \frac{160}{3}H - 15\right)\rho l^2 \mathbf{N}_{,y} dV - \int_\Omega \mathbf{N}_{,x}^T (2m - 160H - 40)\rho l^2 \mathbf{N}_{,x} dV \\
\mathbf{M}_{vv} &= -\int_\Omega \mathbf{N}_{,x}^T (2\mu - 480H - 55)\rho l^2 \mathbf{N}_{,x} dV - \int_\Omega \mathbf{N}_{,y}^T \left(2\nu - 160H - \frac{40}{3}\right)\rho l^2 \mathbf{N}_{,y} dV \\
\mathbf{M}_{ua} &= \int_\Omega \mathbf{N}^T \rho \mathbf{N} dV + \int_\Omega \mathbf{N}_{,x}^T \frac{m}{s}\rho l^2 \mathbf{N}_{,x} dV + \int_\Omega \mathbf{N}_{,y}^T \frac{n}{s}\rho l^2 \mathbf{N}_{,y} dV \\
\mathbf{M}_{vb} &= \int_\Omega \mathbf{N}^T \rho \mathbf{N} dV + \int_\Omega \mathbf{N}_{,x}^T \frac{\mu}{\varsigma}\rho l^2 \mathbf{N}_{,x} dV + \int_\Omega \mathbf{N}_{,y}^T \frac{\nu}{\varsigma}\rho l^2 \mathbf{N}_{,y} dV \\
\mathbf{M}_{uv} &= -\int_\Omega \mathbf{N}_{,y}^T (5 + 320H)\rho l^2 \mathbf{N}_{,x} dV \\
\mathbf{M}_{aa} &= \int_\Omega \mathbf{N}^T \frac{\rho}{s}\mathbf{N} dV \\
\mathbf{M}_{bb} &= \int_\Omega \mathbf{N}^T \frac{\rho}{\varsigma}\mathbf{N} dV
\end{aligned}
\tag{5.83}
$$

$$
\begin{aligned}
\mathbf{K}_{uu} &= -\int_\Omega \mathbf{N}^T \frac{s^2}{tl^2} E\mathbf{N} dV + \int_\Omega \mathbf{N}_{,x}^T \left(180 - qs - \frac{sm}{t}sm\right) E\mathbf{N}_{,x} dV \\
&\quad + \int_\Omega \mathbf{N}_{,y}^T \left(60 - rs - \frac{sn}{t}\right) E\mathbf{N}_{,y} dV - \int_\Omega \mathbf{N}_{,xy}^T \left(qn + rm + \frac{15}{2} + 60H\right) El^2 \mathbf{N}_{,xy} dV \\
\mathbf{K}_{vv} &= -\int_\Omega \mathbf{N}^T \frac{\varsigma^2}{\tau l^2} E\mathbf{N} dV - \int_\Omega \mathbf{N}_{,y}^T \left(20 - \varsigma\vartheta - \frac{\varsigma\nu}{\tau}\right) E\mathbf{N}_{,y} dV + \int_\Omega \mathbf{N}_{,x}^T \left(60 - \varsigma\varpi - \frac{\varsigma\mu}{\tau}\right) E\mathbf{N}_{,x} dV \\
&\quad - \int_\Omega \mathbf{N}_{,y}^T \left(\varpi\nu + \vartheta\mu + \frac{5}{2} - 20H\right) El^2 \mathbf{N}_{,y} dV \\
\mathbf{K}_{ua} &= \int_\Omega \mathbf{N}^T \frac{s}{tl^2} E\mathbf{N} dV + \int_\Omega \mathbf{N}_{,y}^T rE\mathbf{N}_{,y} dV + \int_\Omega \mathbf{N}_{,xy}^T qE\mathbf{N}_{,xy} dV \\
\mathbf{K}_{vb} &= \int_\Omega \mathbf{N}^T \frac{\varsigma}{\tau l^2} E\mathbf{N} dV + \int_\Omega \mathbf{N}_{,y}^T \vartheta E\mathbf{N}_{,y} dV + \int_\Omega \mathbf{N}_{,xy}^T \varpi E\mathbf{N}_{,xy} dV \\
\mathbf{K}_{uv} &= \int_\Omega \mathbf{N}_{,x}^T 120E\mathbf{N}_{,y} dV
\end{aligned}
\tag{5.84}
$$

$$
\begin{aligned}
\mathbf{K}_{aa} &= -\int_\Omega \mathbf{N}^T \frac{E}{tl^2}\mathbf{N} dV \\
\mathbf{K}_{bb} &= -\int_\Omega \mathbf{N}^T \frac{E}{\tau l^2}\mathbf{N} dV
\end{aligned}
\tag{5.85}
$$

and from previous definitions, $q = \dfrac{m}{t}$, $r = \dfrac{n}{t}$, $\varpi = \dfrac{\mu}{\tau}$ and $\vartheta = \dfrac{\nu}{\tau}$.

Different from the square lattice, in this section, there are two element shapes chosen for spatial discretisation of the trapezium lattice: the rectangular and the diamond element shapes, see Figure 5.7. The dimensions of these shapes are chosen to best capture the smallest

wavelength for dispersion relations. The rectangular element is the main FEM shape to be analysed in Table 5.1 because of its versatility in real life applications. A comparison between the two shapes are presented in Table 5.2 with different propagation angles.

Besides, the central difference time scheme is used and analysed at this stage.

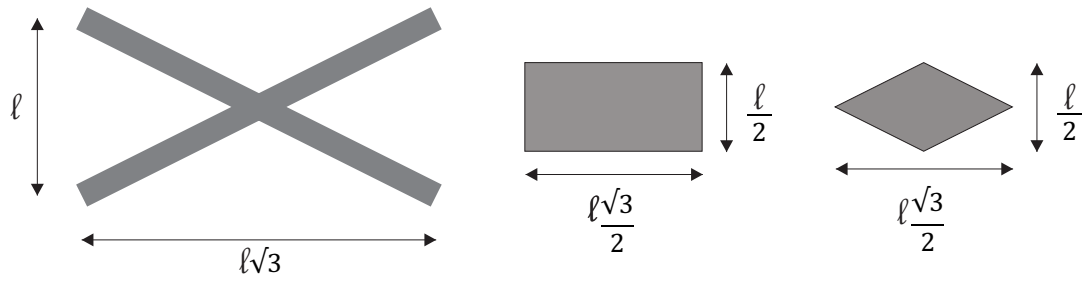

Fig. 5.7 From left to right: The original discrete model, the rectangular FEM shape and the diamond FEM shape

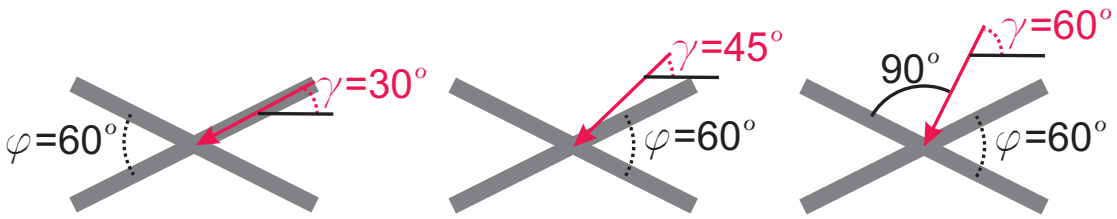

Fig. 5.8 Dispersion analysis for time and space (rectangle element) discretised gradient continuum

Table 5.2 implies that the diamond element of spatial discretisation captures the difficult wave propagation angle easier than the rectangular element.

5.4 Numerical example

The problem is set up as in Figure 5.9. A 2D beam with underlying trapezium microlattice is set up as in Figure 5.9a and the similar arrangement in discretised continuum form is depicted in Figure 5.9b. The discretised element length of the continuum model is equal to the microstructural lengthscale l. The discrete and continuum models are tested against each other. The shapes of the discrete model or the continuum model are all chosen such that the continuum model would be able to simulate similar boundary conditions to those of the discrete model. Forces of the Heavyside function over time, see Figure 3.5, are applied to the left end of the structures. The right-hand side of the structure is fixed. The vertical degrees of freedom

of all nodes are fixed. Therefore, the problem is predicted to behave as the one-dimensional case, see Figure 3.6.

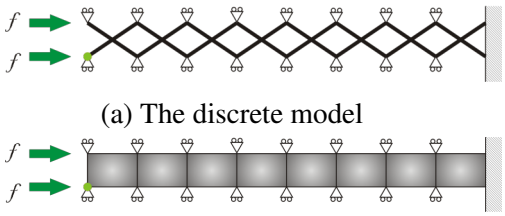

(a) The discrete model

(b) The continuum model

Fig. 5.9 Depiction of numerical problems for the trapezium lattice

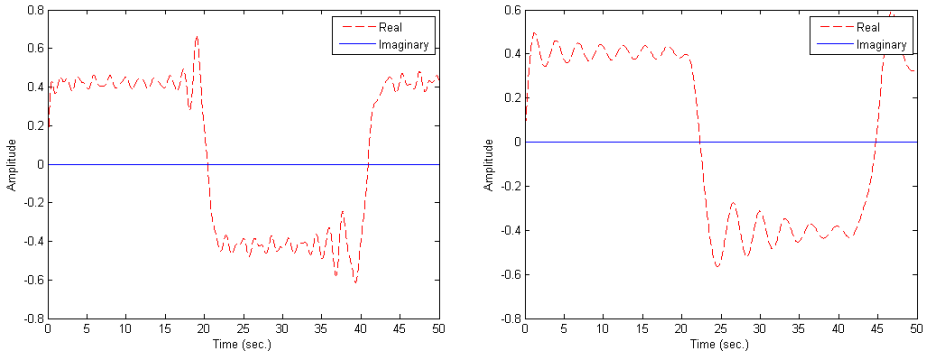

(a) The discrete model

(b) The gradient continuum model

Fig. 5.10 Numerical results for the trapezium lattice- The amplitudes in both graphs depict the horizontal displacement of the light green point in Figure 5.9a and Figure 5.9b, respectively, over time; the time step is 0.05

It is obvious that there would be differences between the two numerical results because the continuum model is limited in its ability to mimic the boundary conditions that are applied to the discrete models. However, in Figure 5.11 plotting both models on the same graph shows a good correspondence between the two models, where the time periods that the wave travels from one end to the other end in the two models are similar. The changing front slopes of the gradient continuum model indicates that there is dispersion.

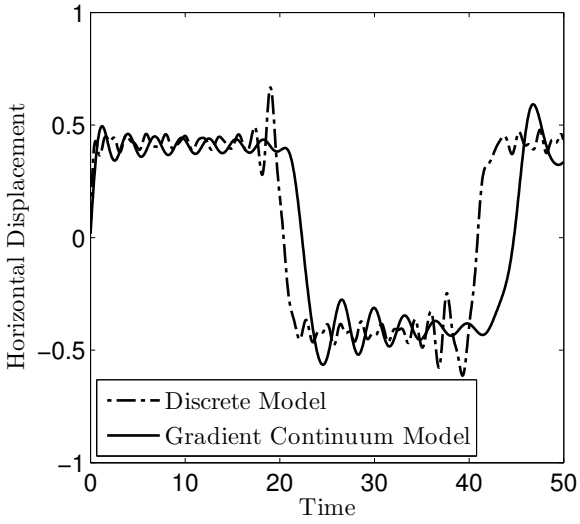

Fig. 5.11 Comparison of the discrete model and the gradient continuum model - Redraws of Figures 5.10a and 5.10b on the same graph.

Stage	Classical model	Gradient model
Continuum model	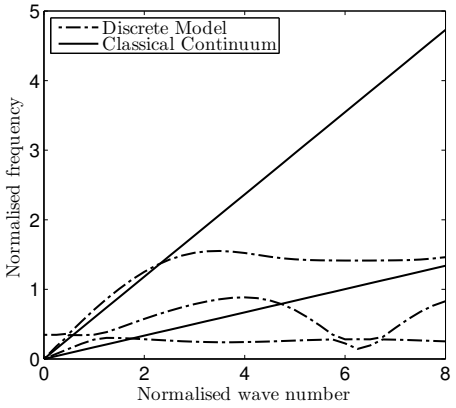	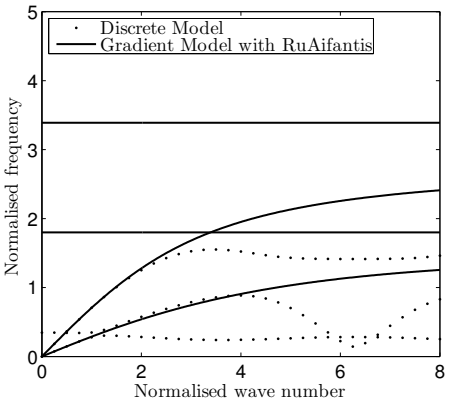
Discretised model in *space*	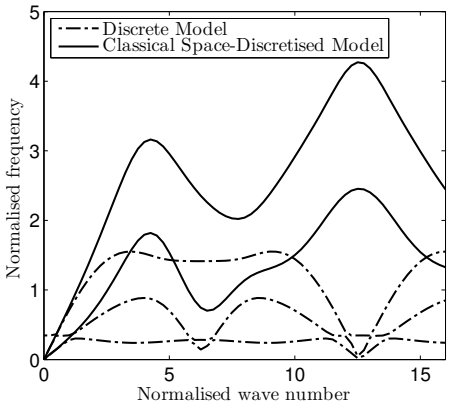	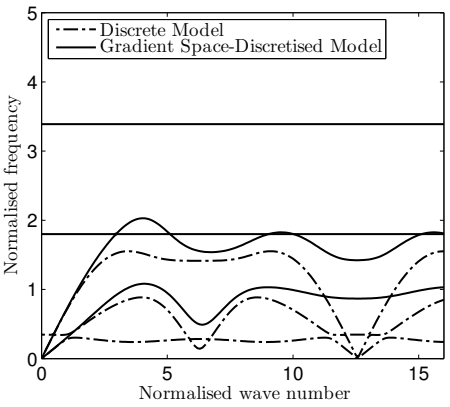
Discretised model in *space and time*	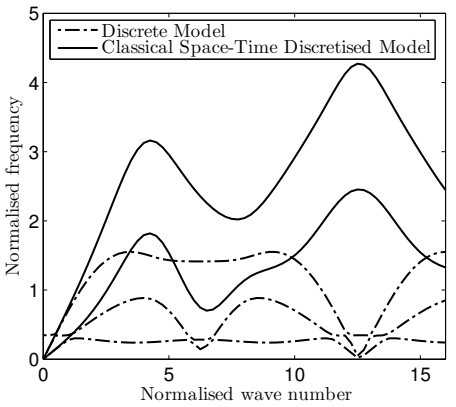	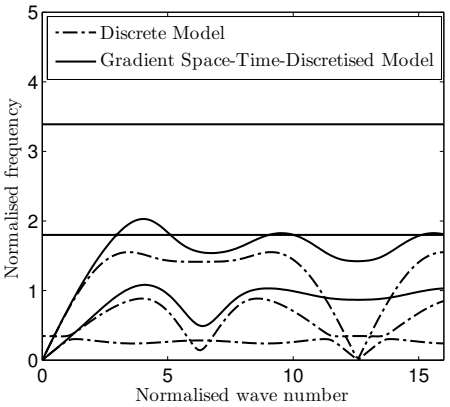

Table 5.1 Trapezium lattice - Comparison the dispersion behaviours of the classical and gradient model under different stages for $\gamma = \pi/6$ using rectangular finite element and time step $\frac{1}{10}$. The normalised wave number has the formula of kl, the normalised frequency $\dfrac{\omega}{c_e}$. For each model, there are two curves, the lower curve represents the shear component and the higher curve represents the compression component.

γ	**Rectangular element**	**Diamond element**
$\pi/6$	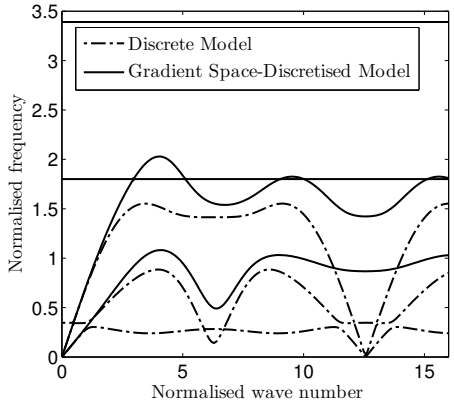	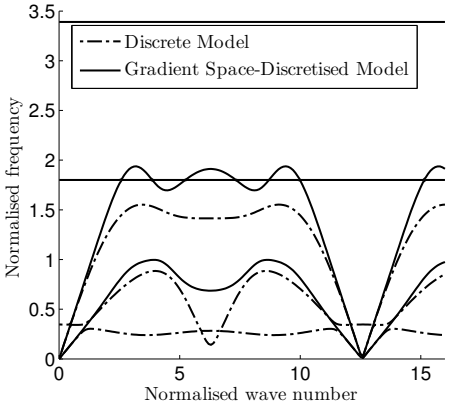
$\pi/4$	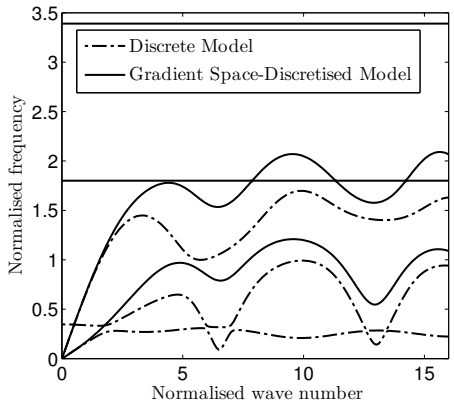	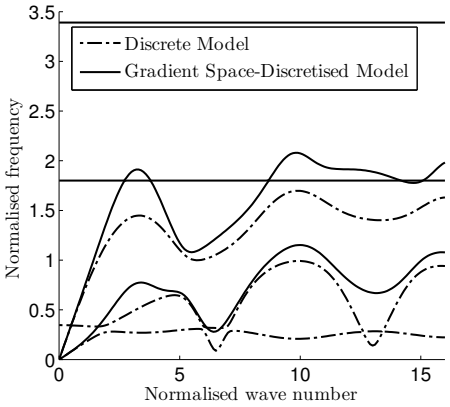
$\pi/3$	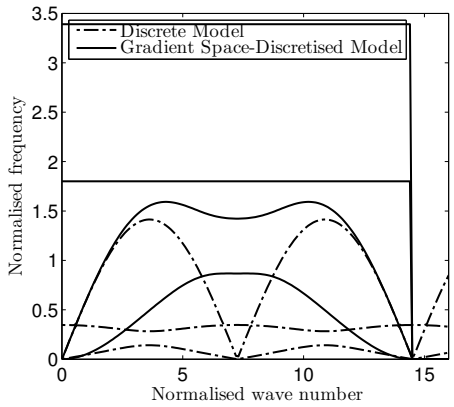	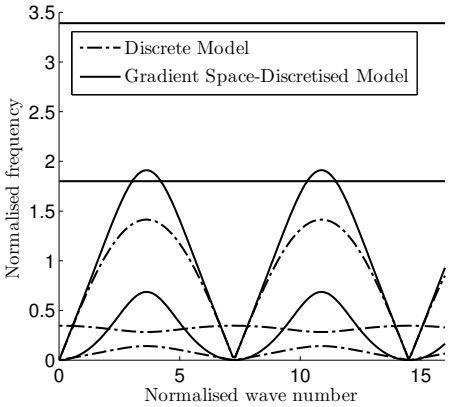

Table 5.2 Trapezium lattice - Comparison of the dispersion behaviours of space-discretised continuum using the rectangular and diagonal elements for different propagation angles γ. The normalised wave number has the formula of kl, the normalised frequency $\frac{\omega}{c_e}$. For each model, there are two curves, the lower curve represents the shear component and the higher curve represents the compression component.

Chapter 6

Wave propagation in the hexagonal lattices

The two-dimensional hexagonal lattice has a very practical application which is the graphite sheet. Compared with the square and trapezium lattices, the hexagonal lattice has a much more complicated geometry for deriving a gradient continuum. This chapter investigates the hexagonal lattice in the following order: the discrete model in Section 6.1, classical and gradient models in Section 6.2. There are no space and time discretised models in this section as no satisfactory FEM hexagonal shape is found in the literature.

6.1 Discrete model of the hexagonal lattice

In this section, the hexagonal lattice is first introduced in the discrete form and then dispersion analysis corresponding to the defined model is presented.

6.1.1 Definition of the hexagonal lattice

This section gives an overview definition of the hexagonal lattice in comparison with the square and trapezium lattice:

- Different from the square lattice in Section 4.1.1 and the trapezium lattice in Section 5.1.1 which have only one joint in the RVE, the hexagonal lattice requires further consideration of a representative volume element. The most simple RVE in the green area of Figure 6.2 are only symmetrical through a vertical line yy, while the second RVE in the yellow area of Figure 6.3 are symmetrical through both main axes but poses difficulties in generating the continuum in later sections. At the end, the new so-called "RVE"

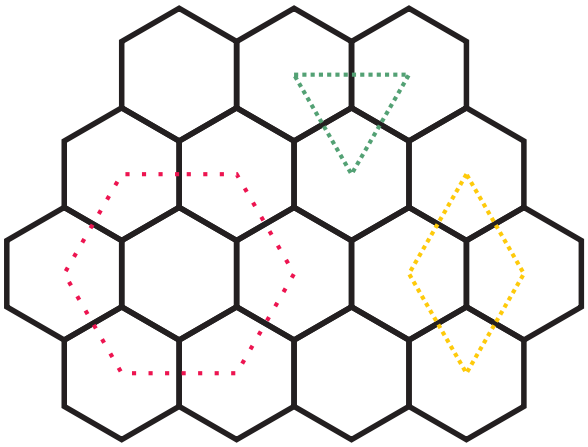

Fig. 6.1 Detailed diagram of a RVE of the hexagonal lattice

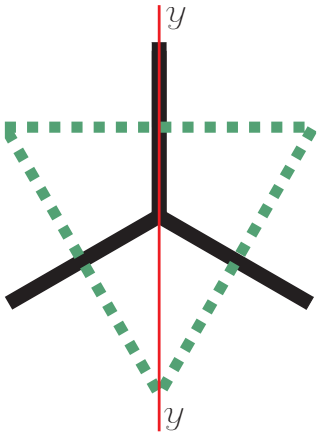

Fig. 6.2 Detailed diagram of a RVE 1 of the hexagonal lattice

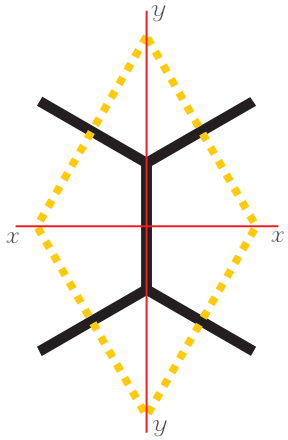

Fig. 6.3 Detailed diagram of a RVE 2 of the hexagonal lattice

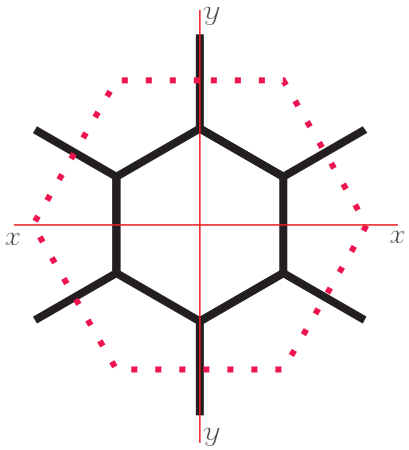

Fig. 6.4 Detailed diagram of a RVE 3 of the hexagonal lattice

in the area of the orange dotted line, see Figure 6.4 was chosen as the optimal model to observe the discrete behaviour and to generate continuum. For the hexagonal geometry, see Figure 6.1, the chosen representative volume element (RVE) requires six joints to ensure the symmetry for simple mathematical formulations, see Figure 6.4. This RVE of the microlattice is modelled as a rigid-joint network of twelve uniform beams having cross section A, length l, material density ρ and Young's modulus E.

- For simplicity, the mass matrix of the beam element is lumped as follows

$$\mathbf{M}^{(e)} = \frac{\rho A l}{2} diag\left(1, 1, \frac{1}{12l^2}, 1, 1, \frac{1}{12l^2}\right)$$

The beam stiffness matrix used is the common two-dimensional stiffness matrix of Euler-Bernoulli beam theory.

6.1.2 Dispersion analysis

The system of twelve beams in Figure 6.4 are chosen to carry out the dispersion analysis. The twelve nodes are numbered anti-clockwise as in Figure 6.5 and from the outer ring to the inner ring and have coordinates $(0,2l)$, $\left(-\sqrt{3}l,l\right)$, $\left(-\sqrt{3}l,-l\right)$, $(-2l,0)$, $\left(\sqrt{3}l,-l\right)$, $\left(\sqrt{3}l,-l\right)$, $(0,l)$, $\left(-\frac{\sqrt{3}l}{2},\frac{l}{2}\right)$, $\left(-\frac{\sqrt{3}l}{2},-\frac{l}{2}\right)$, $(0,-l)$, $\left(-\frac{\sqrt{3}l}{2},\frac{l}{2}\right)$ and $\left(\frac{\sqrt{3}l}{2},\frac{l}{2}\right)$. In this section, u_n and v_n describes the horizontal and vertical displacements of node number n; θ_n stands for the rotation, a_n, b_n and c_n for horizontal, vertical and rotational accelerations. With the mass matrices M and stiffness matrices K defined in Equations (4.1) and (4.2) for each beam of length l, the term $M\overline{a}+K\overline{u}$ can be written where $\overline{a}$ and $\overline{u}$ are the column vectors for dis-

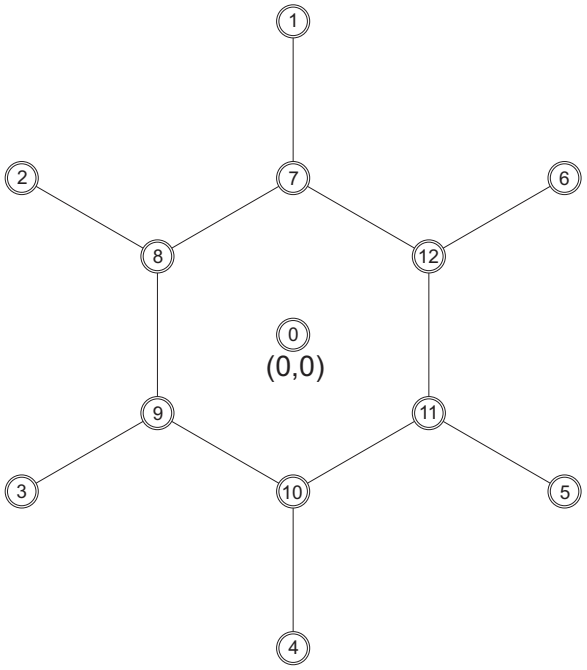

Fig. 6.5 Finite element analysis on the discrete model. Node numbering of the discrete system containing the RVE unit.

placement and acceleration for each beam. In this case, there are six inner nodes that we can assume equilibrium about these nodes (7, 8, 9, 10, 11 and 12 in Figure 6.5) to achieve three equations for each node: one for the x-direction, one for the y-direction and one for θ. The problem is reduced to the following three large equations by summing all six equations in the x-direction, six equations in the y-direction and six equations in θ:

$$\left[\begin{array}{l}\frac{\beta^4L^2}{4}(-2\theta_{10}-\theta_5+2\theta_1+\theta_6+\theta_{12}+2\theta_7-\theta_{11}+\theta_8-\theta_3-\theta_9+\theta_2-2\theta_4)+\\ \left(\left(\begin{array}{l}4u_1+u_2+u_3+u_5+u_6-4u_7+4u_4-4u_{10}-u_9-u_8-u_{12}-u_{11}\\ +\sqrt{3}(-v_8+v_{12}+v_2-v_3+v_9-v_{11}+v_5-v_6)\end{array}\right)\beta^4\right.\\ \left.+\left(\begin{array}{l}\sqrt{3}(v_8-v_{12}-v_2+v_3-v_9+v_{11}-v_5+v_6)+\\ 3u_2+3u_3+3u_6+3u_5-3u_9-3u_8-3u_{12}-3u_{11}\end{array}\right)\beta^2\right)\frac{L}{4}\end{array}\right]E+$$
$$(-a_{12}-a_8-a_9-a_{10}-a_7-a_{11})\frac{3\beta^2\rho L^3}{2}=0 \tag{6.1}$$

$$\left[\begin{array}{l} \frac{\sqrt{3}\beta^4L^2}{4}(\theta_9+\theta_2+\theta_8+\theta_3-\theta_{12}-\theta_5-\theta_{11}-\theta_6)+ \\ \left(\begin{array}{l} \frac{\beta^4L}{4}\left(\begin{array}{l} -3v_9-3v_{11}-3v_{12}+3v_2-3v_8+3v_3+3v_5+3v_6+ \\ \sqrt{3}(-u_8+u_5-u_6+u_{12}+u_2-u_3+u_9-u_{11}) \end{array}\right)+ \\ \frac{\beta^2L}{4}\left(\begin{array}{l} -v_9-v_{11}-v_{12}-v_8+v_2+v_3+v_5+v_6+4v_4-4v_{10}+4v_1-4v_7+ \\ \sqrt{3}(u_8-u_{12}-u_2+u_3-u_9-u_5+u_6+u_{11}) \end{array}\right) \end{array}\right) \end{array}\right] E$$
$$\frac{3\beta^2\rho L^3}{2}(-a_7-a_8-a_9-a_{10}-a_{11}-a_{12})=0 \tag{6.2}$$

$$\left[\begin{array}{l} \frac{\beta^4L^3}{6}(-\theta_4-\theta_1-8\theta_{10}-8\theta_7-\theta_5-\theta_2-8\theta_{11}-8\theta_8-\theta_6-\theta_3-8\theta_{12}-8\theta_9)+ \\ \frac{\beta^2L}{4}\left(\begin{array}{l} \sqrt{3}(-v_2-v_8-v_3-v_9+v_5+v_{11}+v_6+v_{12})+ \\ 2u_{10}-2u_7+u_5-u_2+u_{11}-u_8-u_6+u_3-u_{12}+u_9-2u_1+2u_4 \end{array}\right) \end{array}\right] E$$
$$\frac{\beta^2\delta\rho L^5}{8}(-c_7-c_8-c_9-c_{10}-c_{11}-c_{12})=0. \tag{6.3}$$

After obtaining the three equations of motion, dispersion analysis can be carried out by replacing the displacements with the harmonic plane wave equations (4.6) and substituting in the coordinates (x,y) (mentioned at the beginning of the section) of twelve nodes in Figure 6.5. The substitution is carried out similarly to the square and trapezium lattice. The new system consists of three equation of motions is not displayed here due to its lengthiness and it is unnecessary.

The system is then solved as an eigen-value problem where the variables are $[U,V,W]$; if E, l, ρ, β are predefined, the determinant of the system is a function of $[\omega,k,\gamma]$. For non-trivial solutions for the system, the determinant has to be zero. For each pair of $[k,\gamma]$, there are three corresponding values of ω and all these values are real for the discrete model of the square lattice.

The curves of Figure 6.6 shows all values of the normalised frequency ω against the normalised wave number k for the propagation angle $\gamma=\dfrac{\pi}{3}$.

The Bloch theorem, which is briefly mentioned for the one-dimensional case in Section 2.2 and for a wide range of shapes can be found in Gonella and Ruzzene (2008) and Phani et al. (2006), produces the same results as the discrete model derived above. However, the Bloch theorem in this case performs numerically better than the discrete model; as the propagation angles change, the Bloch theorem achieves more numerically stable cases. Hence, in later sections, the dispersion relations of continuum shall be compared with those of discrete model drawn by using the Bloch theorem.

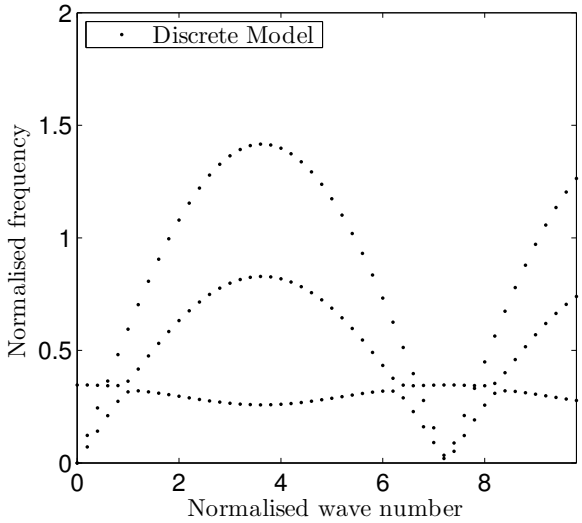

Fig. 6.6 Relationship between normalised frequency and normalised wave number for the discrete 2D hexagonal lattice with $\gamma = \pi/3$

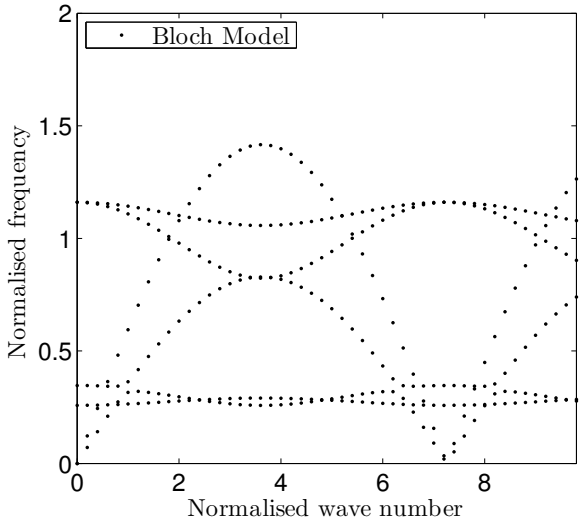

Fig. 6.7 Relationship between normalised frequency and normalised wave number for the discrete 2D hexagonal lattice with $\gamma = \pi/3$ using the Bloch theorem

6.2 Generalised continuum

This section derives the continuum from the discrete hexagonal lattice. Similar to the square and trapezium lattice, we use Taylor's series expansion, to the fourth and third order for spatial variables and rotational variables respectively, to continualise the discrete equation of motions (6.1) and (6.2) and (6.3). The approach is explained in detail in (Lombardo and Askes (2012)). The equations of motion for a RVE in the x-direction, y-direction and rotation in the plane x-y after continualisation are written as:

$$\begin{aligned}
&384\rho\ddot{u}+\frac{416}{35}\rho l^2\ddot{\theta}_{,y}\\
&E\begin{pmatrix}
-48\left(\beta^2+3\right)\left(u_{,xx}+u_{,yy}\right)+96\left(\beta^2-1\right)v_{,xy}\\
-15l^2\left(\beta^2+3\right)\left(u_{,xxxx}+2u_{,xxyy}\right)-5l^2\left(\beta^2+11\right)u_{,yyyy}\\
+20l^2\left(\beta^2-1\right)\left(3v_{,xxxy}+v_{,xyyy}\right)\\
-192\beta^2\theta_y-72\beta^2l^2\theta_{,xxy}-72\beta^2l^2\theta_{,yyy}
\end{pmatrix}=0
\end{aligned} \tag{6.4}$$

$$\begin{aligned}
&384\rho\ddot{v}-\frac{416}{35}\rho l^2\ddot{\theta}_{,x}\\
&E\begin{pmatrix}
-48\left(\beta^2+3\right)\left(v_{,yy}+v_{,xx}\right)+96\left(\beta^2-1\right)u_{,xy}\\
-15l^2\left(\beta^2+3\right)\left(2v_{,xxyy}+v_{,xxxx}\right)-5l^2\left(\beta^2+11\right)v_{,yyyy}\\
+20l^2\left(\beta^2-1\right)\left(u_{,xyyy}+3u_{,xxxy}\right)\\
+192\beta^2\theta_{,x}+72\beta^2l^2\theta_{,xyy}+72\beta^2l^2\theta_{,xxx}
\end{pmatrix}=0
\end{aligned} \tag{6.5}$$

$$\begin{aligned}
&\frac{4\rho l^2\delta}{\beta^2}\ddot{\theta}+24E\left(2\theta+u_{,y}-v_{,x}\right)\\
&+El^2\left(16\theta_{,xx}+16\theta_{,yy}+9u_{,xxy}-9v_{,xyy}+9u_{,yyy}-9v_{,xxx}\right)=0,
\end{aligned} \tag{6.6}$$

where u, v and θ are horizontal, vertical and rotational displacements of the middle node (node $(0,0)$ in Figure 6.5 respectively.

6.2.1 Reduced degree-of-freedom continuum

In this step, the rotational degree of freedom is also eliminated for the reasons that are listed in Section 5.2.1.

Similarly, we rewrite θ with respect to other linear variables as (see Appendix C.2 for full derivation):

$$\theta=\frac{\rho l^2}{24\beta^2E}\delta\left(\ddot{u}_{,y}-\ddot{v}_{,x}\right)+\frac{1}{2}\left(v_{,x}-u_{,y}\right)+\frac{l^2}{48}\left(v_{,xxx}+v_{,xyy}-u_{,xxy}-u_{,yyy}\right). \tag{6.7}$$

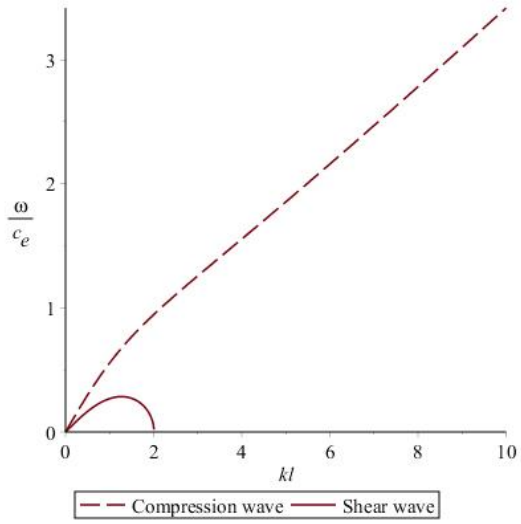

Fig. 6.8 Unstable relationship between normalised frequency and normalised wave number for the continuum of Equations (6.8) and (6.9) with $\gamma = \pi/3$

This step allows us to eliminate θ and reduce the equations of motions (assume that $\beta^2 \ll 1$ due to $\beta \leq \frac{1}{10}$ and $\delta = 1$; hence, we can ignore all terms $O\left(\beta^2 l^2\right)$ and $O\left(l^4\right)$). Substitute the new expression for θ into the primary equations of motion, assume that $\beta^2 \approx 0$, $\delta = 1$ and ignore all terms Ol^4 to get:

$$\begin{aligned} 384\rho\ddot{u} + 8\rho l^2\left(\ddot{v}_{,xy} - \ddot{u}_{,yy}\right) &= 48E\left(3u_{,xx} + u_{,yy} + 2v_{,xy}\right) + \\ &+ 45El^2\left(u_{,xxxx} + 2u_{,xxyy}\right) - 5El^2 u_{,yyyy} + 20El^2\left(3v_{,xxxy} + v_{,xyyy}\right) \end{aligned} \tag{6.8}$$

$$\begin{aligned} 384\rho\ddot{v} + 8\rho l^2\left(\ddot{u}_{,xy} - \ddot{v}_{,xx}\right) &= 48E\left(3v_{,yy} + v_{,xx} + 2u_{,xy}\right) + \\ &+ 15El^2\left(v_{,xxxx} + 2v_{,xxyy}\right) + 55El^2 v_{,yyyy} + 20El^2\left(u_{,xyyy} + 3u_{,xxxy}\right). \end{aligned} \tag{6.9}$$

Similar to the square and trapezium cases, these two equations have unstable dispersion relations, see Figure 6.8; therefore, further steps are taken to achieve stable dispersion relations.

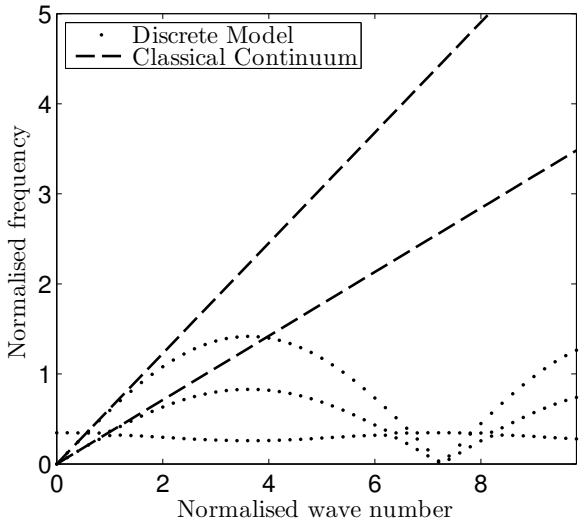

Fig. 6.9 Stable dispersion relationship between normalised frequency and normalised wave number for the classical continuum of Equations (6.8) and (6.9) with $\gamma = \pi/3$. The normalised wave number has the formula of kl, the normalised frequency $\dfrac{\omega}{c_e}$. For each model, there are two curves, the lower curve represents the shear component and the higher curve represents the compression component.

6.2.2 Classical continuum

Similar to previous cases, the equations of motion for classical continuum contains all the second order derivative terms in Equation (6.8) and (6.9):

$$384\rho\ddot{u} = 48E\left(3u_{,xx} + u_{,yy} + 2v_{,xy}\right) \tag{6.10}$$

$$384\rho\ddot{v} = 48E\left(3v_{,yy} + v_{,xx} + 2u_{,xy}\right). \tag{6.11}$$

The classical continuum has linear dispersion relations as seen in Figure 6.9.

6.2.3 Stabilised gradient continuum

Similar to the previous cases, a Padé approximation is used to stabilise the two Equations (6.8) and (6.9). Using the similar method in Section 5.2.3, if we denote Equation (6.8) as $\mathscr{R}$ and Equation (6.9) as $\mathscr{Z}$, we shall calculate (ignoring all terms $(\mathrm{O})\,(l^4)$):

$$\mathscr{R} + B\mathscr{R}_{,xx} + C\mathscr{R}_{,yy} + H\mathscr{Z}_{,xy} \tag{6.12}$$

$$\mathscr{Z} + F\mathscr{Z}_{,xx} + G\mathscr{Z}_{,yy} + H\mathscr{R}_{,xy}, \tag{6.13}$$

where B, C, F, G and H are the multipliers that are determined later so that the new expressions (6.12) and (6.13) shall be stable in the dispersion analysis. The expressions (6.12) and (6.13) in detailed forms are:

$$\begin{aligned}
&384\rho\ddot{u} - (384C-8)\rho l^2\ddot{u}_{,yy} - 384B\rho l^2\ddot{u}_{,xx} + (8+384H)\rho l^2\ddot{v}_{,xy} = \\
&\quad E\left(48\left(\beta^2+3\right)u_{,xx} + 48\left(\beta^2+1\right)u_{,yy} + 96v_{,xy}\right) \\
&\quad + El^2\left[\begin{array}{l}\left(15\beta^2+45+48\left(\beta^2+3\right)B\right)u_{,xxxx} \\ +\left(90-10\beta^2+48\left(\beta^2+3\right)C+48\left(\beta^2+1\right)B+96H\right)u_{,xxyy} \\ \\ \quad +\left(15\beta^2+5+48\left(\beta^2+1\right)C\right)u_{,yyyy}\end{array}\right] \\
&\quad + El^2\left[\left(60-20\beta^2+96B+48H\right)v_{,xxxy} + \left(20+20\beta^2+96C+96H\right)v_{,xyyy}\right]
\end{aligned} \tag{6.14}$$

$$\begin{aligned}
&384\rho\ddot{v} + \rho l^2\left(384F-8\right)\ddot{v}_{,xx} + \rho l^2\left(384H+8\right)\ddot{u}_{,xy} + 384G\rho l^2\ddot{v}_{,yy} = \\
&\quad E\left(48\left(\beta^2+3\right)v_{,yy} + 48\left(\beta^2+1\right)v_{,xx} + 96u_{,xy}\right) \\
&\quad + El^2\left[\begin{array}{l}\left(5\beta^2+55+48\left(\beta^2+3\right)G\right)v_{,yyyy} \\ \\ \quad +\left(50\beta^2+30+48\left(\beta^2+3\right)F+48\left(\beta^2+1\right)G+96H\right)v_{,xxyy} \\ \\ \quad +\left(5\beta^2+15+48\left(\beta^2+1\right)F\right)v_{,xxxx}\end{array}\right] \\
&\quad + El^2\left[\left(20+20\beta^2+96G+48H\right)u_{,xyyy} + \left(60-20\beta^2+96F+144H\right)u_{,xxxy}\right].
\end{aligned} \tag{6.15}$$

Unlike the trapezium case, this time the terms having β^2 are kept to verify the significance of keeping these terms.

If the arbitrary constants have the following values regarding to H, we would achieve the

equation set (6.17) and (6.18):

$$\begin{aligned} C &= \frac{-48\left(\beta^2+3\right)H-20\left(\beta^2+1\right)}{96} \\ B &= \frac{-48\left(\beta^2+1\right)H-20\left(-\beta^2+3\right)}{96} \\ F &= \frac{-48\left(\beta^2+3\right)H-20\left(-\beta^2+3\right)}{96} \\ G &= \frac{-48\left(\beta^2+1\right)H-20\left(\beta^2+1\right)}{96} \end{aligned} \tag{6.16}$$

$$\begin{aligned} &384\rho\ddot{u}-\left(\frac{14448}{25}H+\frac{444}{5}\right)\rho l^2\ddot{u}_{,yy}-384\left(\frac{101}{200}H+\frac{299}{480}\right)\rho l^2\ddot{u}_{,xx}+\left(8+384H\right)\rho l^2\ddot{v}_{,xy}= \\ &E\left(\frac{3612}{25}u_{,xx}+\frac{1212}{25}u_{,yy}+96v_{,xy}\right) \\ &+El^2\left(\left(-\frac{44849}{1000}-\frac{91203}{1250}H\right)u_{,xxxx}+\left(\frac{293}{10}-\frac{91203}{625}H\right)u_{,xxyy}-\left(\frac{5051}{1000}+\frac{91203}{1250}H\right)u_{,yyyy}\right) \end{aligned} \tag{6.17}$$

$$\begin{aligned} &384\rho\ddot{v}+\left(384H+8\right)\rho l^2\ddot{u}_{,xy}-\left(\frac{14448}{25}H+\frac{1236}{5}\right)\rho l^2\ddot{v}_{,xx}-384\left(\frac{101}{200}H+\frac{101}{480}\right)\rho l^2\ddot{v}_{,yy}= \\ &E\left(\frac{3612}{25}v_{,yy}+\frac{1212}{25}v_{,xx}+96u_{,xy}\right) \\ &+El^2\left(-\left(\frac{91203}{1250}H+\frac{15149}{1000}\right)v_{,xxxx}+\left(\frac{24649}{1000}-\frac{91203}{1250}H\right)v_{,yyyy}-\left(\frac{697}{10}+\frac{91203}{625}H\right)v_{,xxyy}\right). \end{aligned} \tag{6.18}$$

This system, if substituting $H=10$ (similar to the trapezium case), under dispersion analysis in Maple, yields the gradient curves in Figure 6.10.

If $H=1$, the gradient compression component shows a more rigorously dispersive behaviour towards the discrete compression curve as in Figure 6.11.

6.2.4 Ru-Aifantis theorem application

Next, we will apply the Ru-Aifantis theorem to the fourth order space derivatives $\mathscr{X}_{iiii}$ of the above set of Equations (6.17) and (6.18) so that we can use C^0 continuity (see footnote 1, page 3) to implement the finite element method. The derivation here is very similar to the trapezium case in Section 5.2.4 and it is described here in detail again to illustrate the versatility of the Ru-Aifantis theorem to different geometries.

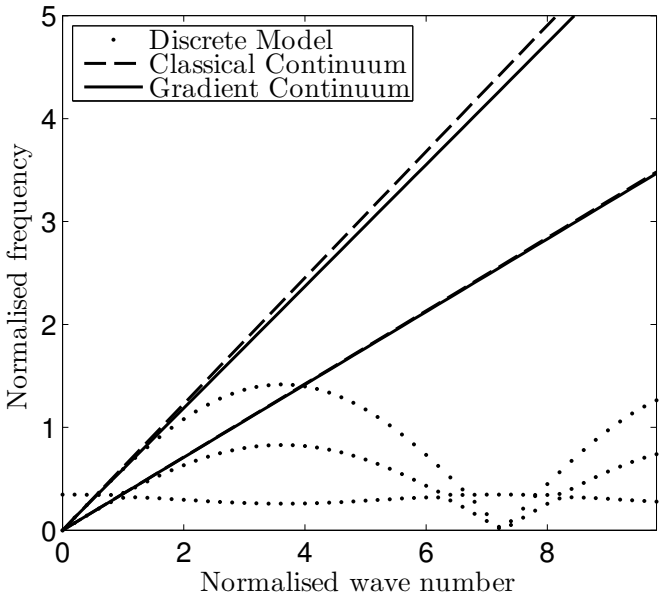

Fig. 6.10 Relationship between normalised frequency and normalised wave number for the new gradient continua– 2D hexagonal lattice with $\gamma = \pi/3$ and $H = 1$. The normalised wave number has the formula of kl, the normalised frequency $\frac{\omega}{c_e}$. For each model, there are two curves, the lower curve represents the shear component and the higher curve represents the compression component.

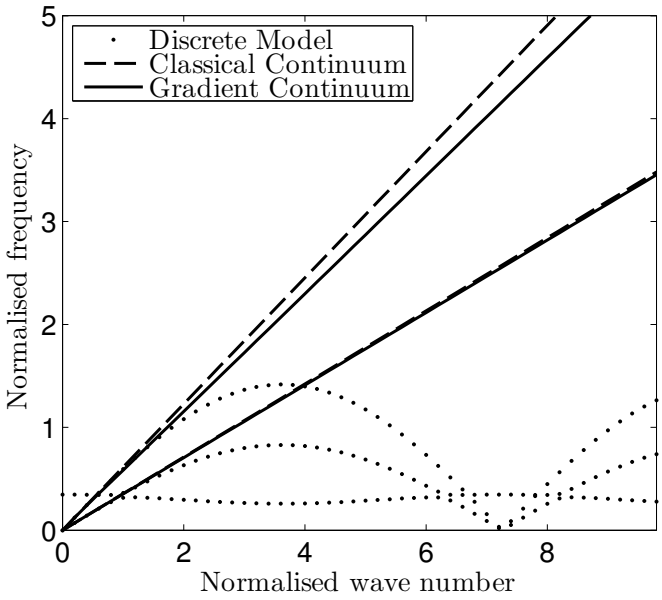

Fig. 6.11 Relationship between normalised frequency and normalised wave number for the new gradient continua– 2D hexagonal lattice with $\gamma = \pi/3$ and $H = 1$. The normalised wave number has the formula of kl, the normalised frequency $\frac{\omega}{c_e}$. For each model, there are two curves, the lower curve represents the shear component and the higher curve represents the compression component.

For Equations (6.17) and (6.18), u and v appear together in the equations. Similar to the one dimensional case and to the two dimensional trapezium lattice, to apply the Ru-Aifantis theory to Equations (6.17) and (6.18), the two new auxiliary displacements a and b are defined as following:

$$a = su - ml^2 u_{,xx} - nl^2 u_{,yy} \tag{6.19}$$

$$b = \varsigma v - \mu l^2 v_{,xx} - \nu l^2 v_{,yy} \tag{6.20}$$

where s, m, n, ς, μ and ν are arbitrary coefficients whose values will be determined later. After eliminating the $\mathscr{X}_i iii$ terms in Equations (6.17) and (6.18), we want to finally achieve this matrix system after FE discretisation:

$$\begin{bmatrix} M_{1,1} & M_{1,2} & M_{1,3} & 0 \\ M_{2,1} & M_{2,2} & 0 & M_{2,4} \\ M_{3,1} & 0 & M_{3,3} & 0 \\ 0 & M_{4,2} & 0 & M_{4,4} \end{bmatrix} \begin{bmatrix} \ddot{u} \\ \ddot{v} \\ \ddot{a} \\ \ddot{b} \end{bmatrix} - \begin{bmatrix} K_{1,1} & K_{1,2} & K_{1,3} & 0 \\ K_{2,1} & K_{2,2} & 0 & K_{2,4} \\ K_{3,1} & 0 & K_{3,3} & 0 \\ 0 & K_{4,2} & 0 & K_{4,4} \end{bmatrix} \begin{bmatrix} u \\ v \\ a \\ b \end{bmatrix} = \begin{bmatrix} f_u \\ f_v \\ 0 \\ 0 \end{bmatrix}, \tag{6.21}$$

with $M_{1,2} = M_{2,1}$, $M_{1,3} = M_{3,1}$, $M_{2,4} = M_{4,2}$, $K_{1,2} = K_{2,1}$, $K_{1,3} = K_{3,1}$ and $K_{2,4} = K_{4,2}$.

To construct such matrices, it is required to consider all four equations from which the matrices are built together. It is obvious that the first and second equations built from the matrices in Equation (6.21) are based on the two Equations (6.17) and (6.18). On the other hand, the third and fourth equations are developed from the definition of a and b - Equations (6.19) and (6.20). In detail, the third equation reads $(M_{3,1}\ddot{u} + M_{3,3}\ddot{a}) - (K_{3,1}u + K_{3,3}a) = 0$, which can be fulfilled with $M_{3,1}\ddot{u} + M_{3,3}\ddot{a} = 0$ and $K_{3,1}u + K_{3,3}a = 0$. It is easier to satisfy these two conditions using the definition of a and b - Equations (6.19) and (6.20).

Consider developing the first equation of the matrix from Equation (6.17), the terms having fourth derivatives, u_{xxxx} and u_{yyyy} on the right hand side of equation (6.17) are replaced by the term $K_{1,3}a$ in the first equation of the matrix. Hence, $K_{1,3}a$ needs to contain the form $qa_{,xx} + ra_{,yy}$ which are equivalent to the main variables by using the definition of a in Equation (6.19), where q and r are arbitrary coefficients whose values shall be determined later:

$$\left.\begin{aligned} qa_{,xx} &= qsu_{,xx} - qml^2 u_{,xxxx} - qnl^2 u_{,xxyy} \\ ra_{,yy} &= rsu_{,yy} - rml^2 u_{,xxyy} - rnl^2 u_{,yyyy} \end{aligned}\right\} \rightarrow \begin{aligned} qm &= \frac{44849}{1000} + \frac{91203}{1250}H \\ rn &= \frac{697}{10} + \frac{91203}{625}H. \end{aligned} \tag{6.22}$$

The condition $K_{1,3} = K_{3,1}$ to preserve the symmetry of the system means that $K_{3,1}u$ also contains $qu_{,xx} + ru_{,yy}$. Moreover, the assumption that $K_{3,1}u + K_{3,3}a = 0$ from the third equation

of the matrix is based on Equation (6.19) leads to $K_{3,1}u{=}qu_{,xx}+ru_{,yy}-\frac{p}{l^2}u$ and $K_{3,3}=-\frac{p}{sl^2}a$ where $\{p/q/r\}$ has the same ratio as $\{s/m/n\}$. This discussion can be presented as follows:

$$\begin{cases} K_{3,1}=K_{1,3} \\ K_{1,3}a \text{ has } qa_{,xx}+ra_{,yy} \\ K_{3,1}u+K_{3,3}a\sim\dfrac{su-ml^2u_{,xx}-nl^2u_{,yy}-a}{l^2}=0 \end{cases} \Rightarrow \begin{cases} K_{1,3}a=\left(-\dfrac{p}{l^2}a+qa_{,xx}+ra_{,yy}\right) \\ K_{3,1}u=\left(-\dfrac{p}{l^2}u+qu_{,xx}+ru_{,yy}\right) \\ \forall\{p/q/r\}=\{s/m/n\} \end{cases}$$

. Therefore, the following relationships are obtained:

$$\begin{cases} \dfrac{m}{s}=\dfrac{q}{p}\rightarrow m=\dfrac{sq}{p}\rightarrow qm=q^2\dfrac{s}{p}=\dfrac{44849}{1000}+\dfrac{91203}{1250}H \\ \dfrac{n}{s}=\dfrac{q}{p}\rightarrow n=\dfrac{sr}{p}\rightarrow rn=r^2\dfrac{s}{p}=\dfrac{697}{10}+\dfrac{91203}{625}H \end{cases} \tag{6.23}$$

and the constants have their values in terms of H according to:

$$q=\sqrt{\frac{1}{t}\left(\frac{44849}{1000}+\frac{91203}{1250}H\right)};r=\sqrt{\frac{1}{t}\left(\frac{697}{10}+\frac{91203}{625}H\right)};\frac{s}{p}=t; \tag{6.24}$$

$$m=\sqrt{t\left(\frac{44849}{1000}+\frac{91203}{1250}H\right)};n=\sqrt{t\left(\frac{697}{10}+\frac{91203}{625}H\right)}. \tag{6.25}$$

Applying the same procedure to the auxiliary variable b yields:

$$\left.\begin{aligned} \varpi\mu=\varpi^2\frac{\varsigma}{\pi}=\frac{91203}{1250}H+\frac{15149}{1000} \\ \vartheta\nu=\vartheta^2\frac{\varsigma}{\pi}=\frac{91203}{1250}H-\frac{24649}{1000} \end{aligned}\right\} \Rightarrow \begin{cases} \varpi=\sqrt{\dfrac{1}{\tau}\left(\dfrac{91203}{1250}H+\dfrac{15149}{1000}\right)}; \\ \vartheta=\sqrt{\dfrac{1}{\tau}\left(\dfrac{91203}{1250}H-\dfrac{24649}{1000}\right)};\dfrac{\varsigma}{\pi}=\tau; \\ \mu=\sqrt{\tau\left(\dfrac{91203}{1250}H+\dfrac{15149}{1000}\right)}; \\ \nu=\sqrt{\tau\left(\dfrac{91203}{1250}H-\dfrac{24649}{1000}\right)} \end{cases} \tag{6.26}$$

With a suitable value of H, the auxiliary variables can be rewritten with respect to t, τ, s

and ς from Equation (6.19) and (6.20) as:

$$a = su - \sqrt{t\left(\frac{44849}{1000} + \frac{91203}{1250}H\right)}l^2u_{,xx} - \sqrt{t\left(\frac{697}{10} + \frac{91203}{625}H\right)}l^2u_{,yy} \tag{6.27}$$

$$b = \varsigma v - \sqrt{\tau\left(\frac{91203}{1250}H + \frac{15149}{1000}\right)}l^2v_{,xx} - \sqrt{\tau\left(\frac{91203}{1250}H - \frac{24649}{1000}\right)}l^2v_{,yy} \tag{6.28}$$

However, for a clear presentation, the more symbolic set of Equations (6.19) and (6.20) is displayed for the rest of the derivation. Further variations of Equations (6.19) and (6.20) are:

$$u = \frac{a}{s} + \frac{m}{s}l^2u_{,xx} + \frac{n}{s}l^2u_{,yy} \tag{6.29}$$

$$v = \frac{b}{\varsigma} + \frac{\mu}{\varsigma}l^2v_{,xx} + \frac{\nu}{\varsigma}l^2v_{,yy}, \tag{6.30}$$

and

$$\frac{sE}{t}\frac{su - ml^2u_{,xx} - nl^2u_{,yy} - a}{l^2} = \frac{sE}{t}\left(-\frac{a}{l^2} + s\frac{u}{l^2} - mu_{,xx} - nu_{,yy}\right) = 0 \tag{6.31}$$

$$\frac{\varsigma E}{\tau}\frac{\varsigma v - \mu l^2v_{,xx} - \nu l^2v_{,yy} - b}{l^2} = \frac{\varsigma E}{\tau}\left(-\frac{b}{l^2} + \varsigma\frac{v}{l^2} - \mu v_{,xx} - \nu v_{,yy}\right) = 0. \tag{6.32}$$

After defining the auxiliary variables in preparation of the Ru-Aifantis theorem application, the left hand side of Equation (6.17) is modified by rewriting $384\rho\ddot{u}$ using Equation (6.29) and introducing $m\rho l^2\ddot{u}_{,xx}$ and $n\rho l^2\ddot{u}_{,yy}$ into the equation:

$$\begin{aligned}
LHS &= 384\rho\ddot{u} - \left(\frac{14448}{25}H + \frac{444}{5}\right)\rho l^2\ddot{u}_{,yy} - 384\left(\frac{101}{200}H + \frac{299}{480}\right)\rho l^2\ddot{u}_{,xx} + (8 + 384H)\,\rho l^2\ddot{v}_{,xy} \\
&= \underbrace{\left(\rho\ddot{a} + m\rho l^2\ddot{u}_{,xx} + n\rho l^2\ddot{u}_{,yy}\right)}_{384\rho\ddot{u}}\underbrace{-m\rho l^2\ddot{u}_{,xx} - n\rho l^2\ddot{u}_{,yy}}_{\text{new terms added}} + \left(\underbrace{n}_{\text{new}} - \frac{14448}{25}H - \frac{444}{5}\right)\rho l^2\ddot{u}_{,yy} \\
&+ \left(\underbrace{m}_{\text{new}} - 384\left(\frac{101}{200}H + \frac{299}{480}\right)\right)\rho l^2\ddot{u}_{,xx} + (8 + 384H)\,\rho l^2\ddot{v}_{,xy} \\
&= \rho\ddot{a} - m\rho l^2\ddot{u}_{,xx} - n\rho l^2\ddot{u}_{,yy} + \left(2n - \frac{14448}{25}H - \frac{444}{5}\right)\rho l^2\ddot{u}_{,yy} \\
&+ \left(2m - 384\left(\frac{101}{200}H + \frac{299}{480}\right)\right)\rho l^2\ddot{u}_{,xx} + (8 + 384H)\,\rho l^2\ddot{v}_{,xy}.
\end{aligned}$$

The terms $-m\rho l^2\ddot{u}_{,xx}$ and $-n\rho l^2\ddot{u}_{,yy}$ are then rewritten using Equation (6.29):

$$\begin{aligned} LHS = &-m\rho l^2\left(\frac{1}{s}\ddot{a}_{,xx}+\frac{1}{s}ml^2\ddot{u}_{,xxxx}+\frac{1}{s}nl^2\ddot{u}_{,xxyy}\right)-n\rho l^2\left(\frac{1}{s}\ddot{a}_{,yy}+\frac{1}{s}ml^2\ddot{u}_{,xxyy}+\frac{1}{s}nl^2\ddot{u}_{,yyyy}\right)\\ &+\left(2n-\frac{14448}{25}H-\frac{444}{5}\right)\rho l^2\ddot{u}_{,yy}+\left(2m-384\left(\frac{101}{200}H+\frac{299}{480}\right)\right)\rho l^2\ddot{u}_{,xx}\\ &+(8+384H)\,\rho l^2\ddot{v}_{,xy}. \end{aligned} \tag{6.33}$$

It is acceptable to ignore all $O\left(l^4\right)$ terms because:

- The lengthscale l of the microlattice materials is very small.
- Hence, the numerical coefficient of $-\mathrm{O}\left(l^4\ddot{u}_{ijkl}\right)$ terms are considerably much smaller than $\mathrm{O}\left(l^2\ddot{u}_{ij}\right)$.

Finally, the left hand side of Equation (6.17) (or Equation (6.33)) is approximated as:

$$\begin{aligned} LHS = &-\rho l^2\left[\left(2m-384\left(\frac{101}{200}H+\frac{299}{480}\right)\right)\ddot{u}_{,xx}+\left(2n-\frac{14448}{25}H-\frac{444}{5}\right)\ddot{u}_{,yy}\right]\\ &+(8+384H)\,\rho l^2\ddot{v}_{,xy}+\rho\left[\ddot{a}-\frac{1}{s}ml^2\ddot{a}_{,xx}-\frac{1}{s}nl^2\ddot{a}_{,yy}\right]. \end{aligned} \tag{6.34}$$

Next, the right hand side of Equation (6.17) is modified; the fourth order derivatives $\mathscr{X}_{iiii}$ are replaced by using Equation (6.29):

$$\begin{aligned} RHS =&E\left(\frac{3612}{25}u_{,xx}+\frac{1212}{25}u_{,yy}+96v_{,xy}\right)+El^2\left(\frac{293}{10}-\frac{91203}{625}H\right)u_{,xxyy}\\ &-El^2\left(\underbrace{\left(\frac{44849}{1000}+\frac{91203}{1250}\right)}_{qm}u_{,xxxx}+\underbrace{\left(\frac{5051}{1000}+\frac{91203}{1250}H\right)}_{rn}u_{,yyyy}\right)\\ =&E\left(\frac{3612}{25}u_{,xx}+\frac{1212}{25}u_{,yy}+96v_{,xy}\right)+\left(\frac{293}{10}-\frac{91203}{625}H\right)El^2u_{,xxyy}\\ &+E\left(qa_{,xx}-qsu_{,xx}+qnl^2u_{,xxyy}\right)+E\left(ra_{,yy}-rsu_{,yy}+rml^2u_{,xxyy}\right). \end{aligned} \tag{6.35}$$

Equation (6.31) is then added to the right hand side:

$$\begin{aligned}
RHS =& E\left[\frac{3612}{25}u_{,xx}+\frac{1212}{25}u_{,yy}+96v_{,xy}+qa_{,xx}+ra_{,yy}-qsu_{,xx}-rsu_{,yy}+(qn+rm)\,l^2u_{,xxyy}\right]+\\
& E\left(\frac{293}{10}-\frac{91203}{625}H\right)l^2u_{,xxyy}+\underbrace{\frac{sE}{t}\left(-\frac{a}{l^2}+s\frac{u}{l^2}-mu_{,xx}-nu_{,yy}\right)}_{=0}\\
=& E\left[\begin{array}{l}s^2\dfrac{u}{tl^2}+\left(\dfrac{3612}{25}-qs-\dfrac{sm}{t}\right)u_{,xx}+\left(\dfrac{1212}{25}-rs-\dfrac{sn}{t}\right)u_{,yy}\\ +\left(qn+rm+\dfrac{293}{10}-\dfrac{91203}{625}H\right)l^2u_{,xxyy}\end{array}\right]+\\
& E96v_{,xy}+E\left[qa_{,xx}+ra_{,yy}-s\frac{a}{tl^2}\right].
\end{aligned} \tag{6.36}$$

Similarly the same procedure is applied to both sides of Equation (6.18). First consider the left hand side of Equation (6.18):

$$\begin{aligned}
& 384\rho\ddot{v}+(384H+8)\,\rho l^2\ddot{u}_{,xy}-\left(\frac{14448}{25}H+\frac{1236}{5}\right)\rho l^2\ddot{v}_{,xx}-384\left(\frac{101}{200}H+\frac{101}{480}\right)\rho l^2\ddot{v}_{,yy}\\
=&\rho\left(\ddot{b}+\mu l^2\ddot{v}_{xx}+\nu l^2\ddot{v}_{yy}\right)-\mu\rho l^2\ddot{v}_{xx}-\nu\rho l^2\ddot{v}_{yy}+\left(\nu-384\left(\frac{101}{200}H+\frac{101}{480}\right)\right)\rho l^2\ddot{v}_{,yy}\\
&+\left(\mu-\left(\frac{14448}{25}H+\frac{1236}{5}\right)\right)\rho l^2\ddot{v}_{,xx}+(384H+8)\,\rho l^2\ddot{u}_{,xy}\\
=&\rho\ddot{b}-\mu\rho l^2\left(\ddot{b}_{,xx}+\mu l^2\ddot{v}_{,xxxx}+\nu l^2\ddot{v}_{,xxyy}\right)-\nu\rho l^2\left(\ddot{b}_{,yy}+\mu l^2\ddot{v}_{,xxyy}+\nu l^2\ddot{v}_{,yyyy}\right)\\
&+\left(2\nu-384\left(\frac{101}{200}H+\frac{101}{480}\right)\right)\rho l^2\ddot{v}_{,yy}+\left(2\mu-\left(\frac{14448}{25}H+\frac{1236}{5}\right)\right)\rho l^2\ddot{v}_{,xx}\\
&+(384H+8)\,\rho l^2\ddot{u}_{,xy}\\
\approx&(384H+8)\,\rho l^2\ddot{u}_{,xy}+\left(2\nu-384\left(\frac{101}{200}H+\frac{101}{480}\right)\right)\rho l^2\ddot{v}_{,yy}\\
&+\left(2\mu-\left(\frac{14448}{25}H+\frac{1236}{5}\right)\right)\rho l^2\ddot{v}_{,xx}+\rho\ddot{b}-\mu\rho l^2\ddot{b}_{,xx}-\nu\rho l^2\ddot{b}_{,yy}.
\end{aligned} \tag{6.37}$$

The right hand side of Equation (6.18) is modified in the following steps:

$$\begin{aligned}
RHS =& E\left(\frac{3612}{25}v_{,yy}+\frac{1212}{25}v_{,xx}+96u_{,xy}\right)+-El^2\left(\frac{91203}{1250}H+\frac{15149}{1000}\right)v_{,xxxx}\\
&+El^2\left(\frac{24649}{1000}-\frac{91203}{1250}H\right)v_{,yyyy}-El^2\left(\frac{697}{10}+\frac{91203}{625}H\right)v_{,xxyy}\\
=&E\left(\frac{3612}{25}v_{,yy}+\frac{1212}{25}v_{,xx}+96u_{,xy}\right)-E\left(\frac{697}{10}+\frac{91203}{625}H\right)l^2v_{,xxyy}\\
&+E\left(\varpi b_{,xx}-\varpi\varsigma v_{,xx}+\varpi\nu l^2v_{,xxyy}\right)+E\left(\vartheta b_{,yy}-\vartheta\varsigma v_{,yy}+\vartheta\mu l^2v_{,xxyy}\right)\\
=&E\left(\frac{3612}{25}v_{,yy}+\frac{1212}{25}v_{,xx}+96u_{,xy}+\varpi b_{,xx}+\vartheta b_{,yy}-\varpi\varsigma v_{,xx}-\vartheta\varsigma v_{,yy}\right)\\
&+E\left(\varpi\nu+\vartheta\mu-\frac{697}{10}-\frac{91203}{625}H\right)l^2v_{,xxyy}+\frac{\varsigma E}{\tau}\left(-\frac{b}{l^2}+\varsigma\frac{v}{l^2}-\mu v_{,xx}-\nu v_{,yy}\right)\\
=&E\left[96u_{,xy}+\varsigma^2\frac{v}{\tau l^2}+\left(\frac{1212}{25}-\varsigma\varpi-\frac{\varsigma\mu}{\tau}\right)v_{,xx}+\left(\frac{3612}{25}-\varsigma\vartheta-\frac{\varsigma\nu}{\tau}\right)v_{,yy}\right]\\
&+E\left(\varpi\nu+\vartheta\mu-\frac{697}{10}-\frac{91203}{625}H\right)l^2v_{,xxyy}+E\left[-\varsigma\left(\frac{b}{\tau l^2}\right)+\varpi b_{,xx}+\vartheta b_{,yy}\right].
\end{aligned}\tag{6.38}$$

Therefore, to be able to use the Ru-Aifantis theorem, Equations (6.17) and (6.18) are modified into:

$$\begin{aligned}
&-\rho l^2\left[\left(2m-384\left(\frac{101}{200}H+\frac{299}{480}\right)\right)\ddot{u}_{,xx}+\left(2n-\frac{14448}{25}H-\frac{444}{5}\right)\ddot{u}_{,yy}\right]\\
&+(8+384H)\rho l^2\ddot{v}_{,xy}+\rho\left[\ddot{a}-\frac{1}{s}ml^2\ddot{a}_{,xx}-\frac{1}{s}nl^2\ddot{a}_{,yy}\right]\\
=&E\left[\begin{array}{l}s^2\frac{u}{tl^2}+\left(\frac{3612}{25}-qs-\frac{sm}{t}\right)u_{,xx}+\left(\frac{1212}{25}-rs-\frac{sn}{t}\right)u_{,yy}+\\ \left(qn+rm+\frac{293}{10}-\frac{91203}{625}H\right)l^2u_{,xxyy}\end{array}\right]\\
&+E96v_{,xy}+E\left[qa_{,xx}+ra_{,yy}-s\frac{a}{tl^2}\right].
\end{aligned}\tag{6.39}$$

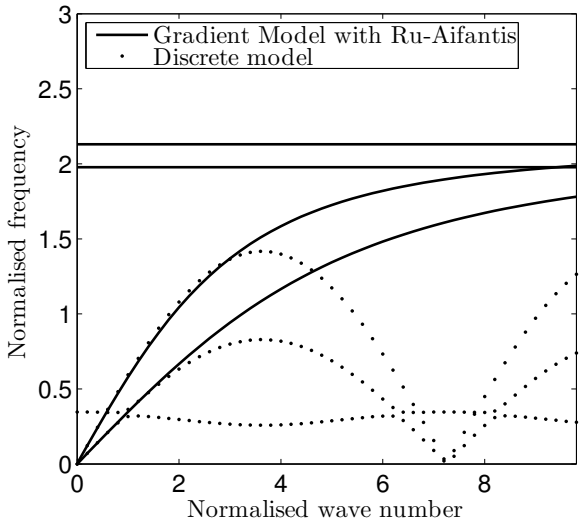

Fig. 6.12 Dispersion analysis for the gradient continuum with the Ru-Aifantis theorem at propagation angle of $\pi/3$. The normalised wave number has the formula of kl, the normalised frequency $\dfrac{\omega}{c_e}$. For each model, there are two curves, the lower curve represents the shear component and the higher curve represents the compression component.

$$
\begin{aligned}
&(384H+8)\rho l^2\ddot{u}_{,xy}+\left(2\nu-384\left(\frac{101}{200}H+\frac{101}{480}\right)\right)\rho l^2\ddot{v}_{,yy}+\\
&\quad\left(2\mu-\left(\frac{14448}{25}H+\frac{1236}{5}\right)\right)\rho l^2\ddot{v}_{,xx}+\rho\ddot{b}-\mu\rho l^2\ddot{b}_{,xx}-\nu\rho l^2\ddot{b}_{,yy}\\
=&E\left[96u_{,xy}+\varsigma^2\frac{v}{\tau l^2}+\left(\frac{1212}{25}-\varsigma\varpi-\frac{\varsigma\mu}{\tau}\right)v_{,xx}+\left(\frac{3612}{25}-\varsigma\vartheta-\frac{\varsigma\nu}{\tau}\right)v_{,yy}\right]\\
&+E\left(\varpi\nu+\vartheta\mu-\left(\frac{697}{10}+\frac{91203}{625}H\right)\right)l^2v_{,xxyy}+E\left[-\varsigma\left(\frac{b}{\tau l^2}\right)+\varpi b_{,xx}+\vartheta b_{,yy}\right].
\end{aligned}
\tag{6.40}
$$

And the other two equations to form the symmetric matrices are as follows; note that two sides of the equations below are identities of Equations (6.27) and (6.28):

$$\rho\left[\ddot{u}-\frac{1}{s}ml^2\ddot{u}_{,xx}-\frac{1}{s}nl^2\ddot{u}_{,yy}\right]-\frac{1}{s}\rho\ddot{a}=\frac{E}{t}\left[-\frac{u}{l^2}+mu_{,xx}+nu_{,yy}\right]+\frac{E}{tl^2}a \tag{6.41}$$

$$\rho\left[\ddot{v}-\frac{1}{\varsigma}\mu l^2\ddot{v}_{,xx}-\frac{1}{\varsigma}\upsilon l^2\ddot{v}_{,yy}\right]-\frac{\rho\ddot{b}}{\varsigma}=\frac{E}{\tau}E\left[-\frac{v}{l^2}+\mu v_{,xx}+\nu v_{,yy}\right]+\frac{E}{\tau l^2}b. \tag{6.42}$$

Figures 6.12 and 6.13 display the dispersion relations of four new Equations 6.37, 6.38, 6.39 and 6.40 compared with ones of the discrete models. In these figures, the gradient model has four curves for the four variables u, v, a and b. Similar to the trapezium lattice case,

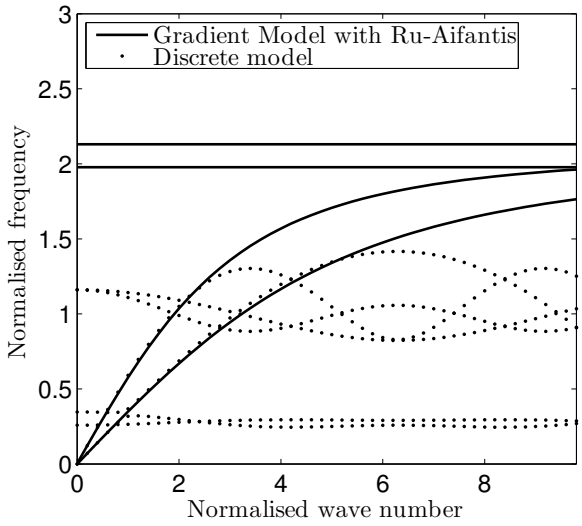

Fig. 6.13 Dispersion analysis for the gradient continuum with the Ru-Aifantis theorem at propagation angle of $\pi/6$. The dispersion relations of the discrete models are derived by the Bloch theorem. The normalised wave number has the formula of kl, the normalised frequency $\frac{\omega}{c_e}$. For each model, there are two curves, the lower curve represents the shear component and the higher curve represents the compression component.

the curves for the variables a and b are straight lines and their positions can be changed by changing the values of arbitrary constants in the application of the Ru-Aifantis theorem.

The discretisation schemes for this set of equation is similar to Equation 5.82. We will not compare the discrete model with discretised continuum of the hexagonal lattice because no simple and efficient hexagonal spatial scheme can be found. If we use a square element in this case, it is predictable that there will be large discrepancies. Moreover, it is not the aim of this thesis to focus on the discretisation scheme.

Chapter 7

Discussion

Based on the results given in previous chapters, this chapter evaluates and discusses the dispersion simulation of micro-lattice materials, especially the discrete, classical and gradient models from one dimension case to different two-dimensional geometries. Through this discussion, advantages and disadvantages of the gradient continuum are collected and compiled. Therefore, limitations can be drawn for the gradient continuum and improvement areas can be defined for future research. The arrangement for this chapter is as follows: Section 7.1 revises and compares all the one-dimensional models, Section 7.2 compiles different aspects of different models of the three two-dimensional lattices, and finally, Section 7.3 integrates all discussion points.

7.1 The one-dimensional case

The one dimensional case is the foundation and benchmark to consider further higher-dimension models. It is important to understand this case with the developments, correspondences and differences between the discrete model, the classical model and the gradient model. Section 3.4 briefly draws some discussion and conclusion to compare with later chapters. This section will add to Section 3.4 a more thorough and systematic observation through the different stages of the 4-step procedure:

- The discrete model is described in Section 3.1 and defined in a particular way to demonstrate how the 4-step procedure (see Section 2.7) is used to derive a continuum from a specific discrete model. It was not chosen on the criterion of the best model to simulate a realistic spring-mass model. Equation (3.2) describing the dispersion relation of the discrete model is periodic and has a ceiling frequency for all values of the wave number k, $\Omega(k) \leq \omega_{max}$, see Figure 3.2. This property is known as the wave filtering ability

of materials with underlying microstructures; no frequency higher than the maximum frequency can propagate through the material.

- The classical model: We can consider the classical model, see Equation (3.9), as the simplest form of the class of generalised continuum without taking into account the effect of the microstructural length l. The dispersion equation has a linear form and the dispersive property of the continuum is absent: the phase velocity is equal to the group velocity. The straight solid line representing the classical model in Figure 3.2 shows a large discrepancy with the discrete model curve for higher wavenumbers. By being discretised in space and time, the classical curves were numerically turned to a periodic function with respect to the wave number k in Figure 3.3. The newly achieved dispersion behaviour of the discretised classical model is caused by numerical discretisation, not by the physical nature of the continuum and is therefore not preferred.

- The gradient model: takes into account of the microstructural length l, see Equation (3.11), and has various forms depending on the value of S when applied Padé approximation is applied:

  – When S is $\frac{1}{12}$, Equation 3.13 has the same number of the order of spatial derivatives on both sides which leads to the dispersion equation (Equation 3.14) having a maximum value $\frac{E12}{\rho l^2}$ as the wave number k tends to infinity. This means only frequencies that are lower than this maximum value are allowed to travel through the defined one dimensional material; when sketched against the wave number k, this wave filtering behaviour is shown by having a horizontal asymptote. Compared to the classical continuum, see Figure 3.2, the gradient continuum can represent the discrete model better on the wave propagation properties.

  – When $S > \frac{1}{12}$, the Ru-Aifantis theorem is deployed to reduce the continuity requirement when implementing FEM method . The system now has an extra auxiliary variable, see Equation (3.23), increasing the number of degrees of freedom which is a disadvantage that we have to accept to gain a more robust numerical implementation.

  When discretised, similar to the classical case, the gradient curve has the same first Brillouin zone as the discrete model when the element length $h = l$, see Section 3.3; and, the maximum frequency value of the gradient model is closer to the discrete value. After all, the procedure produces a gradient model based on the physical properties of the system (the microstructural length l) and closely captures the dispersive behaviour of the discrete model.

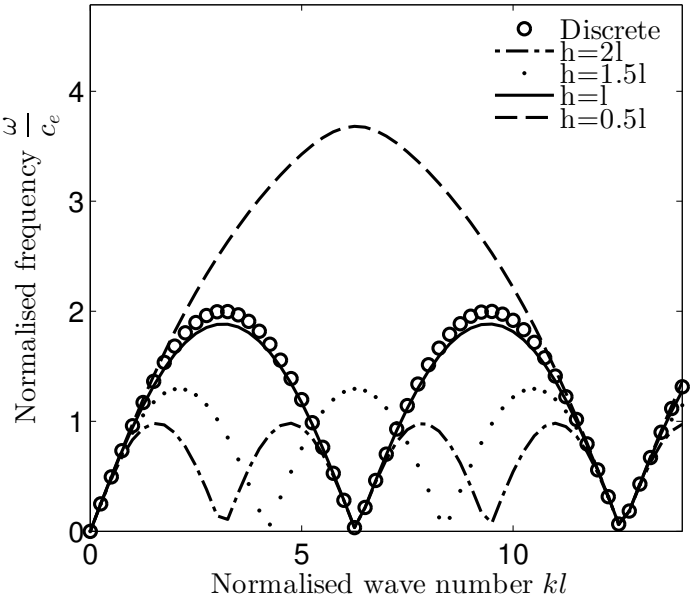

Fig. 7.1 Dispersion relations - Gradient continuum discretised with different element lengths compared with the discrete model

It can be said that the continuum is equivalent to a discretised continuum where the element lengths are infinite small. Figure 2 in Askes et al. (2008) presented the dispersion relations with different discretisation lengths (sizes) but did not compare them with the discrete model. Figure 7.1 demonstrates the effect of the discretisation length choice and compares those discretised continuum with the discrete model. The element length varies from $h = 2l$, $h = 1.5l$, $h = 0.5l$ and $h = l$ which is the best fit. It can be seen that the range of the Brillouin zone is inversely proportional to the element length: for e.g. in Figure 7.1, the continuum which was discretised at $h = 2l$ has the range of the Brillouin zone which is half the one of the discrete model. This property of the discretised continuum is also valid for the two dimensional case.

7.2 The two-dimensional cases

Similar to the one dimensional case, the order of discussion in this section shall be the successive transformation stages for each geometry. It is important to note that the shortest wavelength that the beam model can mathematically transfer is half the shortest wavelength that a spring model allows. Different mass schemes and different beam theories can be used for continualisation and produce results which have the same terms but different coefficients of the terms. We first compare the dispersion behaviour of the classical and gradient model with the discrete model for all three geometries (square, trapezium and hexagonal arrangements) before considering other factors.

7.2.1 General comparison of the analytical form of stages

- Discrete model: The dispersion relations are periodic for both shear and compression waves. This is due to the discrete model are already discretised in space. For the square and trapezium lattices, it is straightforward to derive the discrete model; meanwhile, the hexagonal lattice requires further manipulations to ensure the symmetry and reduce the size of the problem. The Bloch model is a good replacement for the discrete model to find the analytical dispersion relations. The discrete model used in this thesis is only capable of capturing mechanical waves and rotation waves.

- Generalised continuum: The homogenisation (continualisation) process of the discrete models produces sets of three equations representing generalised continuum. The new continuum is often not stable if the Taylor series expansion is utilised up to the fourth spatial order. At this stage, if we keep the high order gradients, we can classify them as non-standard continuum with enhanced gradients or if we do not keep the high order gradients, the continuum belongs to micro-polar theory. The rotational degrees of freedom are then eliminated by being approximated and replaced with translational degrees of freedom; thus, the newly reduced-degree-of-freedom continuum is now classed as a standard continuum with high order gradients.

- Classical continuum: The analytical forms have second order spatial gradients (first order of strain gradient) and no rotation degrees of freedom. They also show a coupling between two displacement variables. Therefore, the classical continuum can be considered as the standard continuum mentioned in Section 2.4 .The dispersion relations of the classical continuum are linear and turned periodic after space discretisation. Linear relationships are predictable because, similar to the one dimensional case, the maximum number of gradient order (combining micro-gradient and spatial gradient order) are the same for both sides of equations, see Equations (4.17) and (4.18). The classical dispersion graph can be said to be a tangent line to the discrete dispersion graph or the classical continuum estimates an inaccurate upper bound dispersion relations.

- Gradient continuum: For the square lattice, we have the gradient model in Lombardo and Askes (2012) to compare with the newly derived model. Figure 4.4 shows that the gradients of the dispersion graphs of both gradient models change with regard to the wavenumber k instead of being constant as the gradients of the classical continuum. However, regarding the terms, the model in Lombardo and Askes (2012) (equations 14a and 14b) is very similar to the one dimensional case with $S = 1/12$, see Equation (3.13), in the view that there are no high strain gradients but inertia-gradients. Due to this

propery, the dispersion curves have maximum frequency values (horizontal asymptotes) and it is safe to say that the Lombardo and Askes (2012) model has an apparent wave filtering effect. On the other hand, the square lattice model developed in this thesis, see Equations (4.23) and (4.24), has a few more terms but most importantly the fourth order spatial gradients (second order strain gradient), which results in a dispersion analysis having a diagonal asymptote as $k \rightarrow$. It can be seen that the newly derived equations lose the opportunity to have a horizontal asymptote but they give better approximation of dispersion relations in the first Brillouin zone to the discrete model than the classical model and the model in Lombardo and Askes (2012). After space discretisation, like the classical continuum, the dispersion relation of the discretised gradient continuum turns periodic. Similarly, for the trapezium and diamond lattices, the slope (horizontal or diagonal) of the asymptote when the wavenumber tends to infinity depends on how the terms are selected. When the high order gradient terms $\mathscr{X}_{iiii}$ are kept, application of the Ru-Aifantis theorem (see footnote1, page 14) is required to enable a robust C^0 continuity numerical discretisation.

7.2.2 Different beam theories and mass schemes used during homogenisation

Two mass schemes are investigated in this thesis: the lumped mass and consistent mass; and two popular beam theories: Euler beam and Timoshenko beam theories. It is reported that the consistent mass scheme and Euler beam often overestimate and the lumped mass and Timoshenko beam theory often underestimate the simulation results. Hence, two combinations are chosen for the homogenisation processes: Euler beam theory together with lumped mass and Timoshenko beam theory with consistent mass scheme. In all three lattices, both combinations produce qualitatively similar equations with different coefficients for the terms.

7.2.3 Effects of the propagation angle

Different from the one dimensional case, the scalar wave number k becomes the magnitude of a vector $\overrightarrow{k} = (k\cos\gamma, k\sin\gamma)$. For the two dimensional discrete models, expectedly, as the propagation angles γ varies, the dynamically linear wave dispersion pattern (the frequency of compression and shear component against the wave number k) repeats periodically for the discrete model due to the geometric symmetry of the lattices, e.g. the dispersion graph is the same for $\gamma = 0$ and $\gamma = 2\pi$ or all angles $\gamma = \gamma_0 + n2\pi$ where $n = 0, 1, 2, 3...$ for all periodic lattices. Moreover, there are special propagation angles γ that the dispersion graph would exhibit special properties such as symmetric propagation (same frequency curves for shear

and compression wave components) or when the wave number vector $\overrightarrow{k}$ is perpendicular to the beams, the shear wave will disappear or its magnitude is significantly smaller than that of the compression components. A desired continuum model will demonstrate isotropic and anisotropic propagation behaviour similar to the discrete model when the forces are exerted at those special angles.

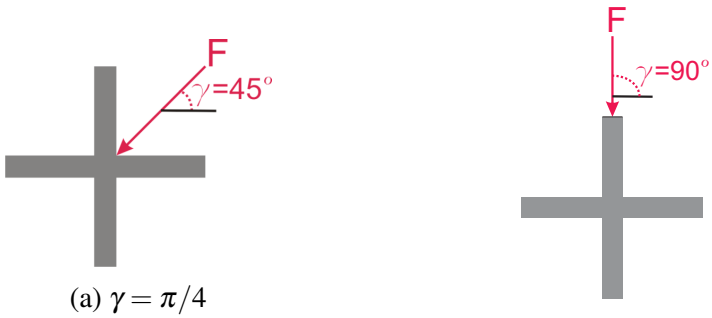

(a) $\gamma = \pi/4$ (b) $\gamma = \pi/2$

Fig. 7.2 The square lattice with different propagation angles γ of external waves

- Square lattice: the wave pattern repeats every $\pi/4$, symmetric propagation (same frequency curve for shear and compression waves) is seen at angles $(2n+1)\pi/4$ where $n = 0, 1, 2, 3...$, the shear wave component disappears for $\gamma = n\pi/2$. Two Figures 7.2a and 7.2b sketch the two different specific angles at which the wave strikes the model. This angle determines the wave number vector $\overrightarrow{k}$. Table 4.1 and Table 4.2 display the symmetry and asymmetry dispersion behaviour at the two special angles of the discrete, classical and gradient models. The magnitudes of shear and compression components of both classical and gradient models are distributed as predicted from the discrete model.

- Trapezium lattice: the wave pattern repeats every π. Let $\alpha \neq \pi/4$ be the opening angle between two intersecting beams. There is no propagation angle where the shear and compression components have the same frequency magnitude. When $\gamma = \left(n+\frac{1}{2}\right)\pi - \frac{\alpha}{2}$ or $\gamma = (n+1)\,\pi - \frac{\alpha}{2}$, the shear wave component has very small magnitude, as expected, because the wave propagates perpendicular to the beam, see Figure 5.8 for $\gamma = \pi/3$. Table 5.2 demonstrates the mentioned behaviour at $\pi/3$ where the shear wave component of the gradient model starts with a small slope. As the wave number k increases at these particular angles, the gradient model cannot capture the low magnitude shear wave component accurately.

- Hexagonal lattice: for such a regular hexagon shape, the wave dispersion repeats every $\pi/6$. Figures 6.12 and 6.13 depicts how the dispersion behaves at the two boundaries

of the repetition region. There is no angle where the compression and shear wave have the same frequency curves. When the shear wave magnitude is small, this effect causes some numerical errors when dispersion analysis is carried out for discretised models because of rounding errors.

7.2.4 Different element sizes and shapes for the finite element model

After deriving the gradient continuum, a discretisation scheme is applied where finite element sizes and shapes are chosen to best estimate a given problem. If is preferred to have a comparable finite element mesh with the discrete model which allows applying similar boundary conditions.

- Square lattice: if we choose the finite element length equal to the minimum length-scale of the discrete beam model, we can accurately compare the frequency curves of the classical continuum and the gradient continuum after discretisation. Table 4.1 shows no difference between the space-only discretised and space-and-time discretised model. If the finite element length is increased, the gradient continuum only closely captures the dispersion behaviour at low range of wave number k. The gradient continuum in Figure 7.3 has the finite element vertical and horizontal lengths twice the length-scale of the discrete model and results in having the period range of wave number k twice longer than the discrete model. This behaviour is very similar to the one-dimensional case. However, the change in element size would not affect the dispersion curve if it is calibrated with the direction of the wave propagation angles. Figure 7.4 displays the dispersion relation of a space discretised gradient continuum using square elements with vertical length $h_v = 2l$ and horizontal length $h_h = l$ when the propagation angle $\gamma = \pi/2$. We can see even though the element size is larger this time, the Brillouin zone period for the discretised continuum is the same as the one of the discrete model. We can also have larger vertical lengths for the square element but still have the same dispersion curve for the same propagation angle. This behaviour can help reduce the computation cost for certain problems.

- Trapezium lattice: if the continuum can be discretised numerically stably by the chosen discretisation scheme, there is no distinguishable difference between the space discretised results and that of space and time discretisation. Table 5.2 shows that different element shapes can affect how the continuum (after being disretised) behaves in dispersion. Even though the dispersion curves of both discrete model and continuum model at the representative volume element level are closely matching, the application of same boundary conditions on both models when there are more elements would be difficult.

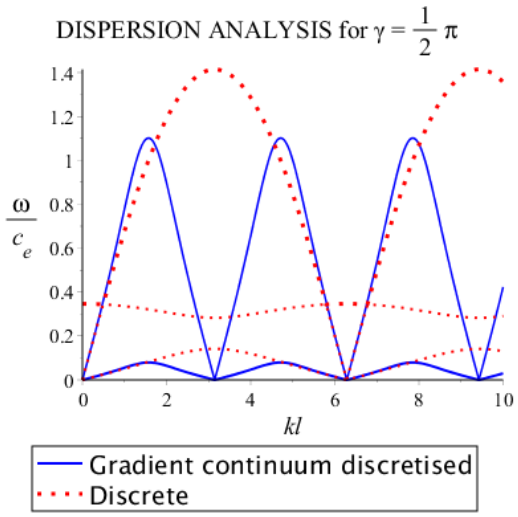

Fig. 7.3 The square lattice with the wave propagation angle of $\gamma = \pi/2$ and the square element shape has vertical length $h_v = 2l$ and horizontal length $h_h = 2l$. For each model, there are two curves, the lower curve represents the shear component and the higher curve represents the compression component, except the discrete model has an extra curve which does not originate from the origin represents the rotational degree of freedom.

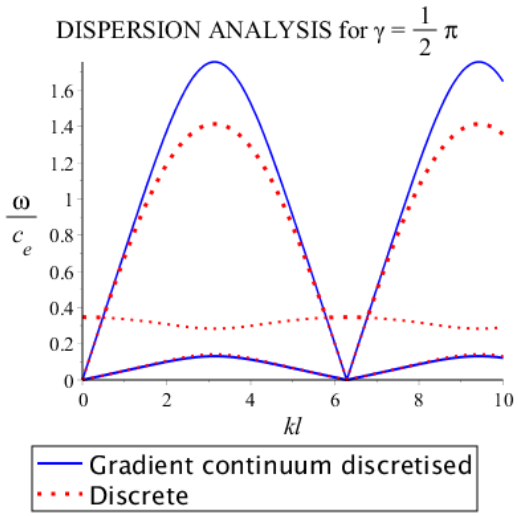

Fig. 7.4 The square lattice with the wave propagation angle of $\gamma = \pi/2$ and the square element shape has vertical length $h_v = 2l$ and horizontal length $h_h = l$. For each model, there are two curves, the lower curve represents the shear component and the higher curve represents the compression component, except the discrete model has an extra curve which does not originate from the origin represents the rotational degree of freedom.

The diamond finite element shape allows the application of boundary conditions and the energy paths to the continuum model to be more similar to the discrete model.

In conclusions, the shape and size of discretisation elements play important roles to help mimic the boundary conditions of the discrete model.

A closer look at the classical model after space discretisation, with lumped mass scheme and the spatial scheme of Equations (4.23) and (4.24), shows that the shear waves have zero frequency magnitudes with respect to all wave numbers. Especially, after space and time discretisation, the shear waves reappear but at a very small magnitude. This may be caused by the chosen time and spatial discretisation scheme. This result gives a message to be careful when using the continuum model for problems where a single frequency force is exerted on the model. Further investigations into this particular phenomenon could be considered in the future.

7.3 Gradient continuum - Advantages and disadvantages

How closely can the gradient continuum match the discrete model?

It is understandable that the analytical forms of all continuum would not be able to produce the periodic dispersion curves of the discrete model because the discrete model is already discretised in space. However, any improvements on the stable continua to get closer matches to the dispersion curves in the first Brillouin zone of the discrete models are preferred since then the newly modified continua possess natural dispersion relations instead of numerical dispersion. Continua enhanced by high order gradients give better dispersive behaviour than the classical continua.

Once being discretised in space, the continuum models are closest to the discrete model when the finite element length is equal to the discrete lengthscale in the one dimensional case and similar element shape in the two dimensional cases. This implies that there is no benefit in using smaller elements. The discretised gradient continua often give better estimations of the maximum frequency than the discretised classical continua. Specific dispersion behaviours at certain propagation angles for each lattice are preserved well by the gradient continuum.

Element shapes and lengths dictate how easy similar boundary conditions to the ones of the discrete models are applied to the continuum model. For example, in the trapezium case, the diamond element shape (on the right in Figure 5.7) distributes the mechanical waves more accurately in Table 5.2 than the rectangle element shape (the middle in Figure 5.7) This may be corrected by changing the chosen space and time discretisation schemes.

In some cases, it is difficult to apply the same boundary conditions to the discrete model and the continuum. However, calibration of the element shape and size to a specific problem

would improve the performance gradient continua.

When is it beneficial to use continua enhanced with high-order gradients?

Based on the results given in previous chapters and the discussion points, we list some cases where it is beneficial to use the gradient continuum:

- When the rotational wave can be ignored, using the gradient continuum can reduce the scale of problems significantly. Or, the rotation degrees of freedom can be ignored initially then get approximated to appear in the system again.
- When using with larger FE elements than the length-scale, the gradient continuum is only reliable for low wave number ranges (see Figure 7.3) or the first Brillouin zone.
- If mathematical manipulation of the discrete model to obtain a stable efficient gradient continuum can be accomplished, the gradient continua should be used instead of the classical continuum.
- If the discretisation element shape and size can be calibrated with the original arrangement of the continuum and the propagation angles, gradient continua could save on computational cost.

Chapter 8

Conclusion

The thesis introduces a four-step procedure to obtain a stable and efficient continuum enhanced with high-order gradients to simulate dynamically linear wave dispersion behaviours from a pre-defined physical discrete model. The method is first demonstrated with the one-dimensional spring-mass system. Then, it is applied to the square, trapezium and hexagonal lattices which are the underlying structures of microstructural materials. The newly derived continua must satisfy three requisite criteria: unconditional stability for dispersion relations while displaying a better dispersive behaviour than the classical continuum, robustness with parameters derived from the physical model and efficiency for easy numerical implementation which require only C^0 continuity for spatial discretisation. The research succeeds in deriving a continuum model which has separate numerical length-scale h and physical length-scale l.

The newly derived continua were compared with the discrete models and classical models. It has been shown that the gradient continua take into account of the inner length-scale of the microstructural material; hence, they can analytically describe the dispersion behaviours better than classical continuum. Moreover, the discretisation stage is also inspected using different element shapes and sizes to observe the calibration possibility of the discretisation scheme to certain problems.

8.1 Further research

During the time the thesis was carried out, there are a few areas of research that help understand the gradient continuum further but have not been investigated in this thesis:

- Investigation on the analytical solutions of discretised continuum for the hexagonal lattice. There is no effective space discretisation shape function for a hexagonal shape in the literature at the moment. Moreover, a short test for which sizes for a square element

to capture the periodic dispersion curve of the discrete model should be carried out.

- Investigation of the implementability of the gradient continuum with the boundary element method.
- A new way to incorporating the rotational degrees of freedom with the high-order gradients while still maintaining the stability of dispersion curve.
- Optimisation on the coefficients of the Padé approximation. In this thesis, the one dimensional case is optimised to have $H = \frac{1}{12}$; meanwhile, the two dimensional cases are much more mathematically complicated, for e.g. a rough estimation of the range for H in the trapezium case is achieved but the best value for H to achieve the best fit can be considered in future works.
- Three-dimensional microlattices: A better understanding for the one and two dimensional cases opens the door to more practical three-dimensional microstructure.

References

E.C. Aifantis. On the microstructural origin of certain inelastic models. *Journal of Engineering Materials and Technology, Transactions of the ASME*, 106(4):326–330, 1984. URL http://www.scopus.com/inward/record.url?eid=2-s2.0-0021502102&partnerID=40&md5=26d6e25d71667fdfec7b5460eda74cd9.

E.C. Aifantis. The physics of plastic deformation. *International Journal of Plasticity*, 3(3): 211–247, 1987. URL http://www.scopus.com/inward/record.url?eid=2-s2.0-0023174893&partnerID=40&md5=86ba5081f0524c8261c09928c72fe852. cited By 419.

E.C. Aifantis. On the role of gradients in the localization of deformation and fracture. *International Journal of Engineering Science*, 30(10):1279 – 1299, 1992.

B.S. Altan and E.C. Aifantis. On some aspects in the special theory of gradient elasticity. *Journal of the Mechanical Behaviour of Materials (UK)*, 7(3):231–282, 1997.

I.V. Andrianov and J. Awrejcewicz. Continuous models for 2d discrete media valid for higher-frequency domain. *Computers & structures*, 86(1):140–144, 2008.

I.V. Andrianov, J. Awrejcewicz, and R.G. Barantsev. Asymptotic approaches in mechanics: New parameters and procedures. *Applied Mechanics Reviews*, 56(1):87–109, 2003. URL http://www.scopus.com/inward/record.url?eid=2-s2.0-5644239856&partnerID=40&md5=e9b498c3c37c4060da3d2fc262cf1b0b. cited By 34.

I.V. Andrianov, J. Awrejcewicz, and D. Weichert. Improved continuous models for discrete media. *Mathematical Problems in Engineering*, 2010, 2009.

A. Askar and A.S. Cakmak. A structural model of a micropolar continuum. *International Journal of Engineering Science*, 6(10):583–589, 1968.

H. Askes and E.C. Aifantis. Gradient elasticity in statics and dynamics: An overview of formulations, length scale identification procedures, finite element implementations and new results. *International Journal of Solids and Structures*, 48(13):1962–1990, June 2011. ISSN 00207683.

H. Askes and A.V. Metrikine. One-dimensional dynamically consistent gradient elasticity models derived from a discrete microstructure Part 2 : Static and dynamic response. 21: 573–588, 2002.

H. Askes, T. Bennett, and E.C. Aifantis. A new formulation and C 0 -implementation of dynamically consistent gradient elasticity. *International Journal for Numerical Methods in Engineering*, 72(February):111–126, 2007.

H. Askes, B. Wang, and T. Bennett. Element size and time step selection procedures for the numerical analysis of elasticity with higher-order inertia. *Journal of Sound and Vibration*, 314(3–5):650 – 656, 2008. ISSN 0022-460X. doi: http://dx.doi.org/10.1016/j.jsv.2007.12.034. URL http://www.sciencedirect.com/science/article/pii/S0022460X08000175.

H. Askes, D.C.D. Nguyen, and A. Tyas. Increasing the critical time step: micro-inertia, inertia penalties and mass scaling. *Computational Mechanics*, 47(6):657–667, 2011. ISSN 0178-7675. doi: 10.1007/s00466-010-0568-z. URL http://dx.doi.org/10.1007/s00466-010-0568-z.

Klaus-Jürgen Bathe. *Finite Element Procedures*. Prentice Hall, 2006.

O.A. Bauchau and J.I. Craig. Euler-bernoulli beam theory. In O.A. Bauchau and J.I. Craig, editors, *Structural Analysis*, volume 163 of *Solid Mechanics and Its Applications*, pages 173–221. Springer Netherlands, 2009. ISBN 978-90-481-2515-9. doi: 10.1007/978-90-481-2516-6_5. URL http://dx.doi.org/10.1007/978-90-481-2516-6_5.

Z.P. Bazant and M. Christensen. Analogy between micropolar continuum and grid frameworks under initial stress. 1972.

T. Bennett and H. Askes. Finite element modelling of wave dispersion with dynamically consistent gradient elasticity. *Computational Mechanics*, 43(6):815–825, November 2008. ISSN 0178-7675.

A. Berezovski, J. Engelbrecht, and M. Berezovski. Waves in microstructured solids: a unified viewpoint of modeling. *Acta Mechanica*, 220(1-4):349–363, 2011. ISSN 0001-5970. doi: 10.1007/s00707-011-0468-0. URL http://dx.doi.org/10.1007/s00707-011-0468-0.

A. Berezovski, J. Engelbrecht, and M. Berezovski. Influence of internal structures on wave dispersion in solids. In *Advanced modelling of wave propagation in solids*, EUROMECH colloquium 540, pages 29–30, 2012.

M. Born and T. von Karman. Über schwingungen in raumgittern. *Physikalische Zeitschrift*, (113):297–309, 1912.

L. Brillouin. *Wave propagation in periodic structures: electric filters and crystal lattices*. Dover books and science. Dover Publications, 1953.

Jr. C.B. Banks and M. Sokolowski. On certain two-dimensional applications of the couple stress theory. *International Journal of Solids and Structures*, 4(1):15 – 29, 1968. ISSN 0020-7683.

C. Chang and J. Gao. Wave propagation in granular rod using high-gradient theory. *Journal of Engineering Mechanics*, 123(1):52–59, 1997. doi: 10.1061/(ASCE)0733-9399(1997)123:1(52). URL http://dx.doi.org/10.1061/(ASCE)0733-9399(1997)123:1(52).

C.S. Chang and J. Gao. Second-gradient constitutive theory for granular material with random packing structure. *International Journal of Solids and Structures*, 32(16):2279 – 2293, 1995. ISSN 0020-7683. doi: http://dx.doi.org/10.1016/0020-7683(94)00259-Y. URL http://www.sciencedirect.com/science/article/pii/002076839400259Y.

J.Y. Chen, Y. Huang, and M. Ortiz. Fracture analysis of cellular materials: A strain gradient model. *Journal of the Mechanics and Physics of Solids*, 46(5):789 – 828, 1998. ISSN 0022-5096. doi: http://dx.doi.org/10.1016/S0022-5096(98)00006-4. URL http://www.sciencedirect.com/science/article/pii/S0022509698000064.

W. Chen and J. Fish. A dispersive model for wave propagation in periodic heterogeneous media based on homogenization with multiple spatial and temporal scales. *Journal of Applied Mechanics, Transactions ASME*, 68(2):153–161, 2001. URL http://www.scopus.com/inward/record.url?eid=2-s2.0-0000258643&partnerID=40&md5=74f399ba9c0e6b9f6cea62a5fdcc7f06. cited By 79.

R.M. Christensen. *Mechanics of composite materials*. John Wiley Sons, Inc., 1979.

M.A. Collins. A quasicontinuum approximation for solitons in an atomic chain. *Chemical Physics Letters*, 77(2):342–347, 1981. URL http://www.scopus.com/inward/record.url?eid=2-s2.0-0002436381&partnerID=40&md5=bc773e4bd963a4fe609b548bbfec9f86. cited By 47.

E.M.P. Cosserat and F. Cosserat. *Théorie des corps déformables*. A. Hermann et fils (Paris), 1909.

R. De Borst, A. Benallal, and R.H.J. Peerlings. On gradient-enhanced damage theories. In N.A. Fleck and A.C.F. Cocks, editors, *IUTAM Symposium on Mechanics of Granular and Porous Materials*, volume 53 of *Solid Mechanics and its Applications*, pages 215–226. Springer Netherlands, 1997. ISBN 978-94-010-6324-1. doi: 10.1007/978-94-011-5520-5_20. URL http://dx.doi.org/10.1007/978-94-011-5520-5_20.

H. Deresiewicz. Stress-strain relations for a simple model of a granular medium. *J. Appl. Mech.*, 25:402–406, 1958.

J. Duffy and R.D. Mindlin. Stress-strain relations and vibrations of a granular medium. *J. Appl. Mech. (ASME)*, 24:585–593, 1957.

J. Engelbrecht, A. Berezovski, F. Pastrone, and M. Braun. Waves in microstructured materials and dispersion. *Philosophical Magazine*, 85(33-35):4127–4141, 2005.

A.C. Eringen. Linear theory of micropolar elsticity. 15:909–923, 1966.

A.C. Eringen. *Mechanics of micro-morphic continua*. Springer-Verlag, 1967.

A.C. Eringen and C.B. Kafadar. *Polar field theories*, volume I, pages 4–73. Academic Press, 1976.

V.I. Erofeyev. *Wave processes in Solids with Microstructure*. Series on Stability, Vibration and Control of Systems, Series A. World Scientific, 2003.

A.G. Evans, J.W. Hutchinson, and M.F. Ashby. Multifunctionality of cellular metal systems. *Progress in Material Science*, 43:171–221, 1999.

J. Fish and W. Chen. Higher-order homogenization of initial/boundary-value problem. *Journal of engineering mechanics*, 127(12):1223–1230, 2001.

J. Fish, W. Chen, and G. Nagai. Non-local dispersive model for wave propagation in heterogeneous media: one-dimensional case. *International Journal for Numerical Methods in Engineering*, 54(3):331–346, 2002. ISSN 1097-0207. doi: 10.1002/nme.423. URL http://dx.doi.org/10.1002/nme.423.

Dyskin A.V. Germanivich, L.N. Virial expansions in problems of effective characteristics. part i. general concepts. *J. Mech. Compos. Mater*, 30.

L.J. Gibson and M.F. Ashby. *Cellular Solids: Structure and Properties*. Cambridge Solid State Science Series. Cambridge University Press, 1999.

S. Gonella and M. Ruzzene. Analysis of in-plane wave propagation in hexagonal and re-entrant lattices. *Journal of Sound and Vibration*, 312(1–2):125 – 139, 2008. ISSN 0022-460X. doi: http://dx.doi.org/10.1016/j.jsv.2007.10.033. URL http://www.sciencedirect.com/science/article/pii/S0022460X07008486.

K.F. Graff. *Wave Motion in Elastic Solids*. Oxford University Press, London, 1975.

Z. Hashin. The differential scheme and its application to cracked materials. *Journal of the Mechanics and Physics of Solids*, 36(6):719 – 734, 1988. ISSN 0022-5096. doi: http://dx.doi.org/10.1016/0022-5096(88)90005-1. URL http://www.sciencedirect.com/science/article/pii/0022509688900051.

R. Hill. Elastic properties of reinforced solids: Some theoretical principles. *Journal of the Mechanics and Physics of Solids*, 11(5):357 – 372, 1963. ISSN 0022-5096. doi: http://dx.doi.org/10.1016/0022-5096(63)90036-X. URL http://www.sciencedirect.com/science/article/pii/002250966390036X.

T.J.R Hughes. *The Finite Element Method: Linear Static and Dynamic Finite Element Analysis*. Dover, 2000.

K. Jakata and A.G. Every. Determination of the dispersive elastic constants of the cubic crystals ge, si, gaas, and insb. *Phys. Rev. B*, 77:174301, May 2008. doi: 10.1103/PhysRevB.77.174301. URL http://link.aps.org/doi/10.1103/PhysRevB.77.174301.

M. Kachanov. Effective elastic properties of cracked solids: Critical review of some basic concepts. *Applied Mechanics Reviews*, 45(8):304–355, 1992. ISSN 0022-5096. doi: http://dx.doi.org/10.1115/1.3119761.

L.P. Khoroshun. Methods of theory of random functions in problems of macroscopic properties of microinhomogeneous media. *Soviet Applied Mechanics*, 14(2):113–124, 1978. ISSN 0038-5298. doi: 10.1007/BF00902836. URL http://dx.doi.org/10.1007/BF00902836.

C. Kittel. *Elementary solid state physics: a short course*. Wiley, 1962.

C. Kittel. *Introduction to Solid State Physics*. Wiley, 1996.

R.S. Kumar and D.L. McDowell. Generalized continuum modeling of 2-d periodic cellular solids. *International Journal of Solids and Structures*, 41(26):7399 – 7422, 2004. ISSN 0020-7683. doi: http://dx.doi.org/10.1016/j.ijsolstr.2004.06.038. URL http://www.sciencedirect.com/science/article/pii/S0020768304003658.

I.A. Kunin. *Elastic Media with Microstructure I: One-Dimensional Models*. Springer, 1982.

I.A. Kunin. *Elastic Media with Microstructure II: Three-Dimensional Models*. Springer, 1983.

R.S. Langley, N.S. Bardell, and H.M. Ruivo. The response of two-dimensional periodic structures to harmonic point loading: A theoretical and experimental study of a beam grillage. *Journal of Sound and Vibration*, 207(4):521 – 535, 1997. ISSN 0022-460X.

M. Lombardo and H. Askes. Elastic wave dispersion in microstructured membranes. *Proceedings of the Royal Society A: Mathematical, Physical and Engineering Science*, page rspa20090516, 2010.

M. Lombardo and H. Askes. Higher-order gradient continuum modelling of periodic lattice materials. *Computational Materials Science*, 52(1):204–208, February 2012. ISSN 09270256.

G.A. Maugin. *Non-linear Waves in Elastic Crystals*. Oxford University Press, 1999.

S.A. Meguid and A.L. Kalamkarov. Asymptotic homogenization of elastic composite materials with a regular structure. *International Journal of Solids and Structures*, 31(3):303 – 316, 1994. ISSN 0020-7683. doi: http://dx.doi.org/10.1016/0020-7683(94)90108-2. URL http://www.sciencedirect.com/science/article/pii/0020768394901082.

A.V. Metrikine. On causality of the gradient elasticity models. *Journal of Sound and Vibration*, 297(3–5):727 – 742, 2006. ISSN 0022-460X. doi: http://dx.doi.org/10.1016/j.jsv.2006.04.017. URL http://www.sciencedirect.com/science/article/pii/S0022460X06003415.

A.V. Metrikine and H. Askes. One-dimensional dynamically consistent gradient elasticity models derived from a discrete microstructure Part 1 : Generic formulation. 21:555–572, 2002.

G.W. Milton and J.R. Willis. On modifications of newton's second law and linear continuum elastodynamics. *Proceedings of the Royal Society of London A: Mathematical, Physical and Engineering Sciences*, 463(2079):855–880, 2007. ISSN 1364-5021. doi: 10.1098/rspa.2006.1795.

R.D. Mindlin. Micro-structure in linear elasticity. *Archive for Rational Mechanics and Analysis*, 16(1):51–78, 1964. ISSN 0003-9527. doi: 10.1007/BF00248490. URL http://dx.doi.org/10.1007/BF00248490.

R.D. Mindlin and H.F. Tiersten. Effects of couple-stresses in linear elasticity. *Archive for Rational Mechanics and Analysis*, 11(1):415–448, 1962. ISSN 0003-9527. doi: 10.1007/BF00253946. URL http://dx.doi.org/10.1007/BF00253946.

T. Mori and K. Tanaka. Average stress in matrix and average elastic energy of materials with misfitting inclusions. *Acta Metallurgica*, 21(5):571 – 574, 1973. ISSN 0001-6160. doi: http://dx.doi.org/10.1016/0001-6160(73)90064-3. URL http://www.sciencedirect.com/science/article/pii/0001616073900643.

H.B. Mühlhaus and F. Oka. Dispersion and wave propagation in discrete and continuous models for granular materials. *International Journal of Solids and Structures*, 33(19):2841 – 2858, 1996. ISSN 0020-7683. doi: http://dx.doi.org/10.1016/0020-7683(95)00178-6. URL http://www.sciencedirect.com/science/article/pii/0020768395001786.

H.B. Mühlhaus and I. Vardoulakis. The thickness of shear bands in granular materials. *Geotechnique*, 37(3):271–283, 1987.

S. Nemat-Nasser and M. Hori. Micromechanics: overall properties of heterogeneous solids. *Applied Mathematics and Mechanics. Elsevier, Amsterdam*, 1993.

W. Nowacki. *Theory of Micropolar Elasticity*. Springer, 1970.

M. Ostoja-Starzewski. Microstructural randomness versus representative volume element in thermomechanics. *Journal of Applied Mechanics*, 69(1):25–35, 2002.

S. Papargyri-Beskou, D. Polyzos, and D.E. Beskos. Wave dispersion in gradient elastic solids and structures: A unified treatment. *International Journal of Solids and Structures*, 46(21): 3751 – 3759, 2009. ISSN 0020-7683. doi: http://dx.doi.org/10.1016/j.ijsolstr.2009.05.002. URL http://www.sciencedirect.com/science/article/pii/S0020768309001966.

E. Pasternak and H.B. Mühlhaus. Generalised homogenisation procedures for granular materials. *Journal of Engineering Mathematics*, 52(1):199–229, 2005. ISSN 0022-0833. doi: 10.1007/s10665-004-3950-z. URL http://dx.doi.org/10.1007/s10665-004-3950-z.

E. Pasternak, H.B. Mühlhaus, and A.V. Dyskin. Finite deformation model of simple shear of fault with microrotations: apparent strain localisation and en-echelon fracture pattern. *Philosophical Magazine*, 86(21-22):3339–3371, 2006. doi: 10.1080/14786430500270392. URL http://dx.doi.org/10.1080/14786430500270392.

I.S. Pavlov, A.I. Potapov, and G.A. Maugin. A 2d granular medium with rotating particles. *International Journal of Solids and Structures*, 43(20):6194 – 6207, 2006. ISSN 0020-7683. doi: http://dx.doi.org/10.1016/j.ijsolstr.2005.06.012. URL http://www.sciencedirect.com/science/article/pii/S0020768305003252.

A.S. Phani, J. Woodhouse, and N.A. Fleck. Wave propagation in two-dimensional periodic lattices. *The Journal of the Acoustical Society of America*, 119(4):1995, 2006. ISSN 00014966.

A.V. Pichugin, H. Askes, and A. Tyas. Asymptotic equivalence of homogenisation procedures and fine-tuning of continuum theories. *Journal of Sound and Vibration*, 313(3-5):858–874, 2008. URL http://www.scopus.com/inward/record.url?eid=2-s2.0-41549131636&partnerID=40&md5=0ad09459617cfcf6f837f4b4eb57598d. cited By 16.

S.S. Rao. *The Finite Element Method in Engineering*. Elsevier Inc., 2011.

C.Q. Ru and E.C. Aifantis. A simple approach to solve boundary-value problems in gradient elasticity. *Acta Mechanica*, 101(1-4):59–68, 1993. URL http://www.scopus.com/inward/record.url?eid=2-s2.0-0002471276&partnerID=40&md5=7ad8a710d03d962271632b3cf5dacee2. cited By 151.

M. B. Rubin, P. Rosenau, and O. Gottlieb. Continuum model of dispersion caused by an inherent material characteristic length. *Journal of Applied Physics*, 77(8):4054–4063, 1995. doi: http://dx.doi.org/10.1063/1.359488. URL http://scitation.aip.org/content/aip/journal/jap/77/8/10.1063/1.359488.

E.T. Selig and J.M. Waters. *Track Geotechnology and Substructure Management*. Thomas Telford Services, 1994.

A.S.J. Suiker, C.S. Chang, and R. de Borst. Surface waves in a stratified half space with enhanced continuum properties. part 2: Analysis of the wave characteristics in regard to high-speed railway tracks. *European Journal of Mechanics - A/Solids*, 18(5):749–768, 1999. doi: 10.1016/S0997-7538(99)00108-4.

A.S.J. Suiker, R. de Borst, and C.S. Chang. Micromechanically based higher-order continuum models for granular materials. In Dimitrios Kolymbas, editor, *Constitutive Modelling of Granular Materials*, pages 249–274. Springer Berlin Heidelberg, 2000. ISBN 978-3-642-63115-3. doi: 10.1007/978-3-642-57018-6_11. URL http://dx.doi.org/10.1007/978-3-642-57018-6_11.

A.S.J Suiker, A.V Metrikine, and R. de Borst. Comparison of wave propagation characteristics of the Cosserat continuum model and corresponding discrete lattice models. *International Journal of Solids and Structures*, 38:1563–1583, 2001.

S. Timoshenko. *History of strength of materials*. McGraw-Hill, 1953.

I. Vardoulakis and E.C. Aifantis. On the role of microstructure in the behavior of soils: Effects of higher order gradients and internal inertia. *Mechanics of Materials*, 18(2):151 – 158, 1994. ISSN 0167-6636. doi: http://dx.doi.org/10.1016/0167-6636(94)00002-6. URL http://www.sciencedirect.com/science/article/pii/0167663694000026. Special Issue on Microstructure and Strain Localization in Geomaterials.

A.A. Vasiliev, S.V. Dmitriev, Y. Ishibashi, and T. Shigenari. Elastic properties of a two-dimensional model of crystals containing particles with rotational degrees of freedom. *Phys. Rev. B*, 65:094101, Jan 2002. doi: 10.1103/PhysRevB.65.094101. URL http://link.aps.org/doi/10.1103/PhysRevB.65.094101.

A.A. Vasiliev, S.V. Dmitriev, and A.E. Miroshnichenko. Multi-field approach in mechanics of structural solids. *International Journal of Solids and Structures*, 47(3–4):510 – 525, 2010. ISSN 0020-7683. doi: http://dx.doi.org/10.1016/j.ijsolstr.2009.10.016. URL http://www.sciencedirect.com/science/article/pii/S0020768309004090.

X.L. Wang and W.J. Stronge. Micropolar theory for two–dimensional stresses in elastic honeycomb. *Proceedings of the Royal Society of London A: Mathematical, Physical and Engineering Sciences*, 455(1986):2091–2116, 1999. ISSN 1364-5021. doi: 10.1098/rspa.1999.0394.

Z. Wang and C.T. Sun. Modeling micro-inertia in heterogeneous materials under dynamic loading. *Wave Motion*, 36(4):473 – 485, 2002. ISSN 0165-2125. doi: http://dx.doi.org/10.1016/S0165-2125(02)00037-9. URL http://www.sciencedirect.com/science/article/pii/S0165212502000379.

W.E. Warren and E. Byskov. Three-fold symmetry restrictions on two-dimensional micropolar materials. *European Journal of Mechanics - A/Solids*, 21(5):779 – 792, 2002. ISSN 0997-7538. doi: http://dx.doi.org/10.1016/S0997-7538(02)01236-6. URL http://www.sciencedirect.com/science/article/pii/S0997753802012366.

Appendix A

The Timoshenko beam theory

The Timoshenko beam theory (Timoshenko, 1953) has the following stiffness matrix:

$$K_{Timo} = \begin{bmatrix} \frac{EA}{L} & 0 & 0 & -\frac{EA}{L} & 0 & 0 \\ 0 & \frac{12EI_z}{L^3(1+\Phi)} & \frac{6EI_z}{L^2(1+\Phi)} & 0 & -\frac{12EI_z}{L^3(1+\Phi)} & \frac{6EI_z}{L^2(1+\Phi)} \\ 0 & \frac{6EI_z}{L^2(1+\Phi)} & \frac{(4+\Phi)EI_z}{L(1+\Phi)} & 0 & -\frac{6EI_z}{L^2(1+\Phi)} & \frac{(2-\Phi)EI_z}{L(1+\Phi)} \\ -\frac{EA}{L} & 0 & 0 & \frac{EA}{L} & 0 & 0 \\ 0 & -\frac{12EI_z}{L^3(1+\Phi)} & -\frac{6EI_z}{L^2(1+\Phi)} & 0 & \frac{12EI_z}{L^3(1+\Phi)} & -\frac{6EI_z}{L^2(1+\Phi)} \\ 0 & \frac{6EI_z}{L^2(1+\Phi)} & \frac{(2-\Phi)EI_z}{L(1+\Phi)} & 0 & -\frac{6EI_z}{L^2(1+\Phi)} & \frac{(4+\Phi)EI_z}{L(1+\Phi)} \end{bmatrix} \tag{A.1}$$

where A is the beam cross-section area, E the elastic modulus, I_z is the second moment of area for the beam cross-section, L the beam length, and

$$\Phi = \frac{12EI_z}{sAGL^2} \tag{A.2}$$

where s is the shear factor (or Timoshenko shear coefficient), G is the shear modulus.

The consistent mass matrix of the Timoshenko beam theory is:

$$M_{Timo} = \begin{bmatrix} \frac{1}{3}\rho AL & 0 & 0 & \frac{1}{6}\rho AL & 0 & 0 \\ 0 & \frac{\rho ALm_1}{(1+\Phi)^2} & \frac{\rho ALm_2}{(1+\Phi)^2} & 0 & \frac{\rho ALm_3}{(1+\Phi)^2} & -\frac{\rho ALm_4}{(1+\Phi)^2} \\ 0 & \frac{\rho ALm_2}{(1+\Phi)^2} & \frac{\rho ALm_5}{(1+\Phi)^2} & 0 & \frac{\rho ALm_4}{(1+\Phi)^2} & -\frac{\rho ALm_6}{(1+\Phi)^2} \\ \frac{1}{6}\rho AL & 0 & 0 & \frac{1}{3}\rho AL & 0 & 0 \\ 0 & \frac{\rho ALm_3}{(1+\Phi)^2} & \frac{\rho ALm_4}{(1+\Phi)^2} & 0 & \frac{\rho ALm_1}{(1+\Phi)^2} & -\frac{\rho ALm_2}{(1+\Phi)^2} \\ 0 & -\frac{\rho ALm_4}{(1+\Phi)^2} & -\frac{\rho ALm_6}{(1+\Phi)^2} & 0 & -\frac{\rho ALm_2}{(1+\Phi)^2} & \frac{\rho ALm_5}{(1+\Phi)^2} \end{bmatrix} \tag{A.3}$$

where ρ is the material density and

$$m_1 = \frac{13}{35} + \frac{1\Phi}{10} + \frac{\Phi^2}{3} \tag{A.4}$$

$$m_2 = \left(\frac{11}{210} + \frac{11\Phi}{120} + \frac{\Phi^2}{24}\right) L \tag{A.5}$$

$$m_3 = \frac{9}{70} + \frac{3\Phi}{10} + \frac{\Phi^2}{6} \tag{A.6}$$

$$m_4 = \left(\frac{13}{420} + \frac{3\Phi}{40} + \frac{\Phi^2}{24}\right) L \tag{A.7}$$

$$m_5 = \left(\frac{1}{105} + \frac{\Phi}{60} + \frac{\Phi^2}{120}\right) L^2 \tag{A.8}$$

$$m_6 = \left(\frac{1}{140} + \frac{\Phi}{60} + \frac{\Phi^2}{120}\right) L^2 \tag{A.9}$$

$$\tag{A.10}$$

These two matrices are used in the continualisation processes in Appendices B.1, C.1 and D.1.

Appendix B

Additional notes on the square lattices

B.1 Continualisation results of the Timoshenko beam theory and consistent mass matrices

This section presents the results of the continualisation process using the Timoshenko beam theories and consistent mass matrices in Appendix A. The following three equations have similar format to the set of equations (4.10), (4.11) and (4.12).

$$\begin{aligned} 2\left(1+3\beta^2\right)\rho\ddot{u} = E\left(\left(1+3\beta^2\right)u_{,xx}+\beta^2 u_{,yy}+\beta^2\theta_{,y}\right) \\ +\frac{El^2}{12}\left(\left(1+3\beta^2\right)u_{,xxxx}+\beta^2 u_{,yyyy}+2\beta^2\theta_{,yyy}\right) \end{aligned} \tag{B.1}$$

$$\begin{aligned} 2\left(1+3\beta^2\right)\rho\ddot{v} = E\left(\left(1+3\beta^2\right)v_{,yy}+\beta^2 v_{,xx}-\beta^2\theta_{,x}\right) \\ +\frac{El^2}{12}\left(\left(1+3\beta^2\right)v_{,yyyy}+\beta^2 v_{,xxxx}-2\beta^2\theta_{,yyy}\right) \end{aligned} \tag{B.2}$$

$$\begin{aligned} \frac{\delta}{6E\beta^2}\left(1+3\beta^2\right)\rho l^2\ddot{\theta}+2\theta = \\ v_{,x}-u_{,y}-\frac{l^2}{6}\left[\left(1-\frac{3}{2}\beta^2\right)\left(\theta_{,xx}+\theta_{,yy}\right)-v_{,xxx}+u_{,yyy}\right] \end{aligned} \tag{B.3}$$

B.2 Rephrasing the rotational degree of freedom

This section provides the derivation process to approximate and replace the rotational degree of freedom with the translational degrees of freedom. The result of this section is used in Section 4.2.1. Different from the method used in Lombardo and Askes (2012), we only use Equation (4.12) to approximate θ. We take the derivatives $\frac{d}{d^2tt}$, $\frac{d}{d^2xx}$ and $\frac{d}{d^2yy}$ of both sides of

Equation (4.12) and rewrite them as follows:

$$2\ddot{\theta} = \ddot{v}_{,x} - \ddot{u}_{,y} - \frac{l^2}{6}\left(\ddot{\theta}_{,xx} + \ddot{\theta}_{,yy} - \ddot{v}_{,xxx} + \ddot{u}_{,yyy} - \frac{\delta \dddot{\theta}}{E\beta^2}\rho\right) \tag{B.4}$$

$$2\theta_{,xx} = v_{,xxx} - u_{,xxy} - \frac{l^2}{6}\left(\theta_{,xxxx} + \theta_{,xxyy} - v_{,xxxxx} + u_{,xxyyy} - \frac{1}{E\beta^2}\rho\ddot{\theta}_{,xx}\right) \tag{B.5}$$

$$2\theta_{,yy} = v_{,xyy} - u_{,yyy} - \frac{l^2}{6}\left(\theta_{,xxyy} + \theta_{,yyyy} - v_{,xxxyy} + u_{,yyyyy} - \frac{\delta}{E\beta^2}\rho\ddot{\theta}_{,yy}\right) \tag{B.6}$$

The right hand sides of above equations are substituted into Equation (4.12) to replace $\ddot{\theta}$, $\theta_{,xx}$ and $\theta_{,yy}$. Ignoring all $O\left(l^4\right)$ terms in the new equation of Equation (4.12), we can rewrite the rotational displacement θ with respect to u and v as Equation (4.14).

Appendix C

Additional notes on the trapezium lattices

C.1 Continualisation results of the Timoshenko beam theory and consistent mass matrices

This section presents the results of the continualisation process using the Timoshenko beam theories and consistent mass matrices in Appendix A. The following three equations have similar format to the set of equations (5.14), (5.15) and (5.16).

$$\begin{aligned}&6720\left(3\beta^2+1\right)\rho\ddot{u}+\\&E\begin{pmatrix}-1260\left(10\beta^2+3\right)\left(3u_{,xx}+u_{,yy}\right)-2520\left(2\beta^2+1\right)v_{,xy}\\-\frac{l^2}{4}\left(10\beta^2+3\right)\left(315\left(u_{,xxxx}+2u_{,xxyy}\right)+35u_{,yyyy}\right)\\-105l^2\left(2\beta^2+1\right)\left(3v_{,xxxy}+v_{,xyyy}\right)\\-1680\beta^2\theta_y-630\beta^2l^2\theta_{,xxy}-70\beta^2l^2\theta_{,yyy}\end{pmatrix}=0\end{aligned} \tag{C.1}$$

$$\begin{aligned}&6720\left(3\beta^2+1\right)\ddot{v}+\\&E\begin{pmatrix}-1260\left(6\beta^2+1\right)\left(v_{,yy}+3v_{,xx}\right)+-2520\left(2\beta^2+1\right)u_{,xy}\\-\frac{l^2}{4}\left(6\beta^2+1\right)\left[315\left(v_{,xxxx}+2v_{,xxyy}\right)+35v_{,yyyy}\right]\\-105l^2\left(2\beta^2+1\right)\left(u_{,xyyy}+3u_{,xxxy}\right)\\+5040\beta^2\theta_{,}y+630\beta^2l^2\theta_{,xyy}+630\beta^2l^2\theta_{,xxx}\end{pmatrix}=0\end{aligned} \tag{C.2}$$

$$\begin{aligned}&\tfrac{16\rho l^2\delta}{\beta^2}\ddot{\theta}+E840\left(3\beta^2+1\right)\left(4\theta+u_{,}y-3v_{,}x\right)+\\&El^2\left(3\beta^2+1\right)\left[70\left(-3\beta^2+2\right)\left(3\theta_{,xx}+\theta_{,yy}\right)\right]\\&+El^2\left(3\beta^2+1\right)\left[315\left(u_{,xxy}-v_{,xyy}\right)+35\left(3u_{,yyy}-v_{,xxx}\right)\right]=0\end{aligned} \tag{C.3}$$

C.2 Rephrasing the rotational degree of freedom

There are two ways to eliminate the rotational degree of freedom: the method used in (Lombardo and Askes (2012)) and the following methods: For easy formulation and simple derivation, we ignore all terms related to l^4 since l is at the microscale, l^4 will have the numerical value negligible compared to other terms. Differentiating both sides of Equation (5.16) twice with respect to time:

$$\ddot{\theta} = \frac{3}{4}\ddot{v}_{,x} - \frac{1}{4}\ddot{u}_{,y} \underbrace{- l^2\left(\frac{\rho}{12\lambda^2 E}\ddot{\ddot{\theta}} + \frac{3}{32}\ddot{u}_{,xxy} - \frac{3}{32}\ddot{v}_{,xyy} + \frac{1}{96}\ddot{u}_{,yyy} - \frac{3}{32}\ddot{v}_{,xxx} + \frac{1}{8}\ddot{\theta}_{,xx} + \frac{1}{24}\ddot{\theta}_{,yy}\right)}_{\text{negligible}} \tag{C.4}$$

We can ignore the terms related to $O\left(l^2\right)$ in Equation (C.4) because when we substitute back into Equation (5.16), these terms then incur terms of $O(l^4)$. The same procedure is applied when differentiating Equation (5.16) twice with respect to x and twice with respect to y, respectively:

$$\theta_{,xx} = -\frac{1}{4}u_{,xxy} + \frac{3}{4}v_{,xxx} \tag{C.5}$$

$$\theta_{,yy} = -\frac{1}{4}u_{,yyy} + \frac{3}{4}v_{,xyy} \tag{C.6}$$

Substitute the three Equations (C.4), (C.5) and (C.6) into equation (5.16) and drop all $O\left(l^4\right)$ terms, we can rewrite θ with respect to other linear variables as in Equation (5.18).

C.3 Find values of H for Padé approximation

During the stabilisation process using Padé approximation (see section 5.2.3), we have set up some conditions for arbitrary constant relative to H, see Equations (5.25). However, to find the suitable value ranges for H that ensure the dynamic stability for all propagation angles and all positive wave numbers is a labourious and complicated task and would require the aid of symbolic mathematic softwares. The quickest way is the "trial and error" method. In this section, we describes the trial and error method and try to give the best details whenever possible without writing out lengthy equations.

First, we rewrite the two Equations (5.27) and (5.28).

$$2\rho\ddot{u} - \left(\frac{3}{32}+\frac{H}{3}\right)\rho l^2\ddot{u}_{,yy} - \left(H+\frac{1}{4}\right)\rho l^2\ddot{u}_{,xx} + \left(\frac{1}{32}+2H\right)\rho l^2\ddot{v}_{,xy} = E\left(\frac{9}{8}u_{,xx}+\frac{3}{8}u_{,yy}+\frac{3}{4}v_{,xy}\right) + El^2\left(-\left(\frac{9}{128}+\frac{H}{16}\right)u_{,xxxx}+\left(\frac{3}{64}+\frac{3}{8}H\right)u_{,xxyy}-\left(\frac{1}{128}+\frac{H}{16}\right)u_{,yyyy}\right) \tag{C.7}$$

$$2\rho\ddot{v} - \left(\frac{11}{32}+3H\right)\rho l^2\ddot{v}_{,xx} - \left(H+\frac{1}{12}\right)\rho l^2\ddot{v}_{,yy} + \left(2H+\frac{1}{32}\right)\rho l^2\ddot{u}_{,xy} = E\left(\frac{1}{8}v_{,yy}+\frac{3}{8}v_{,xx}+\frac{3}{4}u_{,xy}\right) + + El^2\left(-\left(\frac{1}{384}+\frac{H}{16}\right)v_{,yyyy}-\left(\frac{3}{128}+\frac{9H}{16}\right)v_{,xxxx}+\left(\frac{1}{64}-\frac{H}{8}\right)v_{,xxyy}\right) \tag{C.8}$$

Substituting the plane wave equations (4.13) for u and v with $x=0$, $y=0$ and $t=0$ as we normally do for dispersion analysis, we obtain an eigen value problem for (U,V). The determinant K of the matrix is a biquadratic equation of the angular frequency ω:

$$K = A(H,cos(\gamma),k)\omega^4 + B(H,cos(\gamma),k)\omega^2 + C(H,cos(\gamma),k) \tag{C.9}$$

where A, B and C are coefficients which are functions of $(k,cos\gamma,H)$ where k is the wave number, γ is the propagation angle. Note that $cos(\gamma)$ varies in the range $[-1,1]$.

To have non-trivia real solutions for ω, the coefficients in the equation of determinant K must satisfy conditions:

- $A \neq 0$
- Vieta theory (for quadratic equations) to have both positive roots: $-\frac{B}{A} > 0$ and $-\frac{C}{A} > 0$

To find the proper range of H that ensures stable dispersion analysis is out of the scope of this thesis but would be beneficial to optimise the Padé approximants. However, it is easier to check if a certain value of H is suitable for an extensive range of positive wave numbers by substituting that value to K. With the aid of symbolic mathematical solvers, we can easily obtain four analytical solutions ω for $K=0$ and the four solutions (of which two equations will give positive values)will be functions of wavenumber k and the propagation angle γ. Hence, with the value of H chosen, we can plot the two positive solutions with respect to the propagation angle γ varying from 0 to 2π and the wave number k from 1 to 100 covering the first Brillouin zone. Figure C.1 display the plot for two positive solutions of ωs at $H=10$ and infers that the values of square of frequency ω increase as the wavenumber k increases and are stable(positive) for a large range of wavenumbers. This agrees with the two-dimensional graphs of dispersion analysis, in particular Figure 5.5.

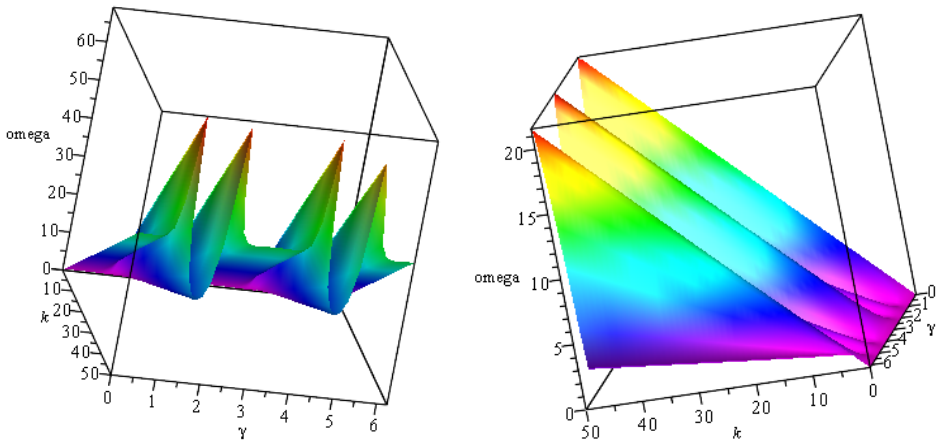

(a) The discrete model (b) The continuum model

Fig. C.1 Dispersion relations (frequency value ω) - Gradient continuum for all possible values of the propagation angles γ and varying wavenumber k for $H = 10$

Appendix D

Additional notes on the hexagonal lattices

D.1 Continualisation results of the Timoshenko beam theory and consistent mass matrices

This section presents the results of the continualisation process using the Timoshenko beam theories and consistent mass matrices in Appendix A. The following three equations have similar format to the set of equations (6.4), (6.5) and (6.6).

$$
\begin{aligned}
&13440\left(3\beta^2+1\right)\rho\ddot{u}+\\
&E\begin{pmatrix}
-1680\left(10\beta^2+3\right)u_{,xx}-1680\left(6\beta^2+1\right)u_{,yy}-3360\left(2\beta^2+1\right)v_{,xy}\\
-525l^2\left(10\beta^2+3\right)\left(u_{,xxxx}+2u_{,xxyy}\right)-175\left(14\beta^2+1\right)u_{,yyyy}\\
-700l^2\left(2\beta^2+1\right)\left(3v_{,xxxy}+v_{,xyyy}\right)\\
-6720\beta^2\theta_{,y}-2520\beta^2l^2\theta_{,xxy}-2520\beta^2l^2\theta_{,yyy}
\end{pmatrix}=0
\end{aligned}
\tag{D.1}
$$

$$
\begin{aligned}
&13440\left(3\beta^2+1\right)\ddot{v}+\\
&E\begin{pmatrix}
-1680\left(10\beta^2+3\right)\left(v_{,yy}\right)-1680\left(6\beta^2+1\right)v_{,xx}-3360\left(2\beta^2+1\right)u_{,xy}\\
-525l^2\left(6\beta^2+1\right)\left(v_{,xxxx}+2v_{,xxyy}\right)-175l^2\left(34\beta^2+11\right)v_{,yyyy}\\
-700l^2\left(2\beta^2+1\right)\left(u_{,xyyy}+3u_{,xxxy}\right)\\
+6720\beta^2\theta_{,y}+2520\beta^2l^2\theta_{,xyy}+2520\beta^2l^2\theta_{,xxx}
\end{pmatrix}=0
\end{aligned}
\tag{D.2}
$$

$$
\begin{aligned}
&\frac{8\rho l^2\delta}{\beta^2}\ddot{\theta}+E840\left(3\beta^2+1\right)\left(2\theta+u_y-v_{,x}\right)+\\
&El^2\left(3\beta^2+1\right)\left[70\left(-3\beta^2+8\right)\left(\theta_{,xx}+\theta_{,yy}\right)\right]\\
&+El^2\left(3\beta^2+1\right)\left[u_{,xxy}-v_{,xyy}+u_{,yyy}-v_{,xxx}\right]=0
\end{aligned}
\tag{D.3}
$$

D.2 Rephrasing the rotational degree of freedom

This section provides the derivation process to approximate and replace the rotational degree of freedom with the translational degrees of freedom. For easy formulation and simple derivation, we ignore all terms related to (l^4) since l is at the microscale, (l^4) will have the numerical value negligible compared to other terms. Differentiating both sides of Equation (6.6) twice with respect to time:

$$\ddot{\theta} = \frac{3}{4}\ddot{v}_{,x} - \frac{1}{4}\ddot{u}_{,y} \underbrace{-l^2\left(\frac{\rho}{12\lambda^2 E}\ddot{\ddot{\theta}} + \frac{3}{32}\ddot{u}_{,xxy} - \frac{3}{32}\ddot{v}_{,xyy} + \frac{1}{96}\ddot{u}_{,yyy} - \frac{3}{32}\ddot{v}_{,xxx} + \frac{1}{8}\ddot{\theta}_{,xx} + \frac{1}{24}\ddot{\theta}_{,yy}\right)}_{\text{negligible}} \tag{D.4}$$

We can ignore the terms related to l^2 in Equation (D.4) because when we substitute back into Equation (6.6), these terms then incur terms of l^4 . The same procedure is applied when differentiating Equation (6.6) twice with respect to x and twice with respect to y, respectively:

$$\theta_{,xx} = -\frac{1}{4}u_{,xxy} + \frac{3}{4}v_{,xxx} \tag{D.5}$$

$$\theta_{,yy} = -\frac{1}{4}u_{,yyy} + \frac{3}{4}v_{,xyy} \tag{D.6}$$

Substitute the three Equations (D.4), (D.5) and (D.6) into equation (6.6) and drop all (l^4) terms, we can rewrite θ with respect to other linear variables as in Equation (6.6).

Index